ENERGY CARRIER ALLOCATION STRATEGY FOR A HYBRID WIND FARM WITH OFFSHORE ELECTROLYSIS

A techno-economic optimization study from a developer's perspective

MASTER OF SCIENCE THESIS

L.M. BOUMA

TU Delft

Eneco

Energy allocation strategy for a hybrid wind farm with offshore electrolysis

A techno-economic optimization study from a developer's perspective

MASTER OF SCIENCE THESIS

by

Lucas Bouma

August 17, 2023

To defend publicly on:

August 31, 2023

Faculty of Electrical Engineering, Mathematics & Computer Science

Delft University of Technology

This thesis has been carried out to obtain a master's degree in the field of Sustainable Energy Technology at Delft University of Technology. The research has been supported by Eneco, whose cooperation is hereby gratefully acknowledged. This work has been read and evaluated by the thesis committee consisting of the following members:

Graduation committee:

Prof. dr. ir. D.A. Von Terzi	TU Delft, Chair
Prof. dr. A.J.M Van Wijk	TU Delft
ir. M. Goorden	Eneco

Preface

With this thesis, I conclude my master's in Sustainable Energy Technology at Delft University of Technology. During my studies, I switched from civil engineering to the faculty of electrical engineering, which is one of the best decisions I ever made. The field of sustainable energy has really fascinated me over the past two years. Due to the technology being relatively new, many answers about incorporating renewables into our daily lives are yet to be found, of which this thesis is an example. However, the master Sustainable Energy Technology has opened my eyes to the vast amount of possibilities we have.

Before moving on to the content, I would like to express my gratitude to several people who supported me during my research. First of all, I would like to thank Marjolijn Goorden. You have been closest to me for the past seven months by meeting with me on a weekly basis. I think I never met a person who is more enthusiastic about this subject than you. I really enjoyed our discussions and you provided me with many useful insights on which I could build my work. Secondly, I would like to thank Prof. Dominic von Terzi. As both my supervisor and chair of the committee, you guided me through the process. We met on a monthly basis to discuss my progress. Your critical view, as well as your expertise, have provided me with many good ideas and made me think more critically myself. At last, I would like to thank Prof. Ad van Wijk. Although we have never met in person up until my defense, I am excited and thankful for you reading and evaluating my work.

Lucas Bouma
Amsterdam, 2023

Abstract

Hydrogen is emerging as a promising energy carrier that can potentially solve the challenges like long-term storage and intermittent power supply associated with a 100%-renewable economy. Moreover, hydrogen can be used in industry sectors such as steel manufacturing and aviation, which struggle with carbon abatement. To increase the supply of green hydrogen, the European Union aims to have at least 40 GW of renewable energy sources connected to electrolysis by 2030. In light of this ambition, the Dutch government recently issued an offshore wind tender that should incorporate 500 MW of offshore electrolysis capacity.

A hybrid farm with offshore electrolysis contains both a hydrogen pipeline and an electricity cable as the export connection to shore. Appropriately sizing these connections to ensure financial feasibility becomes a design challenge for wind farm developers as the technology is still maturing.

This study considers a case study of an offshore hybrid wind farm situated in the European North Sea, connected to the Dutch energy infrastructure. A Python model was developed to simulate the sales and production of hydrogen and electricity on an hourly time scale. The simulation was executed by using historical data for electricity pricing and assuming a perfect forecast from a developer's perspective. The objective function was to determine the optimal ratio between electrolyzer and electricity cable capacity (EC ratio) to maximize the net present value (NPV) of such a project. A sensitivity analysis on various system parameters was performed, and multiple scenarios reflecting potential future circumstances were simulated.

The study revealed that both oversizing and downsizing the total export capacity was not beneficial. Instead, the optimal EC ratio followed a linear trend, where the sum of connection capacities equaled the total farm capacity. The hydrogen price, electricity price, and nominal efficiency of the electrolyzer were identified as key factors influencing the optimal EC ratio.

This research establishes optimal EC ratios for a range of hydrogen prices spanning from €3/kg to €8/kg based on different scenarios. For each scenario, different electricity prices and electrolyzer specifications were defined. The findings indicate that including an electrolyzer in the design is not economically viable for hydrogen prices below €4.00/kg. Conversely, an electrolyzer-dominated system becomes favorable in each scenario when the hydrogen price exceeds €7.50/kg. For prices in between, optimal EC ratios resembling hybrid systems were identified depending on the other key parameters defined by the scenarios.

Contents

List of Figures

List of Tables

Acronyms

AC	Alternating Current
AEM	Anion Exchange Membrane
AWE	Alkaline Water Electrolysis
ASTM	American Society for Testing and Materials
BEV	Battery-powered Electric Vehicles
BOP	Balance Of Plant
CAPEX	Capital Expenditures
DC	Direct Current
EC	Electrolyzer/Cable
EDI	Electrodeionization
EHB	European Hydrogen Backbone
ENTSOG	European Network of Transmission System Operators for Gas
ERD	Energy Recovery Device
EU	European Union
FCEV	Fuel Cell-powered Electric Vehicles
HPL	Hydrogen Pipeline
HPP	High Pressure Pump
HVAC	High Voltage Alternating Current
HVDC	High Voltage Direct Current
IEA	International Energy Agency
IRR	Internal Rate of Return
LCOH	Levelised Cost Of Hydrogen
LHV	Lower Heating Value
MSF	Multi Stage Flash
NPV	Net Present Value
OPEX	Operating Expenses
P2G	Power-to-Gas
P2M	Power-to-Mobility

P2P	Power-to-Power
PEM	Proton Exchange Membrane
PI	Profitability Index
RO	Reverse Osmosis
SEC	Specific Energy Consumption
SMR	Steam-Methane Reforming
SOE	Solid Oxide Electrolyzer
STP	Standard Temperature and Pressure
SWRO	Sea Water Reverse Osmosis
TDS	Total Dissolved Solids
TSO	Transmission System Operator
UPW	Ultra Pure Water

Nomenclature

Greek Symbols

α	Function parameter
ϵ	Pipe surface roughness
η	Efficiency
λ	Friction factor
μ	Dynamic viscosity
Π	Compression ratio
π	Osmotic pressure
ρ	Gravimetric density
σ	Electrical conductivity

Other Symbols

C	Capital expenditure
D	Diameter
E	Energy consumption
G	Specific gravity
g	Gravitational constant
h	Height
k	Gas isentropic coefficient
L	Lenght
M	Molar weight
O	Operating expenses
P	Power
p	Pressure
Q	Flow rate
R	Gas constant
r	Discount rate
S	Capacity
T	Temperature

t	Time
u	Flow velocity
W	Revenue
w	Price
X	Amount
Y	Specific water intake
Z	Compressibility factor
z	Water Depth

Subscripts

ann	Annual
avg	Average
b	Base
cab	Cable
$comp$	Compressor
$curt$	curtailment
dly	Daily
e	Electricity
edi	Electrodeionization
$elec$	Electrolyzer
f	Feed
$farm$	Wind farm
fp	Feed pump
hy	Hydrogen
in	Inlet
$isen$	Isentropic
jck	Jacket
$load$	load
max	Maximum
min	Minimum
nd	Net driving
nom	Nominal
out	Outlet
per	Permeate
$plat$	Platform
ro	Reverse osmosis

sw	Seawater
tps	Topside
trans	Transformer
turb	Turbine
upt	Grid uptake
wt	Water treatment

Chapter 1

Introduction

The focus of this Master of Science thesis is on the design and operation of a hybrid wind farm using offshore electrolysis. In Section 1.1, background information about offshore wind and the significance of hydrogen to the energy mix are outlined. The relevance of the report's subject is provided in Section 1.2. In Section 1.3, the objective and scope of this research are addressed, and Section 1.4 elaborates on the methodology used to answer the research question. And finally, in Section 1.5, the outline of the report is described.

1.1 Background

In recent years, the world has witnessed a growing demand for carbon-free and sustainable energy sources to mitigate global warming and reduce society's dependence on fossil fuels. To meet this demand, significant renewable capacity has been added to the energy mix over the last decade. To pursue the ambition of limiting global warming to no more than two degrees Celsius, as per the Paris Agreement, institutions and organizations set goals and benchmarks to keep track of their performance. Among the renewable technologies in Europe, offshore wind power, in particular, has great potential to be scaled up. As indicated by Figure 1.1, the commissioning of offshore wind farms in Europe has accelerated since 2015 and the total installed capacity added up to 25 GW in 2020 [1]. Moreover, the ambition of the European Commission is to expand this capacity towards 60 GW and 300 GW by 2030 and 2050, respectively [2].

Although the growth of wind power capacity contributes to the mitigation of carbon emissions, it also poses challenges: Due to the intermittency and seasonal dependency of wind power, (i) backup power generation for peak loads and (ii) long-term storage are necessary to achieve a 100% renewable future. Additionally, (iii) the installed wind power capacity currently overloads the electricity grid during peak generation hours, resulting in energy curtailment [3]. This last phenomenon is commonly referred to as grid congestion and is a globally acknowledged issue. The Dutch research organization TNO foresees a power curtailment of 13% due to grid congestion by offshore wind energy alone in the Netherlands by 2030 if the electrification of its society does not accelerate [4].

Hydrogen (H_2) is considered one of the possible solutions to overcome these challenges. Hydrogen gas can be produced with electrolysis by passing an electrical current through water to split it into oxygen and hydrogen. Given that the energy required for electrolysis is generated from renewable power sources, it is possible to produce hydrogen – often referred to as "green hydrogen" – without emitting greenhouse gases. Compared to other fuels, hydrogen gas has the highest gravimetric energy density of 120 MJ/kg, and can be used for many applications:

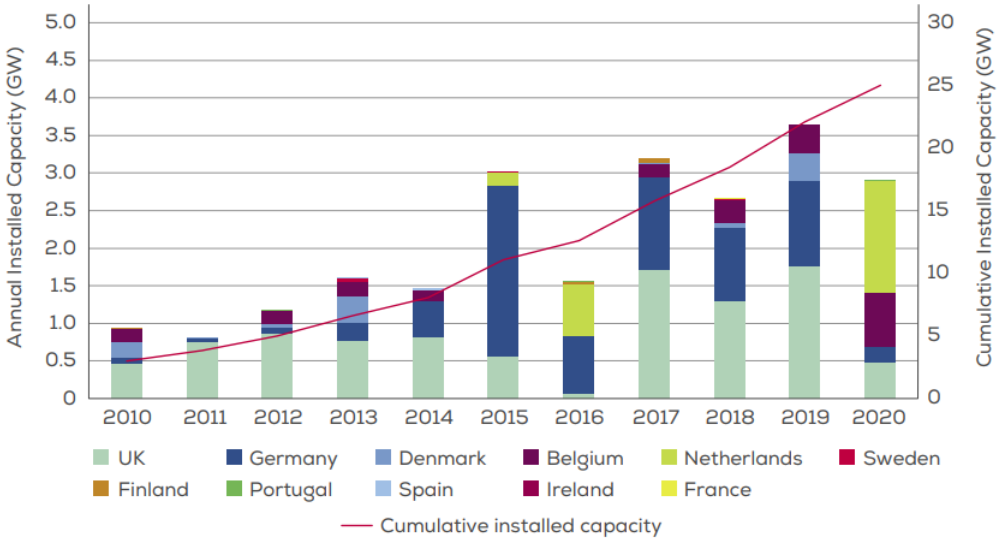

Figure 1.1: Annual installed offshore wind capacity in Europe. The line represents the cumulative installed capacity [1].

Energy storage

One of the main benefits of hydrogen is that it can be stored effectively in the form of gas. Transferring energy across seasons by means of long-term storage is a major challenge of a 100% renewable society. The current battery technology is inadequate for long-term storage due to self-discharge and can therefore only be implemented for short-term and high-cycling storage (day-night schedule). Additionally, large-scale seasonal battery storage would require a vast amount of rare earth materials, making hydrogen an option that is more economically viable. Gaseous storage of hydrogen can be divided into two groups: (i) In fabricated metal tanks and (ii) in underground structures like aquifers and salt caverns. Although hydrogen demonstrates the highest energy density in terms of weight, it is also the fuel with the lowest volumentric energy density. Since the volumetric energy density of hydrogen at standard temperature and pressure (STP, 15°C, 1 bar) is a mere 0.09 kg/m^3, it is usually stored under compression. On a large scale, pressures can reach up to 100 bar and 200 bar for tanks and underground structures, respectively [5].

Hydrogen can also be stored as a liquid or chemically attached to other substances (metal- and chemical hydrides). Both liquefying and bonding hydrogen are established concepts to increase its volumetric energy density, however, both methods require a large amount of energy for them to work as a storage medium. At atmospheric pressure, the boiling point of hydrogen lies at a temperature of $-253°C$, making its liquefaction a very energy-intensive process for which expensive and well-insulated tanks are required [5]. Liquid hydrogen has a volumetric energy density of 70 kg/m^3. Magnesium hydride (MgH_2) and aluminum hydride (AlH_3) are examples of metal hydrides, while examples of chemical hydrides are methanol (CH_3OH) and ammonia (NH_3). Ammonia, in particular, has a very high hydrogen content in its liquid state of 123 kg/m^3 [5]. The challenge with hydrides is the high energy that is required for either the hydrogenation or the dehydrogenation of the chemical compound. Although these methods of storing hydrogen are still maturing, they are currently not applied on a large scale due to their considerable energy consumption [6].

Generating electricity

Hydrogen can be used to produce electricity by using a fuel cell. There are several types of fuel cells, with efficiencies ranging from 40% to 60%. Converting hydrogen to electricity has two main applications: transportation (Power-to-Mobility (P2M)) and grid applications (Power-to-Power (P2P)).

The use of hydrogen as fuel in the transportation sector is a proven concept. However, Fuel Cell-powered Electric Vehicles (FCEV) need to be compared to Battery-powered Electric Vehicles (BEV)) to address the perspective of hydrogen as fuel. For BEV's, the electricity generated by renewable sources can be used directly, avoiding the conversion losses of the electrolyzer and fuel cell. Accounting for these conversion losses, BEV's are theoretically around 50% more efficient compared to FCEV's. However, since FCEV's typically have a longer range and shorter refuel times, long-haul trucks and buses, as well as other vehicles requiring substantial energy reserves and rapid refueling, may benefit from the use of hydrogen in the transportation sector [7].

Due to their fast response time, fuel cells are suitable for grid regulation applications and can serve as dispatchable power plants because of their flexibility. Due to the intermittency of renewables, adding flexibility to the grid is crucial for peak demand, frequency control, mitigation of congestion, and reducing negative price occurrences [8].

Power-to-Gas

Another application of hydrogen would be to use it in its gaseous form, denoted as Power-to-Gas (P2G). Hydrogen gas can either be used without further modifications or it can be converted into methane. Methane can be synthesized from hydrogen in a process called methanation. The basic principle is to combine hydrogen (H_2) with carbon dioxide (CO_2) in the presence of a catalyst, such as nickel or cobalt, to form methane (CH_4) and water (H_2O) via the exothermic reaction:

$$4\,H_2(g) + CO_2(g) \longrightarrow CH_4(g) + 2\,H_2O(g)$$

Applying methanation would be a carbon-neutral way to replace natural gas because the synthesized methane may be injected directly into natural gas infrastructure. However, due to its high flammability, hydrogen gas can also be blended with natural gas up to a percentage of 20% without significant changes in utilization [9]. Many P2G projects already exist around the world for both hydrogen gas as an end product and methanation [10].

Hydrogen as end product

Arguably the best and most obvious way to use hydrogen is as an end product in the existing industry. In the chemical industry, hydrogen is already used intensively to produce ammonia and methanol and in other refineries. The estimated global hydrogen demand in 2021 was 94.3 Mt [11]. The vast majority was produced via the CO2-emitting Steam-Methane Reforming (SMR) method, which uses natural gas or gasoline to create hydrogen. Ammonia production accounts for about 36% of this total demand, methanol production for about 15%, and refining for 42%. Compared to 1975, the industrial demand for hydrogen has more than tripled and it is expected to rise further [12]. Particularly for the industrial sectors which struggle with carbon abatement, such as steel manufacturing and aviation, hydrogen could serve as a green alternative.

1.2 Motivation

As described in Section 1.1, hydrogen is considered vital within the energy transition due to its many applications. As industries are striving for sustainability, the demand for green hydrogen will increase in the coming years. The European Network of Transmission System Operators for Gas (ENTSOG) expects that the demand for hydrogen (non-energy use included) will account for around 20% of the total energy consumption of the European Union (EU) by 2050 [13]. To meet this demand with a zero-carbon footprint, the European Commission plans to install considerable electrolyzer capacity for producing green hydrogen. Their offshore strategy report states that they aim to have at least 40 GW of renewables connected to electrolysis by 2030 [2].

1.2.1 Hybrid wind farms

Currently, large-scale electrolysis is only performed onshore. High-capacity electrolyzers will be installed in coastal regions and connected to offshore wind farms. Farms that produce both electricity and hydrogen are denoted as hybrid wind farms. A schematic diagram of the concept of a hybrid wind farm with onshore electrolysis is presented in Figure 1.2. By adding an electrolyzer to the design, the flexibility of the wind park increases substantially as the generated power can be sold in either the form of electricity or hydrogen. Consequently, in the event of grid congestion, excess energy can be directed toward the electrolyzer instead of being curtailed. From the perspective of wind farm developers, producing hydrogen during periods of low electricity prices could be a profitable strategy. A hydrogen fuel cell could also participate in the ancillary service market, although this has not yet been quantified without subsidies [14].

In addition to onshore electrolysis, growing interest is observed in offshore hydrogen production. Presently, there are several ongoing initiatives that are contemplating the adoption of offshore electrolysis. AquaVentus is a German project that aims to build a large-scale electrolysis plant in the North Sea, along with a network of pipelines to transport the hydrogen to shore. PosHYdon is a Dutch venture that involves retrofitting an offshore oil and gas platform with a green hydrogen production facility. Another project, although still in its early stages, is the North Sea Wind Power Hub, an initiative led by the Dutch-German Transmission System Operator (TSO) TenneT and the Danish TSO Energinet. The project envisions the development of one or more artificial islands located in the North Sea, which will serve as a central hub for the distribution of renewable energy across Europe. They are aiming to incorporate offshore electrolysis into their 100 GW renewable energy system. As stated in their techno-economic feasibility report, they predict that offshore-produced hydrogen can be cost-competitive with onshore-produced hydrogen [15].

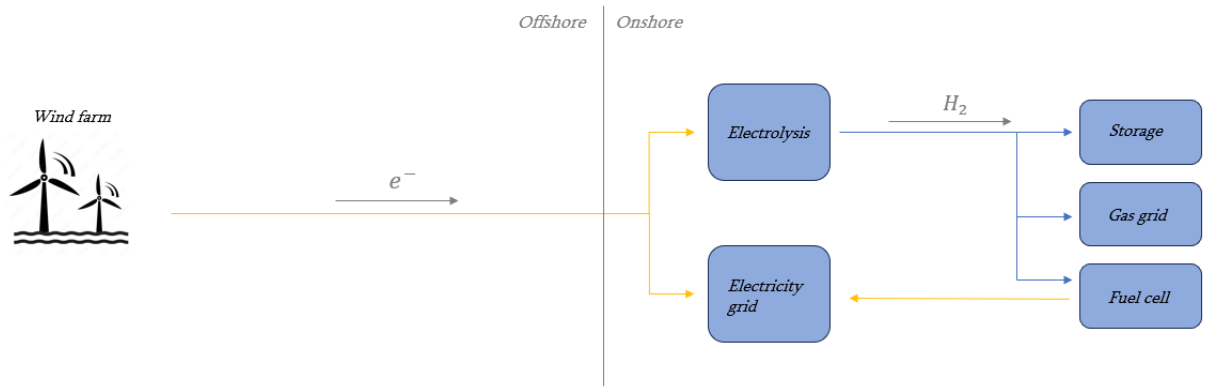

Figure 1.2: Overview of a hybrid wind farm using onshore electrolysis.

1.2.2 Incentives for offshore electrolysis

There are several reasons to explain the increasing interest of wind farm developers in offshore electrolysis. Although the offshore concept will probably cause higher system costs, placing the electrolyzer at sea holds several potential benefits over onshore electrolysis. Among these potential benefits are:

1. Hydrogen pipelines demonstrate superior economic efficiency and reduced energy losses compared to electricity cables. According to the literature, pipelines exhibit reduced installation and maintenance costs compared to High Voltage Direct Current (HVDC) cables [16, 17] and transportation losses for high-pressure gas pipes are substantially lower than those for HVDC cables (0.05%/1000 km and 3.5%/1000 km, respectively) [18]. Additionally, the old gas infrastructure could be used for hydrogen purposes after some modifications [19]. An in-depth analysis of both transportation mechanisms is given in Chapter 2.

2. By installing the electrolyzers offshore, high expenses associated with land-based systems may be avoided. Onshore electrolysis plants are preferably installed in strategically located coastal areas near ports and industrial sites. Consequently, this leads to the creation of certain hot spots where the land-use costs become expensive. At sea, one could build the electrolyzer near the wind farm where sufficient space is available. However, a platform will be necessary to facilitate the offshore system, which will be a costly alternative itself.

3. Compared to onshore electrolysis, offshore electrolysis demonstrates superior scalability due to the vast open space at sea [2]. On land, the availability of space is limited due to restrictions imposed by sites such as residential areas and protected nature reserves, which prohibit the construction of the electrolyzer plant. Considering the aforementioned ambition of the EU to realize 40 GW of electrolyzer capacity, scalability is an important consideration.

4. The European North Sea possesses many salt caverns suitable for storing hydrogen gas. The underground storage in this area allows for a large-scale (TWh) and cost-effective hydrogen storage [20]. Since most of the available salt caverns are offshore, producing hydrogen at sea would offer a more efficient solution as the transportation distance between production and storage would decrease.

An overview of a hybrid wind farm with offshore electrolysis is given in Figure 1.3. Unlike hybrid wind farms with onshore electrolysis, which solely have a single energy connection to the shore, offshore electrolysis systems can transport the energy in two forms: hydrogen gas

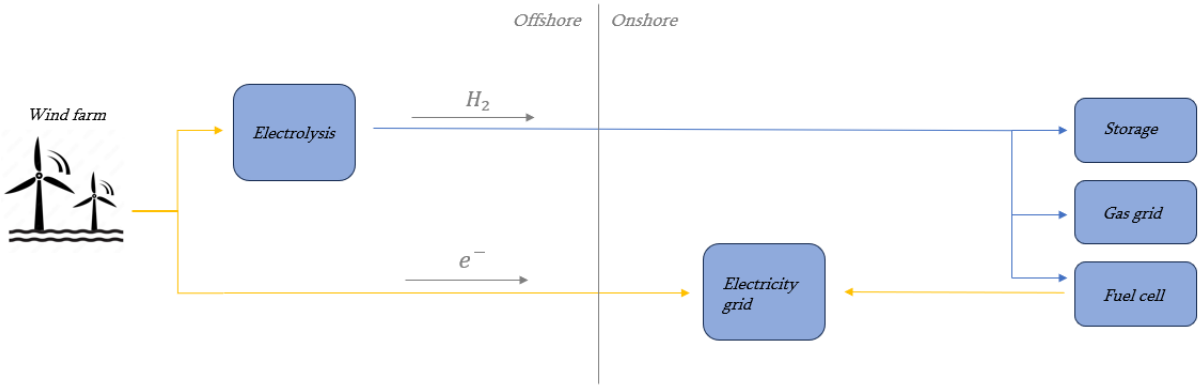

Figure 1.3: Overview of a hybrid wind farm using offshore electrolysis.

and electricity. However, this system layout poses a design challenge for wind farm developers: They must determine the optimal sizing of connections to ensure the economic viability of the project. In other words, they need to estimate the optimal combination of electricity cable capacity and electrolyzer capacity in order to improve the business case. To be able to derive such an estimate, developers need to have insight into what proportion of generated power they should allocate to the electricity grid and what proportion should be directed towards the electrolyzer for hydrogen production.

1.3 Objective and scope

The objective of this research is to provide an energy carrier allocation strategy for a hybrid wind farm with offshore electrolysis. The optimization of the allocation strategy will be from a developer's perspective and will therefore focus on maximizing the profitability of the system.

1.3.1 Financial metrics

There are several financial metrics to assess the profitability of a project, including the Net Present Value (NPV), internal Internal Rate of Return (IRR), and the Profitability Index (PI).

- **NPV** represents the present value of a project and is calculated by adding future cash inflows and outflows to the initial investment. The NPV accounts for the time value of money by discounting future cash flows to their present value. Being an absolute value, it is considered a convenient metric to compare different projects. A positive NPV indicates that the project will generate value, while a negative NPV suggests that value will be lost.
- **IRR** is defined as the discount rate that makes the NPV of a project zero. In other words, it is the rate at which the present value of cash flows equals the initial investment. If a project has an IRR that exceeds the required rate of return, it is considered worthy of investing in.
- **PI** is a financial metric that indicates the profitability of a project. It measures the ratio between the sum of the present value of the cash flows and the initial investment. In principle, it normalizes the NPV for the initial investment and can thus be interpreted as the return on investment rather than an absolute value. A PI greater than one indicates that a project is expected to generate positive returns, while a PI less than one suggests negative returns.

All three financial metrics are considered valid and are used in practice. In this study, however, the focus lies on NPV. Although NPV can be misleading as it does not present any insight into the return on an investment [21], it is often considered a more robust metric than the other two by the literature [22, 23]. Also, in consultation with Eneco, in the case where a company has a higher investment in a project, yet has the ability to generate a greater value over the same time period (= higher NPV), it will opt for that alternative.

However, it should be noted that it is important to consider the risk of a project as well. If a project requires a higher investment and consequently is exposed to a higher risk, the corresponding discount rate increases, which negatively influences the NPV. For the purposes of this study, it was assumed that the degree of risk associated with each investment was identical, thus maintaining a consistent discount rate across all scenarios.

1.3.2 Research question

In this research, the design of a hybrid wind farm with offshore electrolysis will be addressed. The main focus will be on the optimal energy carrier allocation strategy for a hybrid wind farm from a developer's perspective. The research question is formulated as:

What is the optimal ratio between electricity and hydrogen connections to maximize the net present value of a wind farm with offshore electrolysis?

To approach the research question, the following sub-questions need to be answered:

1. *What are the main components of a hybrid wind farm with offshore electrolysis, and what key parameters need to be obtained for modeling the system?*
2. *What parameters influence the system the most, and how does the system respond to variations in these parameters?*

This research will consider a hybrid wind farm in the Dutch European North Sea, which is connected to the energy infrastructure of The Netherlands. The techno-economic optimization of this case study will be from a developer's perspective with the aim of maximizing the NPV. Both the produced hydrogen and electricity will be sold directly to market prices; Storing the hydrogen and electricity for the purpose of future sales at higher prices will be out of the scope of this research. Furthermore, centralized hydrogen production will be assumed in this report. Although decentralized hydrogen production will be briefly addressed in Chapter 2, a detailed comparison between the two will be left out.

1.4 Methodology

In order to answer the research question, a model was built in Python to derive the NPV of a project for certain parameters. To be able to calculate the NPV, it is necessary to obtain the investment costs and future cash flows of the project.

In the initial stages of this research, an extensive literature review was conducted to gain a comprehensive understanding of the layout and configuration of a hybrid wind farm. It is imperative to acquire insights into the main components of the system to effectively model and simulate its operation. Various available technologies were studied, and key parameters regarding these components were obtained. The accuracy of the model relies on the precision of these parameters. Therefore, a wide range of sources, including literature and industry references, were consulted to ensure reliable data for parameter estimation.

Once the outlook of the system was established, it was translated into the Python model. Based on wind generation and electricity pricing, the model simulates the system every hour for a year. The model must account for the investment and operational costs of the components as well as the associated energy losses.

From a developer's perspective, energy pricing forecasts are used to operate the electrolyzer in the best way economically. Every hour of the day, new forecasts come in for the subsequent hour and the electrolyzer is operated accordingly. In this research, the model assumes a perfect forecast. This means that based on historical data, the model runs the electrolyzer in the best way economically by searching for the most profitable combination of hydrogen and electricity sales. Because developers also operate their electrolyzers based on an hourly schedule, the model strategy was considered reasonably reflecting reality for the purpose of this study.

The model assumes that the simulated year is representative of the rest of the system's lifetime so that an NPV can be derived. The calculated NPV will be determined for a set of input parameters. By running the simulation for a range of different parameter values, the optimum configuration can be established.

1.5 Report outline

The structure of this research is outlined as follows:

Chapter 2 provides a detailed overview of the key components that constitute a hybrid wind farm. The objective of Chapter 2 is to offer a comprehensive understanding of the functioning of these diverse system components and to explore the available technologies within this context.

Chapter 3 presents an incremental account of the modeling process. Each system component is explained in terms of its implementation in the model and what specific values were assumed. The processes and parameters are described from both a technical and economic perspective. Towards the end of the chapter, an overview of the system and the strategy for executing the simulation are addressed.

In Chapter 4, the model is verified and the simulation results are presented. An analysis of a base case scenario will be discussed, followed by a sensitivity analysis of several system parameters. At the end of this chapter, the system is evaluated for different scenarios.

In Chapter 5, conclusions are drawn from the results. Several key limitations of this study and recommendations for further research are also described in this chapter.

Chapter 2

System components

In order to effectively build a model of the system, understanding the system components is imperative. This chapter aims to provide a comprehensive literature study on the main elements of a hybrid wind farm and has the following structure: In Section 2.1, two offshore electrolysis configurations are explained, Section 2.2 captures the water treatment of seawater, and an overview of the electrolyzer technologies is found in Section 2.3. Section 2.4 covers the transmission of hydrogen gas and electricity, and finally, in Section 2.5, the compression of hydrogen is addressed.

2.1 Offshore electrolysis

Offshore electrolysis has yet to become a mature technology. Although several small pilots across the world already exist, large-scale systems using the offshore concept are currently not in operation. This section focuses on two main offshore electrolysis configurations that are proposed in the literature: Decentralized (in-turbine) and centralized. An in-depth analysis of the two concepts is beyond the scope of this research, and further in this report, centralized hydrogen production is assumed. The centralized concept entails the necessity of an offshore platform, which is also addressed in this section.

2.1.1 Offshore electrolysis configurations

Decentralized (in-turbine)

Figure 2.1a illustrates the decentralized offshore electrolysis concept. In the decentralized approach, every wind turbine is equipped with a desalinator and an electrolyzer, which can be positioned either adjacent to the turbine or integrated within the turbine itself. The produced hydrogen is transported through pipelines of smaller dimensions to a central platform, where it is gathered, compressed, and subsequently transported to shore via a larger pipeline. The feasibility of the decentralized approach is enhanced as the capacity of individual wind turbines increases: With the installation of more powerful turbines, higher-capacity electrolyzers can be accommodated, and the system begins to benefit from economies of scale [7]. Moreover, the design of the wind turbine could be altered to make it more suitable for hydrogen production [24], and a smaller, less expensive central platform is required compared to the centralized concept. However, when specifying a wind turbine to the needs of the electrolyzer, the rotor design of the wind turbines might change, and these alterations, in turn, have implications for the layout of the wind farm, particularly in terms of turbine placement in relation to wake effects.

Centralized

The centralized concept of offshore electrolysis is presented in Figure 2.1b. In this approach, the power generated by the wind turbines is transported as electricity via inter-array cables to a centralized platform. This offshore platform serves as the hub for the components of the system, including electronic equipment, electrolyzers, desalination units, and compressors. As a result, the centralized configuration demands a larger and more expensive platform compared to the decentralized concept. However, it offers the advantage of a simplified design since there is no need for the installation of small dimension pipelines from each individual wind turbine. By eliminating the requirement for these pipelines, together with the electrolyzer equipment being in one central place, the centralized configuration streamlines the infrastructure, reducing complexity and potentially minimizing maintenance and operational challenges.

In a study by Singlitico et al. [25], they made a comparison between the centralized and decentralized concepts for offshore electrolysis. They compared the different configurations for two scenarios; (i) electricity-driven, where priority is given to the electricity demand and only excess energy is used for producing hydrogen, and (ii) hydrogen-driven, where priority is given to the electrolyzer and only the remaining electricity is fed into the grid. In both scenarios, the researchers discovered that the centralized concept exhibited a lower Levelised Cost Of Hydrogen (LCOH). However, it is important to note that their study focused on simulating a 12 GW artificial island with 4 GW of electrolysis power, and they did not optimize the turbine and farm layout specifically for the decentralized concept. Therefore it is unclear whether the conclusions drawn by Singlitico et al. would be the same if projects of smaller scale are considered, which is the case in this thesis.

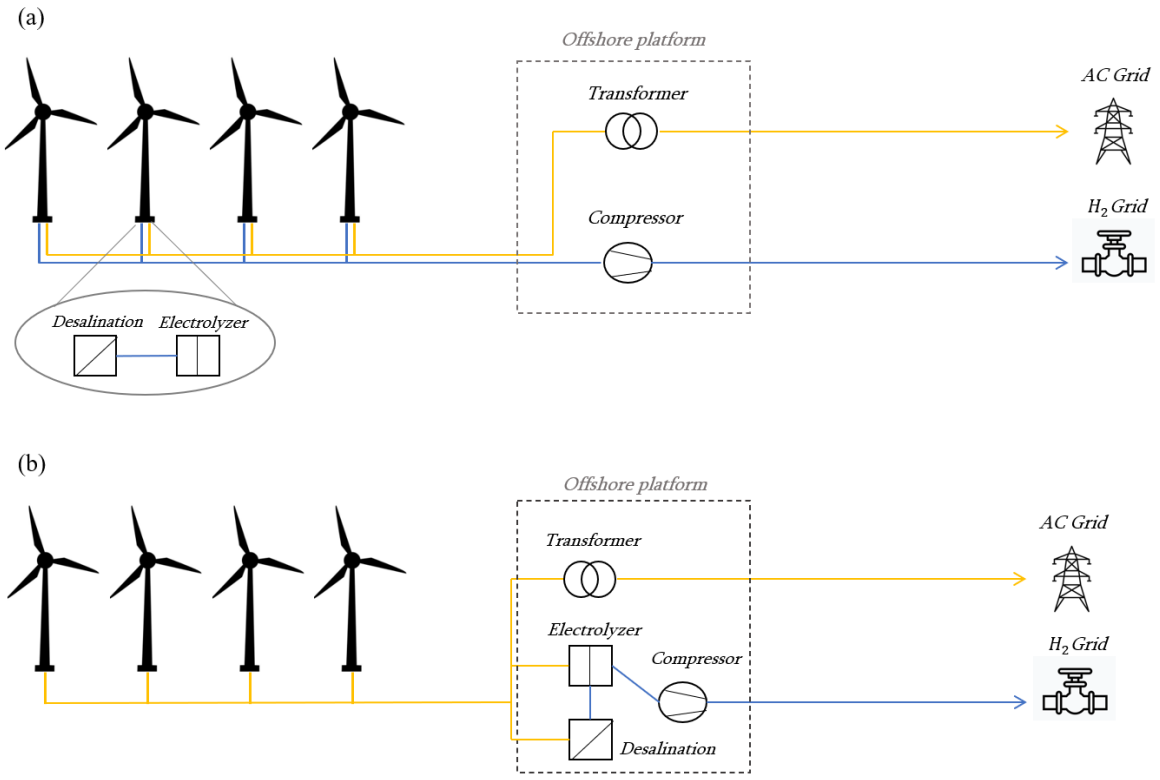

Figure 2.1: Two hybrid wind farm concepts proposed by the literature. With (a) representing the 'in-turbine' configuration and (b) the 'centralized' concept.

2.1.2 Offshore platform

An offshore platform comprises two main components: the support structure and the topside. A schematic representation of an offshore platform is presented in Figure 2.2. The topside serves as the primary area for accommodating the electrolyzer and other Balance Of Plant (BOP) equipment, such as power electronics, compressor stations, and desalination units. Moreover, the topside must also include provisions for a helicopter deck and accommodation facilities. The inclusion of electrolyzer equipment generally necessitates the construction of larger and heavier topsides in comparison to most of the existing oil platforms or electrical substations. The potential re-use of a platform depends on its previous application, where production platforms possess a higher potential for reuse due to their greater carrying capacity. Given that offshore platforms specifically designed for large-scale electrolysis have not been constructed previously, the design and weight of these topsides must be estimated. In a technical report conducted by DNVGL [26], they performed such an estimation and projected that a topside capable of accommodating 1000 MW of electrolysis would have an estimated volume of 193,550 m^3 and a weight of approximately 32,652 tonnes. The topside weight estimated by DNVGL included the electrolyzer and its BOP equipment.

The support structure commonly employed for offshore platforms is the jacket construction. This structure is typically utilized within a depth range spanning from 10 meters to 200 meters and is often secured into the seabed [27]. A jacket construction is composed of a steel framework designed to withstand the demanding environmental conditions experienced offshore, and it is considered capable to support the mass of a topside with electrolyzer equipment [26]. Although other support structures for offshore platforms exist, a jacket support structure has been assumed in this study, which is in line with [26, 28]. Details on the platform topside and support structure are found in Appendix A.

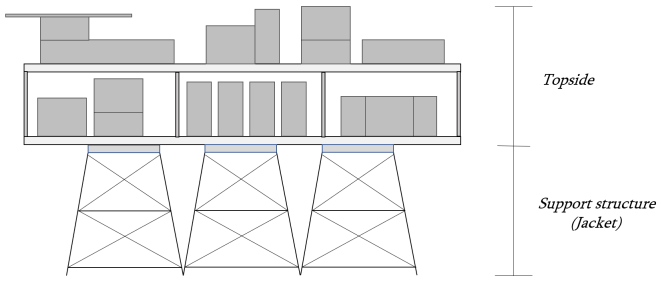

Figure 2.2: Schematic representation of an offshore platform with a jacket support structure.

2.2 Water treatment system

To produce hydrogen gas from electrolysis, the electrolyzer requires highly demineralized water with a resistivity of $18M\Omega$ as feedstock [29]. Although using seawater directly for the purpose of electrolysis is being investigated [30, 31], it may take years for it to be commercially developed. Some even claim that R&D resources could be better spent on other fields of development rather than on direct seawater electrolysis research since the benefits would only be marginal [31]. For these reasons, only demineralized water as feedstock is considered in this study. This section provides an outlook on reverse osmosis combined with electro-deionization as a seawater demineralization system.

2.2.1 Reverse osmosis

The desalination of water can be divided into two main categories: thermal-based and membrane-based processes. Multi Stage Flash (MSF) and Reverse Osmosis (RO) are the dominant technologies within the thermal-based and membrane-based processes, respectively. Due to its energy-intensive character, MSF is hardly used outside the oil-rich Middle East and is therefore not considered a viable technology to implement in the European North Sea. For the purpose of this thesis, only RO will be considered for the system design.

RO has been commercially available since the late 1960s and currently accounts for more than 60% of the world's installed desalination capacity [32]. Osmosis is a naturally occurring process in which a low-concentration liquid diffuses into a high-concentration liquid due to the difference in osmotic pressure. In RO, this process is reversed by pressurizing the fluid with a higher concentration (salt water). The saline seawater is pressurized against a semi-permeable polymer membrane which only allows small particles, like water molecules, to pass through while rejecting the majority of salts. Current thin-film polymer membranes are highly effective and are capable of removing up to 99.8% of the salts [33]. The extent to which the feed water is pressurized against the membrane can be explained by the following formula:

$$p_{nd} = \Delta\overline{p} - \Delta\overline{\pi} \tag{2.1}$$

Where p_{nd} is the net driving pressure, $\Delta\overline{p}$ is the average differential pressure across the membrane, and $\Delta\overline{\pi}$ is the average difference in osmotic pressure across the membrane. $\Delta\overline{\pi}$ depends on the salinity of the feedwater, which is often measured in total Total Dissolved Solids (TDS), and the quality of the produced water (permeate). $\Delta\overline{p}$ represents the pressure difference between the feed stream and the permeate. p_{nd} is then the pressure that is exerted on the membrane. A high net driving pressure results in a high recovery (the percentage of the feed that comes out as desalinated water). As more purified water is produced by systems with a high recovery ratio, the feedwater is generally pressurized to high pressures. However, by increasing the net driving pressure, more unwanted dissolved particles are able to permeate the membrane structure and thereby decreasing the quality of the permeate. Due to this, the recovery of desalination systems highly depends on the TDS content of the feed water. For large-scale Sea Water Reverse Osmosis (SWRO), where the TDS content of seawater lies between 30,000 - 40,0000 mg/L, recoveries of around 45% are customary [34]. The TDS content of the RO permeate is found within the range of 300-500 mg/L.

2.2.2 Electrodeionization

The RO permeate quality does not yet meet the standard for the feed water to the electrolyzer. An additional step in the water purification process is therefore needed to Ultra Pure Water (UPW) with a resistivity of $18M\Omega$. RO is often coupled with Electrodeionization (EDI) to further demineralize the RO permeate [35]. EDI is an electrically driven process that combines ion exchange and electrodialysis to remove positively charged cations and negatively charged anions from the RO permeate. The EDI cell consists of a few compartments which are separated by selective ion-exchange membranes. The selective ion-exchange membranes either allow cations or anions to pass through while rejecting the other and are alternately placed across the EDI cell. A direct electrical current is applied across ion exchange membranes so that an electrical field is created. Due to this electrical field, positively and negatively charged ions in the water are attracted to opposite directions and removed from the feed water.

Since the feed water to the EDI has a low conductivity, the movement of the ions within the water is impaired. Ion-exchange resins are placed in between the membranes to promote the diffusion of the ions. Since the ion mobility decreases when the water conductivity is low, a strong electric field is needed for the deionization. The energy consumption of EDI thus depends on the quality of the feed and the permeate. EDI has been proven to be an effective method for deionizing water with an ion rejection of up to 99.8% and a recovery rate in the range of 85 - 95% [36].

2.2.3 System overview

Figure 2.3 shows an overview of the proposed water treatment system. The saline feed water is pumped upwards by a feed pump and sent to the pre-treatment facility. During the pre-treatment, large particles, sediment, or other organic substances that can cause excessive membrane fouling in the RO assembly are removed from the feed water. Generally, micro-filtration is used during the pre-treatment step. After the pre-treatment, the water stream is pressurized by a High Pressure Pump (HPP) for the RO process. The HPP accounts for the vast majority of the energy consumption of the desalination process. To recover some of this energy, the pressurized reject stream of the RO membranes is sent to an Energy Recovery Device (ERD). The RO permeate is treated with UV light to oxidize any remaining organic compounds. The ionized organic compounds are subsequently removed by the EDI unit to obtain UPW with a resistivity of 18MΩ.

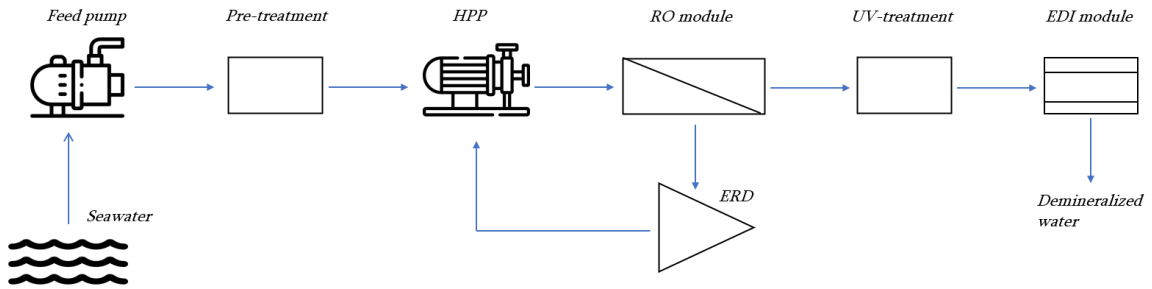

Figure 2.3: Schematic representation of the proposed water treatment system.

2.3 Electrolyzer

The electrolyzer is at the heart of the hydrogen production facility. Using green electricity from the wind farm, the electrolyzer splits pure water into hydrogen and oxygen. Four different types of electrolyzers are described in the literature. This section aims to give a comprehensive overview of these electrolyzer technologies. Three out of the four electrolyzer types have reached a more advanced stage of development, and as a result, they will be discussed in greater detail. The fourth electrolyzer type is still in its early stages of development and will only be briefly addressed.

2.3.1 Alkaline water electrolyzer

Among the current electrolyzer technologies, the Alkaline Water Electrolysis (AWE) is the one that has been developed the most and is already commercially available on MW-scale [37]. AWE uses an aqueous electrolyte with usually 20-40% sodium hydroxide (NaOH) or potassium hydroxide (KOH) [38]. Because these hydroxide-based electrolytes are used, an alkaline environment prevails with a pH value of 13 to 14. The high pH conditions help to facilitate the electrochemical reaction and maintain the stability of the electrolyte. Two electrodes, which are generally nickel-based, are submerged in the liquid electrolyte and separated by a diaphragm which only allows the hydroxide ions to pass through. An overview of the process in an AWE cell is illustrated in Figure 2.4.

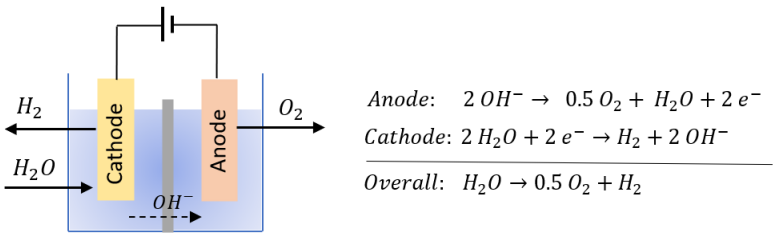

Figure 2.4: The AWE process with the half-reactions occurring at the electrodes.

Because AWE does not employ rare or expensive materials, its capital costs are relatively low. Together with conversion efficiencies reaching up to 80%, AWE is considered the most cost-effective technology to produce hydrogen compared to other electrolyzer types, which is regarded as its key benefit [37, 38]. The electrolysis process occurs at relatively low pressure (1-15 bar) and near ambient temperatures (50-80°C).

The AWE also has some limitations that need to be considered. One of the issues is that the diaphragms used are not perfectly impermeable to the formed hydrogen and oxygen gases. To prevent chemical diffusion of the gases through the diaphragm, a minimal current density is required at all times to maintain an electric potential across the cell. This results in a minimum load operating constraint of around 15% of its nominal capacity [39]. However, if the current density gets too high, the generated gas bubbles can form a non-conductive layer over the electrodes. This phenomenon is known as *screening* and deteriorates the electrolyzer cell efficiency. Therefore, the current density of an AWE is generally limited to a few hundred mA/cm^2 [37]. The current density limitation, together with the liquid electrolyte, causes robust and heavy designs of large-scale AWE installations. Therefore, large and expensive offshore platforms are required to facilitate this technology at sea.

2.3.2 Proton exchange membrane electrolyzer

The Proton Exchange Membrane (PEM) electrolyzer was first introduced in the 1960s and was developed to overcome some of the operational drawbacks of the AWE technology. The membrane electrode assembly is at the core of the electrolyzer and consists of a membrane and the electrocatalysts of the anode and the cathode. Perfluorosulfonic acid membranes are generally used because of their high strength and high proton conductivity [40]. The membrane allows positively charged hydrogen ions (protons) to pass through while rejecting negatively charged ions and electrons. Due to the acidic environment, platinum group metals are required to serve as the electrocatalysts [41]. An overview of the PEM electrolyzer process is presented in Figure 2.5. The oxygen evolution reaction occurs at the anode, and the hydrogen evolution reaction at the cathode.

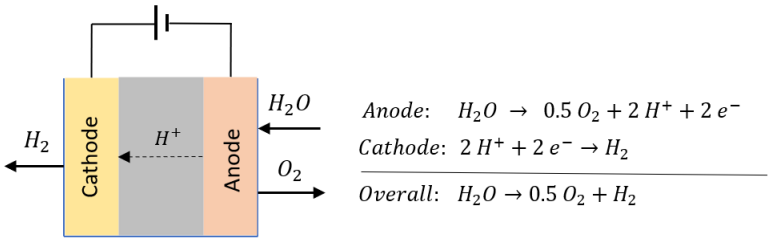

Figure 2.5: The PEM electrolyzer process with the half-reactions occurring at the electrodes

The use of a solid polymer as an electrolyte instead of an aqueous liquid is the main reason for many advantages that the PEM electrolyzer has over the AWE: (i) Due to the solidity of the electrolyte, the cell thickness is reduced, leading to lower Ohmic loss and allowing for high current densities of up to 2 A/cm^2 [42]. (ii) The reduced cell thickness enables less heavy and more compact designs. Compared to the AWE, the PEM electrolyzer requires only half of the space [43]. (iii) Due to the strength of the membrane structure, hydrogen gas can be produced under high pressures within the range of 20-50 bar [41, 42]. (iv) The solidity of the electrolyte reduces the gas crossover, which makes the electrolyzer effective in part-load operation and, therefore, suitable for intermittent renewable energy sources [44].

Although its many benefits, PEM technology tends to be more expensive due to the employment of noble metals such as platinum. It also has a lower lifetime because of its acidic nature and high operating pressures. Similar to the AWE, the PEM electrolyzer operates at temperatures of 50-80°C, but slightly higher efficiencies reaching up to 80% have been established.

2.3.3 Solid oxide electrolyzer

The Solid Oxide Electrolyzer (SOE) has been under development since the 1970s and has gained significant traction in the past decade. The growing interest can be attributed to the superior thermodynamic properties exhibited by the electrolyzer cell [45]. In Figure 2.6, a schematic diagram of an SOE cell is presented. The electrolyte consists of a solid ceramic material capable of conducting oxygen ions, which is sandwiched between two thin electrodes. A key characteristic of the SOE cell is that it operates at high temperatures ranging from 700°C to 900°C. Consequently, the SOE cell utilizes water vapor, rather than liquid water, as the source for hydrogen production. Water splitting in the vapor phase requires less energy compared to water splitting in the liquid phase. Additionally, since no thermal energy is lost during the process, it is possible to achieve efficiencies approaching 100% [37]. The low energy requirement for the electrolysis process may offer an economic advantage since the electricity cost accounts for a large portion of the price of hydrogen production [46]. Moreover, since the

SOE does not employ rare and expensive materials, the technology has the potential to achieve remarkable affordability once it reaches full commercial development [38].

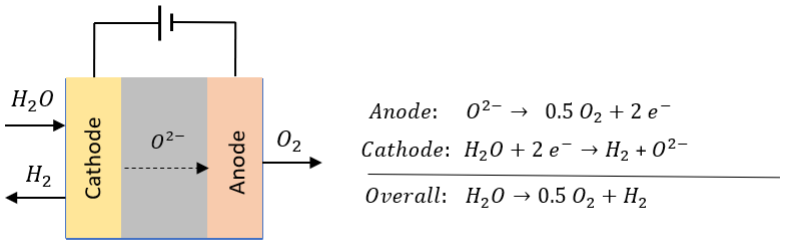

Figure 2.6: The SOE process with the half-reactions occurring at the electrodes

The primary challenge associated with SOE lies in sustaining the elevated operating temperature and connecting a suitable heat source. While some forms of industrial waste heat have the potential to serve as a viable option for supplying the necessary heat to the electrolyzer [38, 46], the majority of industrial processes can not be used at heat source to the SOE [46]. Further, the high-temperature operation environment contributes to a relatively limited lifespan. Prolonging the lifetime of the SOE is one of the main interest fields of development. At present, the technology remains commercially unavailable, and the implementation of large-scale installations is still pending.

In Table 2.1, some key specifications of AWE, SOE, and PEM electrolyzer types are summarized. The values presented in the table were taken from different studies and indicate typical operating conditions and performances.

2.3.4 Alkaline anion exchange membrane

The alkaline Anion Exchange Membrane (AEM) electrolyzer is still in the early stages of development. The concept behind AEM is to combine the advantages of AWE and PEM. Hence, it uses a low-concentration alkaline solution with a solid polymer membrane capable of transferring anions (OH^-). Due to the solidity of the membrane, it is able to operate at elevated pressures of around 30 bar, and the electrodes are both Ni-based, eliminating the need for noble metals. Although the technology shows promising characteristics, its effectiveness has yet to be determined, and currently, there is limited information available regarding its performance. An in-depth description has therefore been left out. Further insights can be found in [47, 48], where the AEM technology is explained in more detail and the future development is addressed.

Table 2.1: Key specifications per electrolyzer technology [37, 38, 39, 40, 42, 43].

Specification	**AWE**	**PEM**	**SOE**
Electrolyte	Aqueous solution	Solid polymer	Solid ceramic
Charge carrier	OH^-	H^+	O^{2-}
Efficiency (P2H)	60-75%	60-80%	90-95%
Operating pressure	1-15 bar	20-50 bar	1-10 bar
Operating temperature	50-80°C	50-80°C	700-900°C
Lifetime (full load hours)	~90,000 hr	~70,000 hr	~30,000 hr
Load range (of nom. capacity)	15-100%	0-100 %	20-100%
Start/stop cycling	weak	good	weak
Ramp up/down response	fast	fast	slow

2.4 Energy Transmission

The wind farm's generated energy must be transported to the grid. For a hybrid wind farm with offshore electrolysis, this can be done in the form of electricity or hydrogen gas. For long-distance transportation, HVAC or HVDC cables and pipelines are used to transport electricity and gas, respectively. This section aims to provide insight into both transportation mechanisms.

2.4.1 Hydrogen transmission

The cheapest way to transport large quantities of hydrogen gas is via steel pipelines. Gas transportation through pipelines relies on pressure differentials over the transmission distance. The pressure at the inlet of the pipe is higher than at the pipe outlet, which causes the gas to flow towards the outlet. Due to factors such as elevation differences, wall friction, and heat exchange with the surroundings, there will be a pressure drop along the pipeline. The temperature changes and the decrease in pressure lead to a reduction in the volumetric density of the hydrogen gas, resulting in an increase in flow velocity, thereby accelerating the pressure drop, and so on. Hence, the pressure drop within the pipeline shows a parabolic gradient [49], as indicated by Figure 2.7. After reaching a specific distance, the gas pressure decreases to a certain threshold, causing the gas flow to stop. To avoid this, compression stations are placed along the pipe to re-pressurize the gas. The distance between these compression stations is usually 80-100 km, depending on the elevation, the pipe geometry, flow velocity, ambient temperature, and pipe insulation [50].

Pipeline transportation of hydrogen gas may be compared to that of natural gas (methane, CH_4). Repurposing existing natural gas pipelines for the transmission of hydrogen could decrease the total capital cost by 75-90 % [19] and is thus considered a cost-effective method for building a new hydrogen infrastructure. From a technical point of view, hydrogen pipelines have identical technical requirements to those of methane, with certain modifications. Due to the corrosive nature of hydrogen, existing pipelines need to be covered with a protective coating to reduce embrittlement and extend their durability. Also, when evaluating the efficiency of a hydrogen gas pipeline, it is commonly compared to that of natural gas. During transportation, there is a possibility of fugitive emissions occurring along the high-pressure gas pipeline, resulting in an approximate loss of 0.02%-0.05% per 1000 km per year [18].

The European Hydrogen Backbone (EHB) is an initiative of 32 energy infrastructure operators. The EHB envisions a pan-European hydrogen transmission network consisting of both repurposed and new pipelines [51]. A map of the projected hydrogen pipeline infrastructure in 2040, proposed by the EHB, is found in Appendix B.

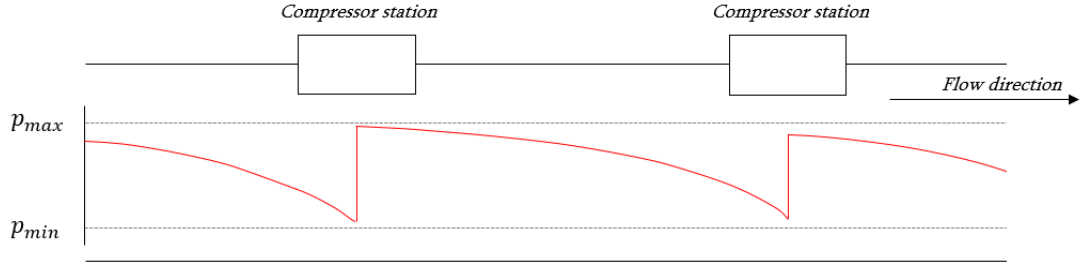

Figure 2.7: The use of multiple compressor stations to maintain the pressure within certain boundaries.

2.4.2 Electricity transmission

Initially, the transportation of electricity from offshore wind farms relied solely on HVAC transmission lines. However, as wind farms are being installed farther offshore, resulting in longer transport distances, the use of HVDC transmission lines is becoming increasingly popular [52]. This shift is primarily driven by the lower resistive losses and installation costs associated with HVDC cables compared to HVAC cables, which becomes crucial when considering long-distance electricity transportation. In HVAC cables, the interaction between the Alternating Current (AC) and its self-generated magnetic field leads to a concentration of the current near the surface of the cable. This phenomenon is known as the *skin effect*. As a consequence, the effective conductive area of the cable is reduced, and the resistance within the cable increases. Additionally, HVAC cables work with 3 cables (three-phase) instead of one. These factors contribute to a greater power loss in the form of heat which is avoided in HVDC lines. According to Miao et al. [18], the power losses in a HVAC line and HVDC line are around 6.7% per 1000 km and 3.5% per 1000 km, respectively.

In addition to their superior transportation efficiency, HVDC cables also exhibit lower costs per kilometer due to their simpler design [52, 53]. Unlike HVAC cables, HVDC cables can withstand higher voltages since Direct Current (DC) does not induce its own magnetic field. Typically, HVDC lines operate at voltages ranging from 400 kV to 1100 kV [18], while HVAC lines generally fall within the range of 200 kV to 400 kV [54, 55]. As a result, HVDC lines can transport more power through the same cross-sectional cable area, allowing for higher power capacities and greater efficiency.

In Figure 2.8, schematic designs of HVAC and HVDC are shown. While HVDC cables enable more efficient electricity transport, their system design is more complex due to the inclusion of converter stations. Typically, wind farms generate AC with voltage levels typically around 33 kV or 66 kV. Both HVAC and HVDC designs utilize a step-up transformer to increase the voltage for long-distance transmission. However, in the case of HVDC, an additional step is required where the AC is converted to DC through a rectifier. Upon reaching the main AC grid at the shore, the DC power is then converted back to AC using an inverter. These converter stations entail additional costs and power conversion losses, which can be avoided with HVAC transmission. Hence, there exists a trade-off between transport efficiency and cable cost on one hand and converter station expenses on the other. For subsea electricity transport, the break-even distance is typically around 60 km, beyond which HVDC becomes a more economically favorable option [18, 56].

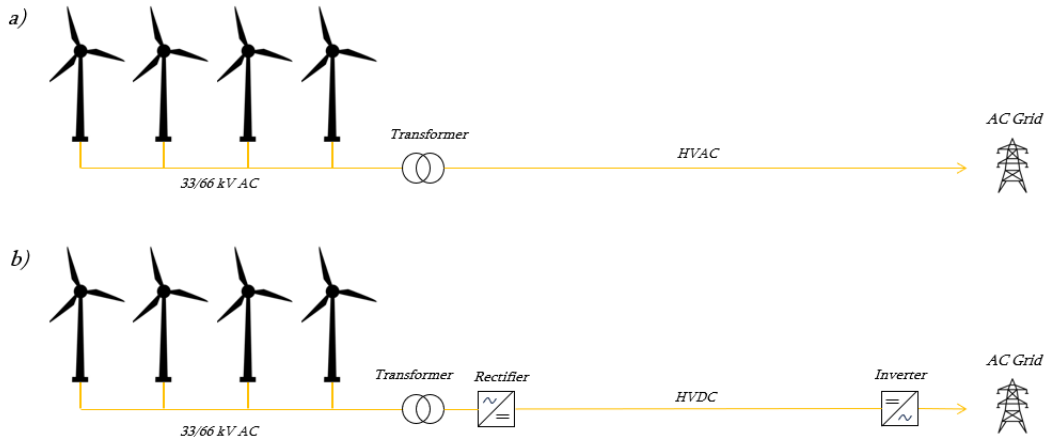

Figure 2.8: Simplified design of a) a HVAC transmission line and b) a HVDC transmission line.

2.5 Compressor

The compression of hydrogen is necessary for storage and transportation purposes due to its low volumetric density. However, compared to natural gas, the compression of hydrogen typically requires more energy due to differences in molecular properties. Hydrogen molecules are lighter and have a lower density, necessitating more work to compress them. The literature discusses two main types of compressors for hydrogen compression [49, 57]: Reciprocating compressors and centrifugal compressors. This section provides a comprehensive discussion of these two compressor types.

2.5.1 Reciprocating compressor

A reciprocating compressor, depicted in Figure 2.9, is a type of positive displacement compressor. It utilizes a piston to compress gas in a continuous manner. The compression process starts when the piston descends from its top dead center (TDC), creating a low-pressure environment within the cylinder. As a result, the suction valve opens, allowing the gas to enter. Subsequently, as the piston reaches the bottom dead center (BDC), the suction valve closes and begins its upward stroke. During this upward motion, the piston reduces the volume of space in the cylinder, leading to an increase in vapor pressure. Once the pressure in the cylinder surpasses the pressure in the discharge line, the discharge valve opens, enabling the release of the compressed gas.

Reciprocating compressors are well-suited for low to moderate hydrogen flow rate applications and high-pressure requirements [57]. When it comes to compressing hydrogen to high pressures, a multi-stage reciprocating compressor system is often employed. In this configuration, the discharge line of one reciprocating compressor serves as the inlet line for the next compressor in the sequence. This arrangement allows for incremental pressure increases across multiple stages. Pressures as high as 85 MPa have been successfully achieved using this multi-stage setup [58].

Despite being a widely utilized and mature technology, the reciprocating compressor does have certain limitations. Given the requirement for high-purity hydrogen gas, the use of oil lubricants is typically avoided during hydrogen compression. Although the piston is equipped with rider bands, the absence of lubricants leads to faster embrittlement. Additionally, the reciprocating compressor is not well-suited for handling high flow rates as it would necessitate either excessively large cylinders or cycling speeds. To accommodate high flow rates, the next section will explore the use of centrifugal compressors, which offer a viable alternative.

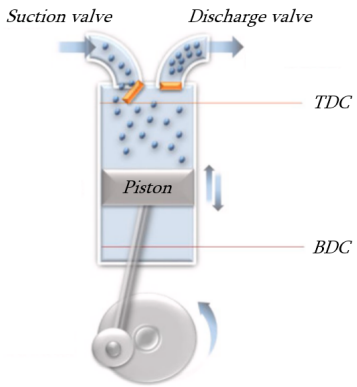

Figure 2.9: Schema of a reciprocating compressor [57].

2.5.2 Centrifugal compressor

A centrifugal compressor is a dynamic compressor that is often used in natural gas pipeline transportation and in other circumstances that require high gas throughput and moderate pressure ratios [57]. A schematic of the centrifugal compressor is shown in Figure 2.10. A centrifugal compressor generally has several stages of an impeller combined with a diffuser. An impeller is a disc consisting of numerous small blades. The impeller, driven by an electrical rotor, exerts a rotational speed on the incoming gas, resulting in momentum transfer and acceleration. The accelerated gas passes through a diffuser, where its pressure is increased. The outlet of the diffuser connects to the subsequent stage in the compressor. With each successive stage, the gas pressure is gradually increased. As the gas tends to heat up after each stage, it is commonly subjected to cooling processes during the compression operation [59].

Centrifugal compressors find extensive use in natural gas pipelines, making them a convenient choice for hydrogen applications as well. However, a thermodynamic challenge arises due to the difference in molecular weight between hydrogen and natural gas. Hydrogen has a molecular weight that is eight times lower than that of natural gas. Consequently, achieving the same compression ratio necessitates the impeller's rotational speed to be nearly 3 times higher (square root of 8) [49, 57, 59]. Nevertheless, there are limitations to what extent the impeller speed can be increased due to material strength constraints and concerns regarding hydrogen embrittlement [57].

Centrifugal compressors designed specifically for hydrogen applications are currently in the developmental stage [49, 57]. Although still under development, it is foreseeable that these compressors will play a significant role in the future, addressing the challenges associated with the properties of hydrogen.

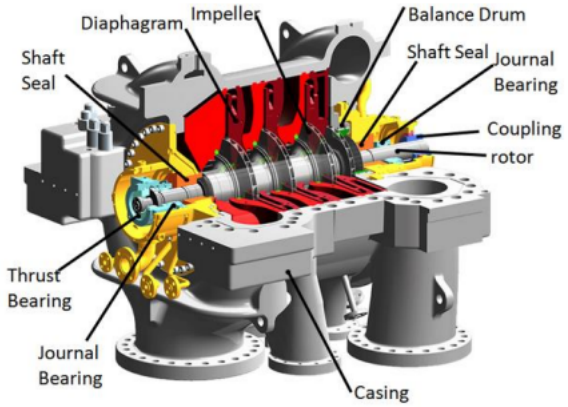

Figure 2.10: Schema of a centrifugal compressor [57].

Chapter 3

Modeling the system

In Chapter 2, a comprehensive overview of the key elements comprising a hybrid wind farm was provided. In order to simulate the system, a Python model was built to determine the net present value of a hybrid wind farm containing offshore electrolysis. To ensure the efficacy of the model, it is imperative to accurately estimate and formulate the performances and costs associated with the various components. To obtain accurate estimations, extensive research was conducted, including consultations with literature sources, vendors, and developers.

This chapter presents an incremental account of the simulation process (both technical and financial) for each component and is structured as follows: In Section 3.1.1, the wind farm and the platform are described, and Section 3.2 elaborates on the modeling of the water treatment system. The electrolyzer is addressed in Section 3.3, after which the simulation of the energy transmission and compression are captured by Section 3.4 and 3.5, respectively. Finally, in Section 3.7, the model strategy and the used data sets are explained.

3.1 Wind Farm

The initial step in the simulation process is to model the wind farm, which supplies electrical energy to the system. By considering the power generation profile of the wind farm, the model will determine the amount of electricity that can be directly sold and the portion that can be allocated for hydrogen production through the electrolyzer. As such, it is imperative to accurately represent this component in the model.

To simulate the wind farm, wind data was taken from 55°N 7°E, near the coast of Denmark. The location can be found in Appendix C. The reason for choosing this site is given in Section 3.7. Wind farm power generation, wind data, and turbine specifications have all been provided by Eneco. A histogram of the used wind data and the fitted Weibull distribution curve are presented in Figure 3.1a.

3.1.1 Wind turbine

The proposed wind farm will consist of IEA reference turbines with a rated capacity of 15 MW [60]. Some technical data regarding the used wind turbine is provided in Table 3.1. The power curve of the wind turbine can be found in Figure 3.1b. The size of the wind farm is one of the main input parameters to the model and will be adjusted to perform a sensitivity analysis found in Chapter 4. The area of the site of the wind farm is assumed to be sized according to the capacity of the wind farm. Additional wake effects were therefore assumed to be negligible and that the power generation thus scales linearly with the total capacity of the farm.

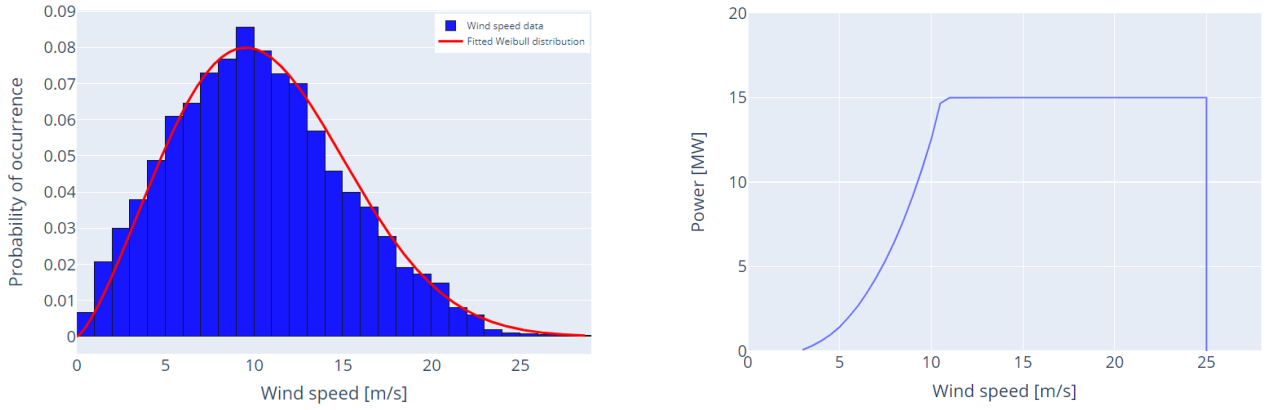

(a) (b)

Figure 3.1: Wind farm specifications with (a) a histogram of used wind speed data with in red the fitted Weibull distribution. The Weibull distribution has a scale parameter c of 12.05 and a shape parameter k of 2.35. And (b) the power curve of the considered 15 MW wind turbine.

Table 3.1: Technical data for the used wind turbine.

Parameter	**Value**	**Unit**
Rated Power	15	MW
Hub Height	145	m
Rotor diameter	240	m
Cut-in wind speed	3	m/s
Rated wind speed	11	m/s
Cut-out wind speed	25	m/s
Inter-array voltage	66	kV

3.1.2 Economic analysis

For the estimation of the wind farm CAPEX, a model developed by Vieira et al. [61] was used. In their study, the researchers evaluated a database of 95 offshore European wind farms to establish trends between CAPEXand several farm parameters such as total capacity, water depth, and turbine capacity. They found the following multiple linear regression model ($R^2 = 0.91$) to determine the total CAPEX of a wind farm:

$$C_{farm} = \alpha_0 + \alpha_1\sqrt{S_{farm}} + \alpha_2 S_{turb} + \alpha_3 z_{avg} + \alpha_4 \tag{3.1}$$

Where C_{farm} is the total capital cost of the wind farm $[M€]$, $\alpha_i; i = [0, 1, 2, 3, 4]$ are model parameters [-], S_{farm} the farm capacity $[MW]$, S_{turb} the turbine capacity $[MW]$, and z_{avg} the average water depth $[m]$. Values of the function parameters are taken from [61] and are found in Table D.1 in Appendix D.

The linear regression function in Equation 3.1 exhibits a coefficient of determination (R^2) of 0.91, indicating a strong alignment with historical data. Consequently, the cost function has been employed in this research to assess the CAPEX associated with the wind farm. Assuming a constant average water depth of 30 meters and a fixed turbine capacity of 15 MW, the wind farm's cost can be modeled in relation to its capacity. Since the square root of the total wind farm capacity is taken, the relationship becomes nonlinear, illustrating economies of scale. Figure E.1 in Appendix E presents the outcome of this analysis, which has been considered reasonable by Eneco.

It should be noted that the cost model utilized in this study relies on historical data, and it is plausible that the cost of wind energy may decrease in the future. However, when examining the costs of offshore wind farms commissioned between 2000 and 2020, a definitive declining trend cannot be established. Given this analysis, it is reasonable to assume that the cost estimation derived from historical data remains valid for near-future considerations. The specific cost of an offshore wind farm in M€/MW is presented in Figure E.2 in Appendix E.

In addition to CAPEX, the wind farm will incur OPEX. The OPEX is an annual cost spent on operation and maintenance. For offshore wind farms, the OPEX is considered a substantial factor and accounts for 20-30% of the total wind farm life cycle costs [62, 63]. Assuming a farm lifetime of 25 years and an OPEX portion of 25%, the following is obtained for OPEX costs per annum:

$$\frac{O_{farm,tot}}{C_{farm} + O_{farm,tot}} = 0.25 \longrightarrow O_{farm,ann} = 0.013 C_{farm} \tag{3.2}$$

Where $O_{farm,tot}$ is the total cumulative farm OPEX over the whole lifetime, C_{farm} is the total farm CAPEX, and $O_{farm,ann}$ are the annual OPEX.

Based on the calculation in Equation 3.2, the OPEX of the wind farm is equal to 1.3% of the farm CAPEX. A detailed derivation of the OPEX can be found in Appendix E.

3.1.3 Platform

The offshore platform serves as a hub for accommodating the electrolyzer, electrical equipment, coolers, and other BOP equipment. As outlined in Section 2.1.2, the platform consists of a topside with a jacket support structure. In a report by DNVGL [26], estimates for platform mass and costs are provided for various sizes of electricity connections and electrolyzers. The report indicates that platform costs, mass, and volume exhibit a roughly linear relationship with the capacity sizes of these two. Their estimations have been adopted in this research, and one of the scenarios, along with the derivation of the cost function presented underneath, can be found in Appendix A.

The cost of the offshore platform as a function of the electricity connection size and the electrolyzer capacity can be formulated as:

$$C_{plat} = (84.651 S_{cab} + 139.281 S_{elec}) \times 10^3 \times 1.5 \tag{3.3}$$

Where C_{plat} is the CAPEX of the platform [€], S_{cab} is the capacity of the electricity cable [MW], and S_{elec} is the capacity of the electrolyzer [MW]. The OPEX of the platform is assumed to be 2.0% of the platform CAPEX per year.

3.2 Water treatment system

As described in section 2.2, the water treatment system will consist of RO coupled with EDI to demineralize seawater. Regarding this system, the following three components are modeled for the simulation: (i) the seawater intake pump, (ii) the RO assembly, and (iii) the EDI assembly. Values for the used parameters regarding the water treatment system are found in Table D.2 in Appendix D.

3.2.1 Feed pump

The seawater intake pump pumps the seawater upwards from sea level to the height of the platform. The following equation calculates the required power:

$$P_{fp} = \frac{Q_f \rho_{sw} g h}{\eta_{fp}} \tag{3.4}$$

Where P_{fp} is the required feed pump power $[W]$, Q_f the seawater feed flow rate $[m^3/s]$, ρ_{sw} the gravimetric density of seawater (1025 kg/m^3), g the gravitational constant (9.81 m/s^2), h the height of the platform above sea level $[m]$, and η_{fp} the pump efficiency.

The seawater flow rate is determined by the feed demand of the electrolyzer and the recovery ratios of the desalination processes and can be derived in m^3/s using the following:

$$Q_f = \frac{Q_{elec}}{R_{ro} R_{edi}} \tag{3.5}$$

Where Q_{elec} is the feed flow rate demanded by the electrolyzers $[m^3/s]$ and R_{ro} and R_{edi} are the recovery ratios of the RO process and the EDI process, respectively. It is worth noting that the feed pump power is calculated by only accounting for the change in potential energy of the seawater and that friction losses in the system are neglected.

3.2.2 Desalinator system

The desalinator system consists of an RO-EDI unit to produce ultrapure water from seawater. The total energy consumption of the desalination (E_{wt}) is calculated by adding the energy consumption of the RO assembly (E_{ro}) and the RO assembly (E_{edi}):

$$E_{wt} = E_{ro} + E_{edi} \tag{3.6}$$

Kim et al. [34] analyzed the energy consumption of over 70 large-scale RO plants. They established a linear relationship between the energy consumption and the TDS content of the feed water. The relationship is found in Appendix F in Figure F.1. A TDS content of 35,000 mg/L was assumed for the water of the North Sea. According to the linear relationship, the Specific Energy Consumption (SEC) of the RO plant would then be 4 kWh/m^3. This value accounts for pre-treatment, RO-assembly, and post-treatment together [34].

Warandi et al. [64] produced ultrapure water with electric conductivities ranging from 0.2–1 $\mu S/cm$ using EDI. In their experiment, they used tapwater with an electrical conductivity of 248 $\mu S/cm$ as feed to the EDI and measured the energy consumption for various product conductivities. The results of their experiment have been plotted and can be found in Figure F.2. Based on the results of the experiment, the following relationship was found:

$$E_{edi} = -0.395\sigma_{per}^2 - 1.404\sigma_{per} + 2.684 \tag{3.7}$$

Where E_{edi} is the energy consumption of the EDI process $[kWh/m^3]$ and σ_{per} is the electrical conductivity of the permeate $[\mu S/cm]$.

In this study, it was assumed that the RO permeate (after post-treatment) has the same conductivity as the tap water in the experiment of Warandi et al. The required level of water purity depends on the type of electrolyzer and manufacturer. Although both types of electrolyzers require deionized water, alkaline electrolyzers generally have a higher tolerance for impurity than PEM electrolyzers. The American Society for Testing and Materials (ASTM) defined deionized water types as ranging from pure to less pure. In this research, it was assumed that the PEM electrolyzer requires a water quality of ASTM type I ($\leq 0.056\mu S/cm$).

3.2.3 Economic analysis

The CAPEX of the water treatment installation depends on the size of the electrolyzer. A system with a high-capacity electrolyzer will require more UPW since more hydrogen will be produced. Shokri et al. performed a techno-economic analysis on a RO desalination plant and showed that the investment cost mainly depends on how much water the system needs to produce. According to them, the CAPEX of a RO system is in the range of €900-2500/m^3/day. Since this research considers the water treatment facility to be built offshore, the most conservative value of €2500/m^3/day has been assumed.

The OPEX of a water treatment system accounts for a considerable part of the total system costs. Membrane fouling in the RO system causes membrane replacement on a regular basis (a few years, depending on the salinity of the feed water and the operating pressure), and chemicals are needed during the pre- and post-treatment. According to the literature, the annual OPEX of a water treatment facility can amount to up to 10% of the capital investment [65, 66].

The costs of the EDI unit were assumed to be comparable to those of the RO unit. An overview of the economical parameters of the water treatment system is presented in Table 3.2. A detailed derivation of the total CAPEX related to the electrolyzer capacity is found in Appendix F.

Table 3.2: Economic parameters regarding the water treatment system.

Parameter	**Value**	**Unit**
Specific capital cost RO	2500	€/m^3/day
Specific capital cost EDI	2500	€/m^3/day
Total CAPEX	20750	€/S_{elec}
OPEX water treatment	10	% of CAPEX

3.3 Electrolyzer

Four electrolyzer types have been discussed in Section 2.3. The AEM and SOE technologies are still in development and not yet commercially available. Additionally, effectively providing the SOE with enough heat to sustain its operational temperatures remains a significant challenge offshore. AWE is a well-established technology, however, due to its robust physique and weak dynamic response, it is considered a less attractive option than PEM for offshore purposes. Shipping and platform installation may become too expensive in order to facilitate large-scale alkaline electrolysis offshore. For these reasons, only PEM electrolysis will be further considered in this research.

3.3.1 Technical specifications

Eneco has provided information on the PEM electrolyzer used in this study. The vendor of the electrolyzer will remain anonymous due to confidentiality reasons. Technical data of one PEM electrolyzer module is given in Table 3.3. The module has a minimum load constraint of 5% of its nominal capacity, which must be ensured when the module is in operation. The power consumption is 52 kWh/kg, and the module efficiency is based on the Lower Heating Value (LHV) of hydrogen, which is 33.3 kWh/kg.

Table 3.3: Technical data on the PEM electrolyzer.

Parameter	**Value**	**Unit**
Stack power consumption	52	kWh/kg
Efficiency (LHV, full load)	64	%
Capacity	18	MW
Operating pressure	30	Bar
Operating range	5-100	% of nominal power
Demin water consumption	10	L/kgH_2
Lifetime (full load hours)	70,000	hr

3.3.2 Minimal load constraint

According to Table 3.3, the electrolyzer module has a minimum load constraint of 5% of its nominal capacity while the module is in operation. However, a system would comprise multiple electrolyzer modules and one could decide to switch off some of these in periods of low wind availability. By deactivating some of the modules, the minimum load constraint of the system as a whole would fall lower than 5% of the total installed electrolyzer capacity.

However, when switching the modules on and off, the system must deal with startup and shutdown times due to which the response of the system. To this date, limited data is available on the operational response and adaptability of a PEM electrolyzer. Some research studies suggest that the cold startup and shutdown of a PEM electrolyzer module can be accomplished within a matter of minutes [38, 67], which is considered a short timeframe in comparison to alternative electrolyzer technologies. Given this rapid response rate, a system operator could activate or deactivate the modules based on wind forecasts, and any potential losses due to delays may be marginal.

Despite the ability of electrolyzer modules to rapidly switch on and off, a constant minimal load constraint of 5% of the total installed electrolyzer capacity was assumed in this study. The reason behind this choice is that the electrolyzer is not the only component to consider. Other BOP components, such as desalination units and compressors, also demand a minimal load to

be operated effectively. Additionally, various on-platform facilities like accommodations and control rooms necessitate continuous operation, requiring a certain energy demand. Hence, a minimum load constraint of 5% of the total electrolyzer capacity was deemed reasonable.

3.3.3 Part load operation

An important aspect when considering an electrolyzer is its operation while in part load. Kopp et al. [68] studied the efficiency curve of a PEM electrolyzer based on the load percentage relative to its nominal capacity. They found a slight increase in conversion efficiency at loads lower than the nominal capacity. The curve from their data has been reproduced in this research and is presented in Figure 3.2. The nominal efficiency of the electrolyzer used in this study is 64%, which is found at full load. To model the efficiency of the electrolyzer for a given load, the following set of equations that describes the blue line in Figure 3.2 is used:

$$f(x) = \begin{cases} 4.76 * 10^{-2}x^3 - 1.68x^2 + 19.6x - 0.87, & 0 \leq x \leq 15 \\ 4.73 * 10^{-4}x^2 - 0.19x + 77.7, & 15 < x \leq 100 \end{cases} \tag{3.8}$$

Where $f(x)$ is the efficiency of the electrolyzer [%] given a load x, which is expressed as relative to the nominal capacity of the electrolyzer [% of nominal capacity].

Due to the superior performance in part load operation, the following two points must be considered by the model:

1. It may be beneficial to oversize the electrolyzer relative to the wind farm. Since the wind farm will be operating at rated power for a considerable amount of time (29% according to the data), it could be advantageous to oversize the electrolyzer so that it will operate at a higher efficiency during maximum power output.

2. Depending on the electricity price and farm power output at a given point in time, it may be beneficial to sell part of the power as electricity and part of the power as hydrogen. This means that for each hour, the model has to consider the possible combinations and choose the most profitable one.

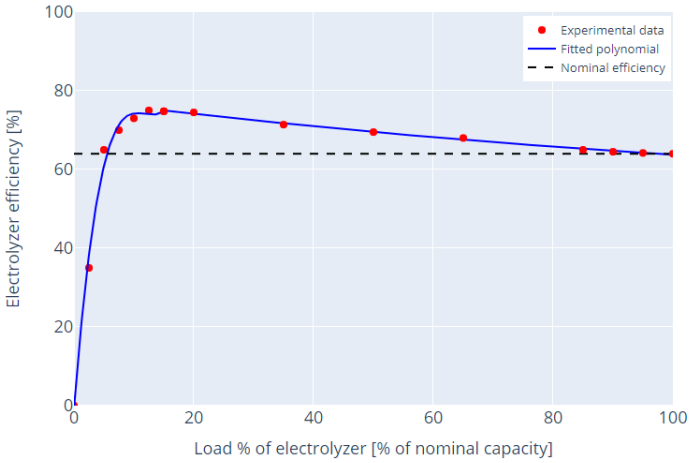

Figure 3.2: PEM electrolyzer efficiency based on load percentage relative to its nominal capacity. The experimental data was taken from Kopp et al. [68]

.

3.3.4 Economic analysis

The costs associated with PEM electrolyzers are typically expressed in euro per kilowatt (€/kW). As advancements continue to be made and increased investments are allocated towards development due to the rising demand for electrolysis, it is anticipated that the cost of this technology will decrease over time. However, accurately predicting the price trend for PEM electrolyzers remains challenging, particularly as the technology is still in the process of maturing for large-scale applications.

For instance, in a technical report prepared by the IEA for the G20 summit in Japan in 2019 [43], a price range of 650 €/kW to 1500 €/kW was projected for PEM electrolysis by 2030, highlighting a significant variation. Considering the offshore nature of this installation, a conservative value of 1300 €/kW was assumed for the electrolyzer within this research. Next to the costs for the electrolyzer, there is also an expense for the BOP of the electrolyzer unit. This involves piping, cooling, installation, insurance, etc. From Eneco's experience, the BOP of an electrolyzer adds up to another €700/kW. The associated annual OPEX was assumed to be 1.5% of the CAPEX [56].

An additional aspect to take into account is the lifespan of the electrolyzer stack. The projected lifetime of the proposed electrolyzer stack is 70,000 full load hours. This duration is significantly shorter compared to the lifespans of other system components. Upon reaching the lifetime of the electrolyzer, components such as electrodes and the membrane will necessitate replacement. It is assumed that these replacement costs will amount to 50% of the initial electrolyzer CAPEX (€1300/kW), which will incur in the year of replacement. It should be noted that there is limited information available regarding the impact of part load operation on the lifetime of the electrolyzer. In this study, it was assumed that part load operation does not have any impact on the lifespan, and the replacement criterion was based on the 70,000 full load hours.

3.4 Transmission

As outlined in Section 2.4, the generated energy can be transported either as electricity through cables (HVAC or HVDC) in the form of electricity or as hydrogen gas through pipelines. To perform the simulation, the model must incorporate the design considerations based on the input parameters and provide cost estimates accordingly.

TenneT, the Dutch electricity grid operator, has set a target to build multiple 2 GW offshore substations in the North Sea by 2030 under their '2GW program' [69]. The objective is to enable nearby wind farms to link to these substations, allowing the energy to be transmitted to the mainland through HVDC cables. In exchange for this service, Tennet levies an annual fee based on the capacity of the connection. Similarly, Gasunie, the Dutch gas grid operator, intends to construct an offshore hydrogen pipeline [51]. This pipeline will facilitate the hydrogen connection of hybrid wind farms, with Gasunie charging an annual fee proportionate to the connection's capacity. Appendix G contains a map of the Dutch North Sea layout envisioned by TenneT and Gasunie.

As a result of the proposed energy infrastructure, the connection points for both electricity and hydrogen will be located within close proximity to the wind farm, with distances below 30 km. Consequently, the following holds regarding the simulation:

1. Since distances between compression stages are usually between 80-100 km, which is described in 2.4.1, the hydrogen pipeline will be equipped with a single compressor station located at the inlet.
2. For the transportation of electricity, an HVAC cable will be utilized, eliminating the requirement for a rectifier. As outlined in Section 2.4.2, HVDC would become favorable to HVAC for subsea distances longer than 60 km.

In the subsequent sections of this report, a transmission distance of 30 km was assumed for both the transportation of electricity and hydrogen.

3.4.1 Hydrogen pipeline

The cost of a hydrogen pipeline per kilometer is influenced by the pipe diameter, where a larger diameter corresponds to higher costs. The cost estimates for the hydrogen pipeline are sourced from a graph presented by Gondal et al. [50], which established the relationship between diameter and associated expenses. The results are found in Table 3.4.

Based on the capacity of the electrolyzer, the model needs to determine the required pipe diameter. To derive this, the model utilizes the general flow equation for steady-state isothermal flow, taken from [70]:

$$Q_{hydr} = 1.1494 \times 10^{-3} \frac{T_b}{p_b} \sqrt{\frac{(p_{in}^2 - p_{out}^2)}{G_{hydr} T_{avg} L Z \lambda}} D^{2.5} \tag{3.9}$$

Where Q_{hydr} is the hydrogen gas flow rate measured at Standard Temperature and Pressure (STP) $[m^3/d]$, T_b is the base temperature (288.15 K), p_b the base pressure (101 kPa), p_{in} and p_{out} are the pressures at the pipe inlet and outlet $[kPa]$, respectively, G_{hydr} is the specific gravity of hydrogen (Air = 1.0), T_{avg} is the average gas flowing temperature $[K]$, L is the pipeline length $[km]$, Z is the dimensionless compressibility factor, λ is the dimensionless friction factor, and D is the inner diameter of the pipe $[mm]$.

In this study, it was assumed that there is no elevation difference along the pipeline and that the grid pressure of the offshore gas infrastructure by Gasunie operates at 70 bar. The upper limit for compression at the pipe inlet was assumed to be 100 bar, which means that the model has to size the diameter of the pipeline such that the total pressure drop will not exceed 30 bar. Aside from the maximal allowable pressure drop, the model also has to deal with a maximal flow velocity constraint, which is given as 50% of the erosional velocity [70]:

$$u_{max} = 0.5u^* \tag{3.10}$$

Where u_{max} is the maximum acceptable flow velocity $[m/s]$, and u^* is the erosional velocity $[m/s]$, given by:

$$u^* = 100\sqrt{\frac{ZRT_{avg}}{29G_{hydr}p}} \tag{3.11}$$

With R the gas constant (8.314 $Jmol^{-1}K^{-1}$), and p the absolute gas pressure $[kPa]$. The flow velocity at any point in the pipeline is given by:

$$u = 14.7349\frac{Q_{hydr}p_bZT}{D^2T_bp} \tag{3.12}$$

Based on the calculations, it was determined that the pressure drop in the pipeline is marginal due to the relatively short transport distance of 30 kilometers. Therefore, the primary factor influencing the sizing of the pipeline is the maximum flow velocity. The limited pressure drop for hydrogen transport over short distances has also been shown by a study by Wlodek et al. [71]. It should be mentioned that both the study conducted by Wlodek and this research assumed isothermal gas flow. In order to obtain a more realistic calculation of pressure drop in pipelines, it is necessary to consider heat transfer effects. Kuczynski et al. [72] conducted such a derivation and analysis, revealing that when heat transfer is taken into consideration, the pressure drop is slightly higher compared to isothermal flow. However, for the purposes of this study, an estimation based on isothermal flow conditions was deemed sufficient. The results are presented in Table 3.4. For further details regarding the pipe design, see Appendix H.

The OPEX of a hydrogen pipeline is relatively high, which can be mainly attributed to leak testing and avoiding hydrogen embrittlement of the materials. In this research, an OPEX of 7% of the CAPEX was assumed for the pipeline [18]. An estimate for the annual grid tariff has been provided by Gasunie and is taken as €1400/kg/h/year. Where 'kg/h' is the maximum hydrogen flow that a system is expected to feed into the grid at any time. Further, pipeline transportation losses (0.05%/1000 km [18]) were assumed to be negligible due to the short transportation distance.

Table 3.4: Estimated pipeline cost for different pipe diameters.

Diameter ["]	**Flow rate [kg/s]**	**Expected CAPEX [€/km]**
2	0.01 - 0.26	300,000
4	0.26 - 1.03	330,000
6	1.03 - 2.31	380,000
8	2.31 - 4.11	410,000
10	4.11 - 6.45	490,000
12	6.45 - 9.24	580,000

3.4.2 HVAC cable

As previously mentioned in this section, an HVAC cable is utilized for transmitting electricity to a 2-GW substation. Unlike HVDC, the utilization of an HVAC cable simplifies the design process by eliminating the need for rectifiers. However, it is important to note that HVAC cables incur higher costs and exhibit greater energy loss compared to HVDC.

The operating voltage of HVAC lines can vary depending on the specific design criteria. Commonly utilized voltage levels for HVAC systems include 132 kV, 220 kV, and 400 kV. Higher voltage levels in cables generally offer increased transport capacities, but they also exhibit a higher cost. Additionally, transporting electricity at higher voltages typically results in lower energy losses. In certain scenarios, it may be advantageous to install two low-voltage cables rather than a single high-voltage cable and vice versa. Therefore, conducting a cost-benefit analysis becomes crucial in order to achieve the optimal electrical design.

When determining the optimal design, key considerations include the distance of electricity transportation and the overall system capacity. Djapic and Strbac [73] have presented an analysis focused on offshore transmission systems for wind farms with capacities up to 1500 MW and transport distances ranging from 25 km to 100 km. This analysis takes into account factors such as cost, energy losses, and system efficiency to determine the most favorable electrical design for the given parameters. However, optimizing the electrical design for each scenario is beyond the scope of this research. For the purpose of this study, it was considered sufficient to solely estimate the cost of HVAC lines given a certain required transport capacity.

To estimate the CAPEX associated with the HVAC cable, the model utilizes a linear cost function presented in Equation 3.13. This cost function is derived from the cost estimates provided by Djapic and Strbac [73].

$$C_{cab} = (1.36P_{cab} + 206.13) \times 10^3 \tag{3.13}$$

Where C_{cab} is the CAPEX of the cable [€/km] and P_{cab} is the transport capacity of the cable [MW].

Once the HVAC cable is installed, it usually does not have many operation and maintenance costs [18, 54]. In this study, the annual OPEX of the HVAC line was taken as 0.5% of the total CAPEX [18]. In addition to the annual OPEX, a yearly fee must be paid to TenneT, which is determined based on the capacity of the electricity connection. TenneT has provided an estimated fee of €42,000/MW/year. The losses incurred by an HVAC line amount to roughly 6.7% per 1000 km. In the context of this research, the transmission distance is limited to a mere 30 km, thereby assuming that the transportation losses for electricity are negligible.

3.5 Compressor

In Section 2.5, two main types of compressors that are used for hydrogen compression were proposed: Reciprocating compressors and centrifugal ones. To determine the suitable compressor type, the diagram presented in Figure I.1 in Appendix I was used. The delivery pressure at the Gasunie hydrogen grid was assumed to be 70 bar and the pressure drop in the pipeline from the wind farm to the grid was relatively low based on the general flow equation, given by Equation 3.9. In order to effectively transport the hydrogen gas from the wind farm to the grid, it needs to be compressed to a pressure of 75 bar.

3.5.1 Compressor system

The volumetric hydrogen flow produced by the hybrid farm is considered to be low to moderate and the initial pressure of the hydrogen gas was assumed to be equal to the outlet pressure of the electrolyzer (30 bar). As a result, a two-stage reciprocating compressor was deemed sufficient for compression from 30 to 75 bar, where each compressor stage has a compression ratio of 1.58. Between each stage, the gas is cooled to make the process less adiabatic and more isothermal [74]. A schematic representation of the compressor system is presented in Figure 3.3. As indicated by the figure, the total hydrogen flow can be distributed over multiple compressor stations, where each station is composed of two stages and a cooler. Distributing the flow over multiple stations has two significant benefits: (i) The system is able to handle larger hydrogen flows, and (ii) in case of a malfunction or maintenance in a single station, the system can still compress hydrogen via other stations.

To derive the required compression power, the following formula is used:

$$P_{comp} = \frac{P_{comp,isen}}{\eta_{isen}} \tag{3.14}$$

Where P_{comp} is the required compressor power $[kW]$, η_{isen} is the isentropic efficiency of the compressor [%], and $P_{comp,isen}$ is the isentropic compression power $[kW]$ given by:

$$P_{comp,isen} = 2.31 \frac{k}{k-1} \frac{T_{out} - T_{in}}{M} (Q_{comp} \times 10^{-3}) \tag{3.15}$$

With k as the gas isentropic coefficient of hydrogen [-], T_{out} and T_{in} the temperature of the gas at the outlet and inlet of the compressor $[K]$, respectively, M is the molar weight of hydrogen $[g/mol]$, and Q_{comp} the compressor throughput $[kg/h]$.

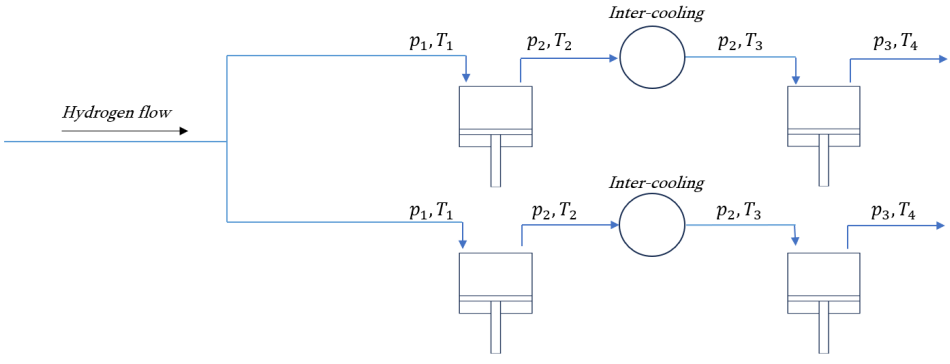

Figure 3.3: Schematic example of the reciprocating piston compressor system. In this example, the hydrogen flow is distributed over two compressor stations with inter-cooling devices.

For one compressor stage, the rise in temperature can be calculated with:

$$\frac{T_{out}}{T_{in}} = \Pi^{(k-1)/k} \tag{3.16}$$

Where Π is the compression ratio [-], and k is given by:

$$k = \frac{c_p}{c_v} \tag{3.17}$$

With c_p the specific heat of hydrogen at constant pressure $[kJ/kgK^{-1}]$, and c_v the specific heat of hydrogen at constant volume $[kJ/kgK^{-1}]$. For more details regarding the compression power calculation, see Appendix I.

3.5.2 Economic analysis

According to Jepma and Van Schot [75], the CAPEX of a compressor system can be estimated by the required compressor power. In their report, they assumed the CAPEX to be €2,800 per kW of compressor power. In order to relate this to the capacity of the electrolyzer, Equation 3.15 can be used. The resulting cost equation is presented underneath and the derivation is found in Appendix I.

$$C_{comp} = 52 \times 10^3 S_{elec} \tag{3.18}$$

Where C_{comp} is the compressor CAPEX [€]. The annual OPEX was assumed to be 3% of the CAPEX [56, 75].

3.6 System overview

In Figure 3.4, a schematic overview of the system is presented. When the wind farm produces electricity, it can either decide to sell it directly to the grid via a TenneT substation or sell it as hydrogen via the offshore gas grid of Gasunie. The symbols depicted in the figure are explained in Table 3.5.

When the system chooses to produce hydrogen, it has to deal with the energy consumption of the water treatment facility, the electrolyzer, and the hydrogen compressor. As mentioned in Section 3.4, the transportation losses of both electricity and hydrogen to the grid are assumed to be negligible due to the short transportation distance.

In both the electricity and hydrogen paths, a transformer needs to be incorporated to adjust the voltage levels. In the hydrogen case, a step-down transformer is required to reduce the voltage from 66 kV to several hundred volts, to make it compatible with the hydrogen production components. Conversely, for the electricity path, a step-up transformer is used to elevate the voltage from 66 kV to several hundred kV for the purpose of HVAC transmission. By running the generated power through a transformer, there are some resistive heat losses that need to be accounted for. In this study, the efficiency of the transformer, η_{trans}, was assumed to be 98% [76].

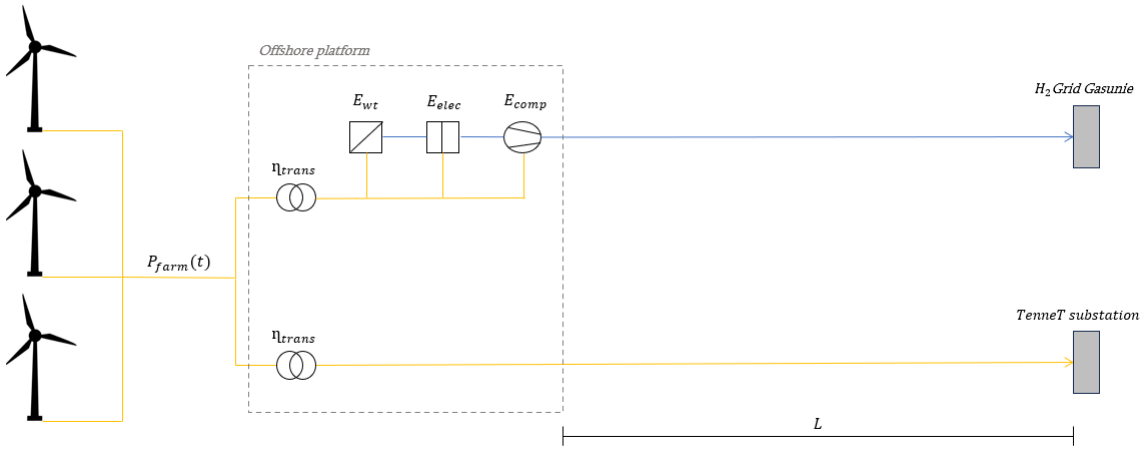

Figure 3.4: Schematic overview of the proposed system. The yellow lines represent the electricity path, and the blue lines indicate the hydrogen path.

Table 3.5: Symbols used in Figure 3.5.

Parameter	Symbol	Unit
Wind farm power	$P_{farm}(t)$	MW
Transformer efficiency	η_{trans}	%
Energy consumption water treatment	E_{wt}	kWh/m^3
Energy consumption electrolyzer	$E_{elec}(P_{load})$	kWh/kg
Energy consumption compressor	E_{comp}	kWh/kg
Transportation distance	L	km

3.7 Model strategy

For the purpose of this research, the revenue and costs of a wind farm with offshore electrolysis will be simulated for a certain set of input parameters. The model takes the following input parameters:

- Capacity of the wind park in MW
- Hourly hydrogen price in €/kg
- Hourly electricity price in €/MWh
- Electrolyzer capacity in MW
- Electricity cable capacity MW

The objective of each simulation is to derive the maximum NPV of a project with a certain set of input parameters. The NPV is a financial metric indicating the total value of a project accounting for the time value of money. It considers the net cash flows throughout the lifetime of a project and tells an investor whether to undertake the project or not. An investment with a positive NPV is expected to create value, while an investment with a negative NPV is expected to destroy value. Also, the higher the NPV, the more profitable a particular project is. The NPV is calculated using the following equation:

$$NPV = -investment + \sum_{n=1}^{N} \frac{NCF_n}{(1+r)^n} \tag{3.19}$$

Where the *investment* resembles the total capital cost of the project assumed to be spent in year 0, N is the expected lifetime of the project in years, NCF_n is the net cash flow in year n, and r is the discount rate in %.

It can be concluded from equation 3.19 that in order to maximize the NPV of a project, the model has to aim for the highest yearly cash flow. More specifically, the model has to decide whether to produce and sell hydrogen or sell electricity at a given point in time. However, the model also has to deal with some constraints, such as transmission limitations and minimal load of the electrolyzer. A schematic overview of the model strategy is given in Figure 3.5. The symbols that are used in this figure are explained in Table 3.6. The model has the following options:

1. *Grid uptake*: In periods when the wind farm generates not enough power to sustain the minimal load of the electrolyzer, it may take up energy from the electricity grid against market prices, only to meet the minimal load constraint of the electrolyzer.
2. *Curtailment*: In the event of negative electricity prices, or when the generated power is greater than the capacity of the electrolyzer and cable combined, the model can decide to curtail energy if that benefits the revenue.
3. *Sales of energy*: In most of the time, when electricity and hydrogen prices are positive and the farm produces energy, the model will sell the energy in either the form of electricity, hydrogen, or both. It has to consider the possible combinations of electricity and hydrogen sales depending on the capacities of the electrolyzer and cable, and the generated power at that time. The combination of sales that results in the highest cash flow has to be chosen.

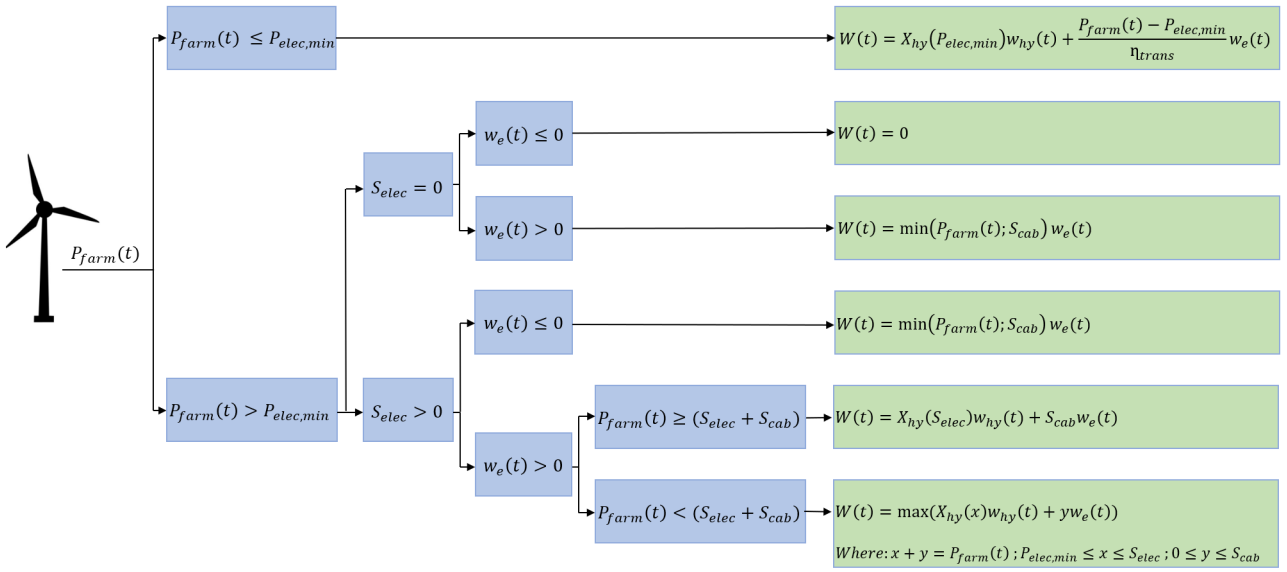

Figure 3.5: Model strategy to maximize cash flow.

Table 3.6: Clarification table regarding the symbols used in Figure 3.5.

Parameter	**Symbol**	**Unit**
Wind farm power	$P_{farm}(t)$	MW
Electrolyzer minimal load	$P_{elec,min}$	MW
Electrolyzer capacity	S_{elec}	MW
Electricity cable capacity	S_{cab}	MW
Hydrogen price	$w_{hy}(t)$	€/kg
Electricity price	$w_e(t)$	€/MWh
Transformer efficiency	η_{trans}	%
Amount of hydrogen	$X_{hy}(P)$	kg

Note that the quantity of hydrogen produced ($X_{hy}(P)$) is dependent on the amount of power supplied to the electrolyzer. Additionally, when the system draws electricity from the grid, it must pass through a transformation in order to match the voltage requirements of the hydrogen production plant. Therefore the amount of electricity that needs to be bought is given by the difference between generated power and the minimum load requirement of the electrolyzer divided by the transformer efficiency (η_{trans}).

3.7.1 Data sets

The simulation by the model research is based on hourly data sets for electricity prices, hydrogen prices, and wind power output for one year. The following considerations were taken into account regarding the data sets:

1. The electricity prices are related to the wind power output: Electricity prices tend to fluctuate according to the "supply and demand" principle. This implies that in times of high wind energy output, the electricity price tends to drop and vice versa. Therefore it is important to use data sets of wind power output and electricity prices of the same year and location.

2. The share of wind energy in the energy mix is relevant: The extent to which the wind power output influences the electricity price depends on the share of wind energy in the energy mix.

3. The hydrogen price was assumed constant: Unlike the electricity price, the hydrogen price is not expected to fluctuate heavily. This can be related to the storage ability of hydrogen. When the hydrogen demand is low, the excess gas can be stored for times when the demand rises again. As a result, the hydrogen gas network will not be as easily overloaded as the electricity grid, and therefore the market stabilizes.

Since more wind energy will be added to the mix in the coming years, it may be assumed that wind power will have a greater impact on the Dutch electricity market in the future than it currently does. This paper focuses on a wind farm that is not expected to be operational before 2030; as a result, a bigger proportion of wind power in the energy mix needs to be taken into account. According to the IEA, Denmark had a wind power share of around 50% of its total electricity supply in 2018 [77], where this was only 10% in The Netherlands [78]. Due to this difference, data sets of hourly electricity prices and wind power generation in Denmark from 2018 were used in this research. Because the average Danish electricity price in 2018 was €44.05 per MWh, according to the data set, it was indexed to a mean price of €75 per MWh to resemble the Dutch market more accurately. The extent to which the data set was indexed has been discussed with Eneco. More details on the used data sets are found in Appendix J.

3.7.2 Model assumptions

For the purpose of the simulation, the model incorporates the following assumptions:

- The model simulates production and sales per hour for one year.
- The lifetime of the system is 25 years[1].
- The discount rate, r, is 7%.
- The simulated year is representative for the whole lifetime of the system.
- There is no battery bank available; generated energy is assumed to be directly sold to market prices or it is curtailed.
- Energy curtailment is free.
- The system requires a minimal load equal to 5% of the total electrolyzer capacity, as explained in Section 3.3.2.
- To ensure that the electrolyzer meets its minimum load requirement during periods of low power generation, the system can draw electricity from the grid at prevailing market prices. Therefore, it is necessary to incorporate an electricity connection with a capacity that is at least equal to the minimum load requirement of the electrolyzer.
- Hydrogen price is constant throughout the year.
- The model operates under the assumption that the system operator possesses a perfect forecast. This implies that, given specific capacities for the electrolyzer and electricity cable, the model will optimize the energy sales strategy based on historical data to maximize profitability. As explained in Section 1.4, this assumption is considered reasonable compared to reality.

[1]The lifetime of the system is based on the lifetime of the system components such as the wind turbines and compressors. From a developer's perspective, the economic lifetime (15 or 20 years) of the project might also be interesting. However, for the purpose of this research, only a lifetime of 25 years has been considered

Chapter 4

Results

In this chapter, the results of the simulation are presented. The chapter is structured as follows: In Section 4.1, the model is verified by using a set of dummy input variables. An analysis of a baseline case scenario is provided in Section 4.2, and in Section 4.3, a sensitivity analysis is performed on various parameters. Finally, in Section 4.4, the system is simulated for different scenarios.

4.1 Model verification

Before running the simulations, the model was verified in order to ensure that it performed as intended. For the purpose of this verification, a set of dummy parameters was used to cover all possible executions that the model can make in just a few hours of simulation. The electrolyzer capacity, cable capacity, and hydrogen price were held constant at 350 MW, 250 MW, and €5 per kg, respectively. The two varied parameters were the generated power of the wind farm and the electricity price. This setup, with the varying wind farm power and electricity price, is also in line with the actual simulation.

The results of the verification process are presented below. To cover all the possible executions, five hours were simulated. Table 4.1 presents the input and output values. Figure 4.1 shows a graph of the results.

As indicated by the results, the model has been successfully verified and is able to execute the model strategy as presented in Figure 3.5.

Table 4.1: Clarification table regarding the symbols used in Figure 3.5.

Hour	**Farm power [MW]**	**Electricity price [€/MWh]**	**Power electrolyzer [MW]**	**Power cable [MW]**	**Power curtailed [MW]**	**Grid Uptake [MW]**
1	400.0	60.0	350.0	50.0	0.0	0.0
2	175.0	140.0	17.5	157.5	0.0	0.0
3	500.0	-10.0	350.0	0.0	150.0	0.0
4	10.0	140.0	17.5	0.0	0.0	7.7
5	400.0	88.0	226.2	173.8	0.0	0.0

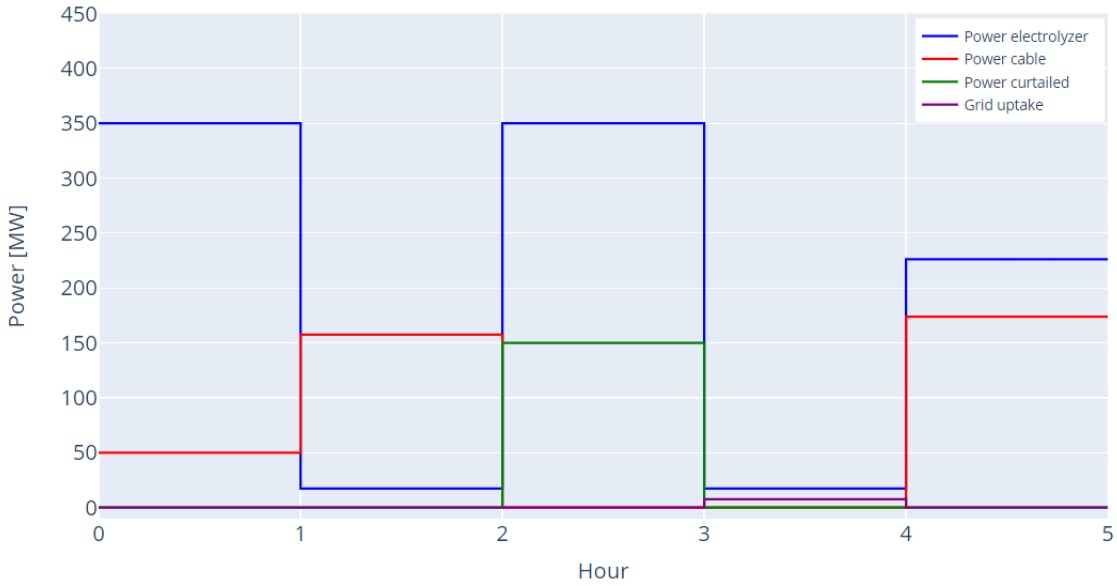

Figure 4.1: Output results of the verification process.

During the verification process, the following executions are made by the model:

- *First hour*: In the first hour, the wind farm generates 400 MW, which can be fully covered by the electrolyzer and cable size. Based on the market prices, producing hydrogen is more profitable than selling electricity directly. As a result, the full electrolyzer capacity of 350 MW is utilized for hydrogen production. Since the electricity price is positive, the remainder of the generated power (50 MW) is allocated to the cable for electricity sales. There is no grid uptake or energy curtailment.
- *Second hour*: During the second hour, it is more profitable to sell electricity instead of hydrogen. The wind farm generates a power of 175 MW, of which 17.5 MW is directed to the electrolyzer to sustain the minimal load constraint. The remainder of 175.5 MW can be fully covered by the capacity of the cable and is sold as electricity. There is no grid uptake or energy curtailment.
- *Third hour*: In the third hour, the electricity price is negative, and the wind farm's power output is 500 MW. The electrolyzer will operate at its full capacity of 350 MW. The remaining 150 MW is not sold as electricity since that would negatively influence the revenue and is therefore being curtailed. There is no grid uptake.
- *Fourth hour*: In the fourth hour, the wind farm only generates 10 MW, which is insufficient to meet the electrolyzer's minimal load demand. The system will draw 7.7 MW from the electricity grid in order to run the electrolyzer at 17.5 MW. Note that the uptake from the grid is slightly higher than the 7.5 MW the system needs because transformer losses are incorporated.
- *Fifth hour*: In the fifth hour, the sales of electricity and hydrogen are almost equally profitable. The generated power is 400 MW, which is less than the capacities of the electrolyzer and cable combined. In periods when these two conditions hold, the model will look for the most profitable combination of energy allocation. Operating the electrolyzer in part-load increases its conversion efficiency, which the system can take advantage of. For the given parameters, the model directs a power of 226.2 MW to the electrolyzer and 173.8 MW to the cable. There is no grid uptake or energy curtailment.

4.2 Baseline case analysis

To assess the performance of the system, a simulation was run for a baseline case scenario. In this section, the outcomes of this baseline case simulation are analyzed and discussed. The aim of this section is to give an insight into the behavior of the system.

The following parameters were set for the baseline case:

- A wind farm capacity of 1000MW.
- An average electricity price of €75 per MWh.
- A hydrogen price of €6 per kg.

4.2.1 Connection sizes and NPV

The baseline case scenario was simulated using different capacities for the electricity cable and the electrolyzer. The outcomes are depicted in Figure 4.2a. The cable capacity was limited to the wind farm's rated capacity since it is unnecessary to oversize the cable, considering the wind farm is not expected to generate more electricity than its rated power. To explore the potential benefits of operating the electrolyzer in the part-load regime, the electrolyzer was slightly oversized and its maximum size was set at 120% of the farm capacity. The minimum capacity of the electricity cable was set according to the minimum load requirement of the maximum electrolyzer capacity, which in this case was 60 MW (5% of 1200 MW).

The graph presents the findings through a heatmap, with darker shades of green representing a higher NPV compared to lighter shades. The corresponding values of NPV, measured in billion euros, are displayed on the color bar located to the right of the heatmap. Note that for most of the connection scenarios, the NPV is negative. Several key observations can be derived from the graph:

1. The findings of the baseline case reveal that oversizing the electrolyzer in relation to the farm capacity does not yield any advantages. As illustrated in the graph, the NPV declines when the electrolyzer's capacity surpasses the total capacity of the farm. This implies that although the electrolyzer operates more efficiently in partial-load conditions, it fails to outweigh the additional costs incurred by the system.

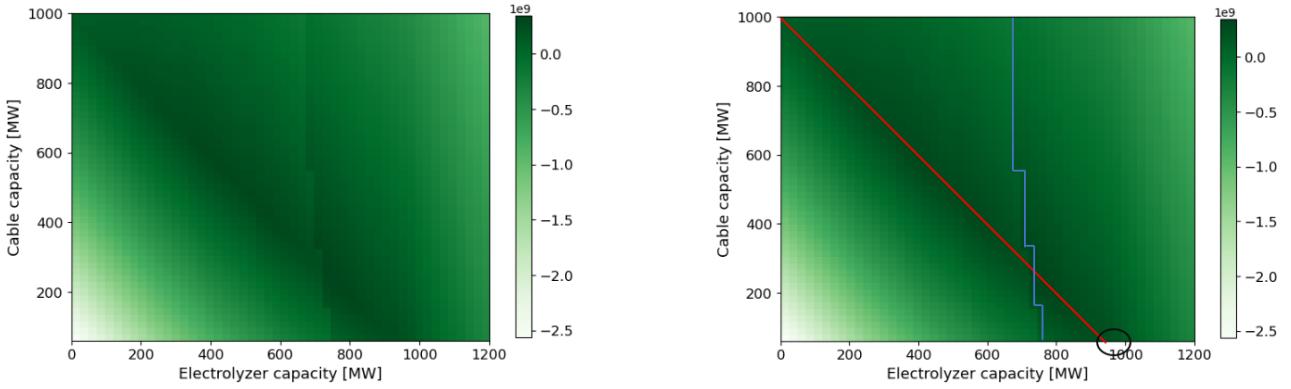

(a) (b)

Figure 4.2: Results of the baseline case simulation. Figure (a) shows the NPV [Billion €] of the baseline case scenario for various cable and electrolyzer capacities; Figure (b) is an analysis of figure (a) with in red: The linear relationship between cable and electrolyzer capacity for which the sum of the two equals the total wind farm capacity. And in blue: The combination of cable and electrolyzer capacity for which the stacks of the electrolyzer only need one replacement throughout the system's lifetime.

2. The graph shows a linear trend characterized by a high NPV. This trend is represented by the red line in Figure 4.2b. For each point along this line holds that the sum of the electrolyzer capacity and cable capacity is equal to the overall size of the farm. Consequently, it can be concluded that deviating from the farm's capacity by either oversizing or downsizing the total connection capacity relative to the farm is not beneficial. Note that this linear relationship crosses the x-axis slightly before reaching a 1000 MW electrolyzer size because the minimum cable size was set at 60 MW in this particular example. As a result, the line intersects the x-axis at 940 MW.
3. The results also reveal the presence of a step function at which the NPV increases. This step function is indicated by the blue line Figure 4.2b. This line represents a threshold indicating that the electrolyzer stacks require only one replacement over the lifetime of the system instead of two. Increasing the electrolyzer's capacity results in a decrease in full-load operating hours, which extends its lifespan. Given that the system operates for 25 years, it becomes financially beneficial if the electrolyzer's durability exceeds or equals 13 years.

4.2.2 Optimal connection configuration

Figure 4.2a demonstrates that in order to determine the optimal connection ratio between electricity and cable capacity, the model only needs to explore the linear trend where the combined connection capacities match the total capacity of the wind farm. The NPV along the relationship is illustrated below in Figure 4.3. For every electrolyzer capacity, there exists a corresponding cable capacity that ensures that the total connection size is equal to the wind farm's capacity (1000 MW).

The leftmost side of the graph, where the capacity of the electrolyzer equals zero, represents an all-electric scenario with no inclusion of an electrolyzer. The graph indicates that the NPV of the baseline case gradually increases by adding more electrolyzer capacity to the system up until an electrolyzer size of 400 MW. By increasing the electrolyzer size beyond 400 MW, the extra costs of the electrolyzer outweigh the benefits, and the NPV starts to gradually decrease.

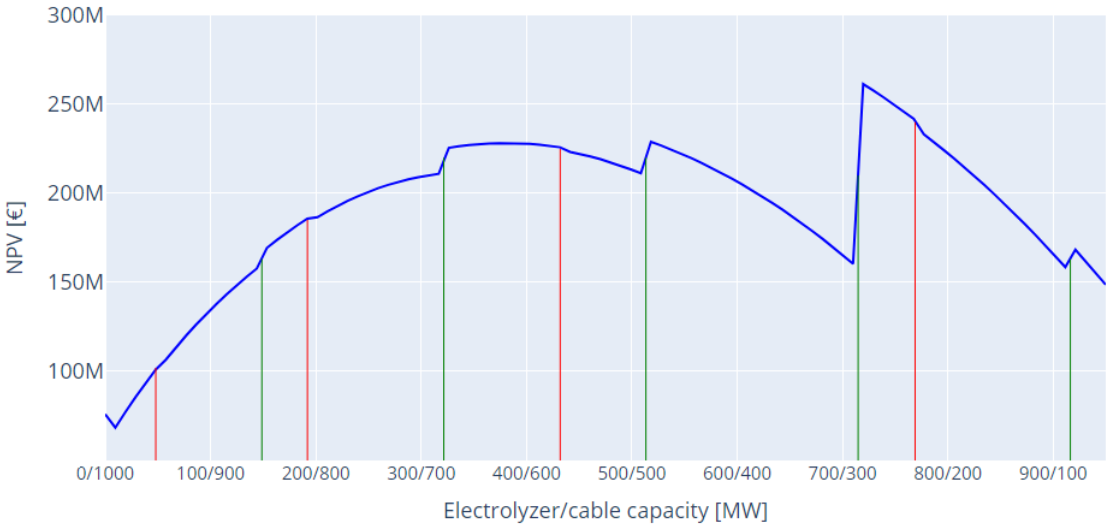

Figure 4.3: NPV as a function of connection ratio. The total connection size adds up to the total capacity of the wind farm (1000MW).

The curve also shows sudden increases, which are indicated by the green vertical lines. At these points, the electrolyzer's stack lifetime is extended by one year. As a result, the replacement of the electrolyzer stacks is discounted by an extra year, which benefits the NPV. At a certain point, the electrolyzer's stack lifetime reaches 13 years, which means that the replacement is necessary only once instead of twice during the lifetime of the system. This leads to a significant jump in NPV. For the baseline case, this point is found at an electrolyzer size of 720 MW and a cable capacity of 280 MW, which also represents the optimum configuration of connections for this specific scenario. The optimal configuration yields an NPV of 261 million euros.

Additionally, Figure 4.3 reveals minor decreases in the NPV at specific points, denoted by the red lines. At these points, the electrolyzer capacity reaches a threshold that requires a larger hydrogen pipeline diameter in order to transport the produced hydrogen. However, the graph indicates that the expenses associated with the pipeline are relatively minimal compared to the overall system costs because of the minor decline in NPV. One contributing factor to this is the assumption of a relatively short transportation distance to the offshore hydrogen grid, set at 30 km.

Table 4.2 presents the energy distribution for the optimal baseline case configuration. In this scenario, 18.3% of the total generated electricity is directly sold to the electricity grid, while 79.4% is allocated to the electrolyzer for hydrogen production. The remaining energy is accounted for by transformer losses and curtailment.

Despite the relatively high capacity of the electrolyzer, set at 720 MW, some energy is still being curtailed by the system. Energy curtailment occurs during hours when electricity prices are negative or when the connection capacity is insufficient to transport all the produced energy. Since most hours of negative electricity prices happen when the wind farm is operating at its rated capacity, there is still a curtailment of 280 MWh during those hours.

Table 4.2: Energy distribution for optimum baseline case scenario.

Parameter	**baseline case optimum**	**Unit**
Total generated electricity	4,714,716	MWh
Electricity directly sold	862,125	MWh
Electricity to electrolyzer	3,775,913	MWh
Hydrogen produced	72,732,519	kg
Electricity curtailed	12,876	MWh
Grid uptake	31,115	MWh
NPV	261,322,245	EUR

4.2.3 Hydrogen energy consumption

During the operation of the system, a decision is made by the model regarding the optimal use of the electricity. It considers whether to directly sell the electricity, curtail, or use it to produce hydrogen at a particular hour. To be able to determine its execution, the model must account for the energy losses when producing hydrogen.

The model calculates the hourly energy requirement for hydrogen production. The energy consumption for desalinating and demineralizing a cubic meter of water remains constant over time. Similarly, the energy required to compress a kilogram of hydrogen from 30 bar to 75 bar remains unchanged. The energy consumption of the electrolyzer, on the other hand, varies based on its load relative to its nominal capacity. Table 4.3 shows the energy consumption per component for producing a kilogram of hydrogen when the electrolyzer operates at nominal efficiency (full load).

Table 4.3: Energy consumption for hydrogen at $\eta_{elec,nom}$.

Process	**Energy consumption [kWh/kg]**	**Share**
Water treatment	0.07	0.13%
Electrolysis	52.03	98.06%
Compression	0.96	1.81 %
Total	53.06	100%

The table clearly demonstrates that the majority of the energy consumption required for producing one kilogram of hydrogen is accounted for by the electrolyzer. The values presented in the table reflect a scenario where the electrolyzer operates at its nominal efficiency of 64%. When the electrolyzer operates at a higher efficiency during part-load operation, its energy consumption decreases. Nevertheless, even if the electrolyzer were to achieve 100% efficiency, the electrolysis process would still contribute almost 97% to the overall energy consumption.

4.2.4 CAPEX and OPEX

To fully understand the system, it is necessary to look at which components incur the highest cost on the project. For the baseline case optimum, with a 1000 MW wind farm, 720 MW electrolyzer, and 280 MW cable, the total CAPEX and OPEX were:

- CAPEX: €4,446 million
- CAPEX: €92 million/year

Figure 4.4a illustrates the distribution of CAPEX among the different system components, while Figure 4.4b presents the breakdown of OPEX. The 'BOP' category in both figures combines the water treatment system, compressors, and platform.

In the optimal baseline case scenario, where the electrolyzer size accounts for 72% of the total system's connection capacity, the majority of the CAPEX is attributed to the electrolyzer and the wind farm. The CAPEX associated with the pipeline and electricity cable are almost negligible. However, a significant portion of the OPEX is allocated to transportation costs due to the annual grid fees associated with the transportation of electricity and hydrogen, which need to be paid to the Dutch grid operators. Note that these graphs reflect investment costs and annual costs; the electrolyzer stack replacement is not included.

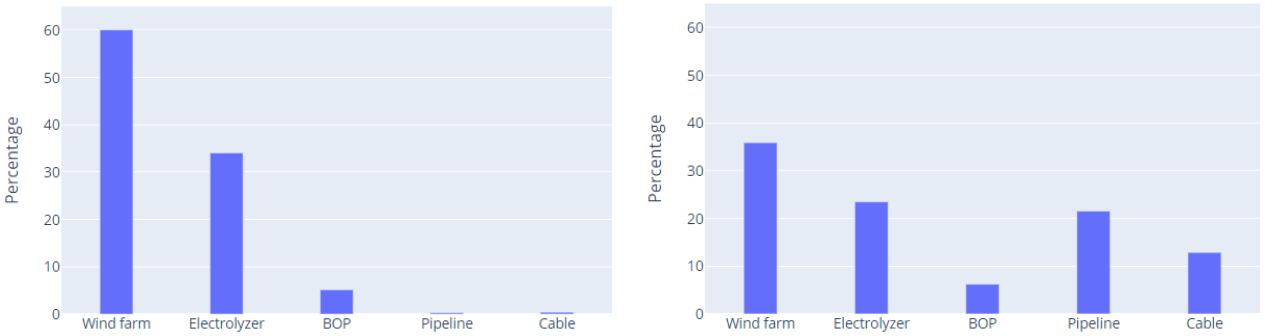

(a) (b)

Figure 4.4: Economic analysis per system component. In Figure (a), the share of each component to the total CAPEX is depicted. Figure (b) presents the percentage of the components to the total OPEX.

4.3 Sensitivity analysis

The previous section focused on analyzing the system's performance specifically for the baseline case scenario. However, this is just one scenario among many. The overall outlook and performance of the system are influenced by a range of parameters, which, in reality, may deviate from the assumptions made for the baseline case.

In this section, a sensitivity analysis is performed on several parameters that possibly have a significant effect on the system. To be able to compare the influence of the parameters on each other, every parameter described in this section is adjusted arbitrarily by plus and minus 15 percent in relation to the baseline case. The sensitivity analysis measures the impact of these adjustments on both the NPV and the optimal Electrolyzer/Cable (EC) ratio, using the baseline case as a reference. The results of the sensitivity analyses are summarized in Table 4.4 at the end of this section. Aside from the sensitivity analysis on the wind farm capacity in Section 4.3.1, only the linear trend established in Section 4.2.1 was investigated.

4.3.1 Wind farm capacity

To evaluate the sensitivity of the wind farm capacity, simulations were conducted considering both an 850 MW farm and an 1150 MW farm, representing variations of ±15% from the baseline case. The outcomes of these simulations are presented in Figure 4.5a and Figure 4.5b, respectively.

Compared to the baseline case simulation, the EC ratio remains unaffected. With all other parameters unchanged, the system and its optimal connection scale linearly with the total capacity of the farm. The graphs show a resemblance to Figure 4.2a, with only the axes being altered. However, there is a variation in the NPV for the optimal scenario. Since the baseline case reflects a positive scenario, scaling up the system enhances the NPV, whereas scaling it down diminishes the NPV.

When negative NPV scenarios are scaled up, the losses increase, as depicted in the graphs. In the case where the total farm capacity is 850 MW, the color bar range is approximately between -2.0 billion and 0.0. For the case with a total farm capacity of 1150 MW, the color bar range is approximately between -2.5 billion and 0.5 billion. This wider range stresses the extra losses for negative NPV scenarios and extra gains for positive ones.

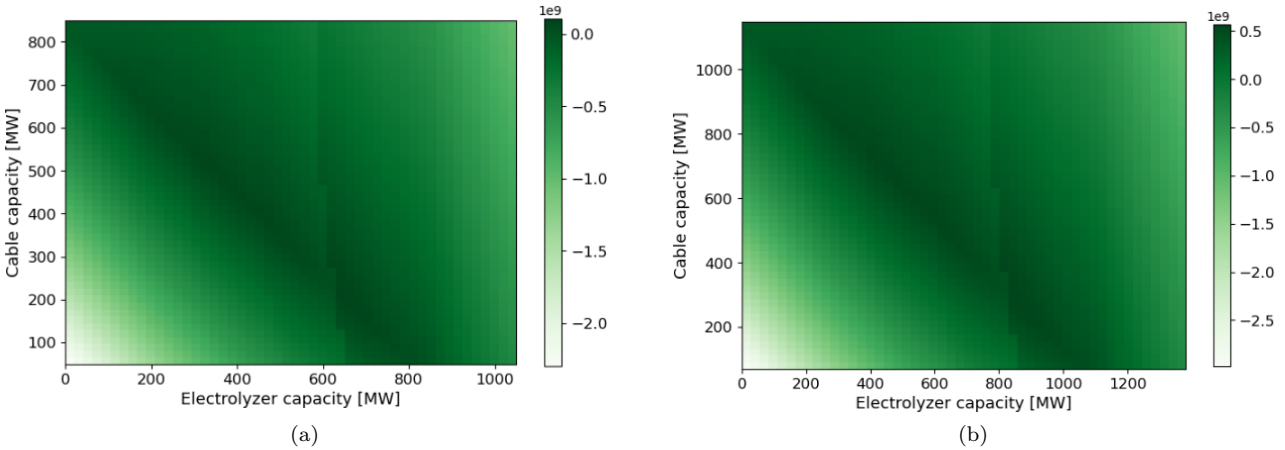

(a) (b)

Figure 4.5: Results of the sensitivity analysis on the capacity of the wind farm. Figure (a) illustrates the NPV for a farm with 850 MW capacity, and Figure (b) shows the NPV for an 1150 MW wind farm.

4.3.2 Wind farm costs

As pointed out in Section 4.2.4, the wind farm incurs the highest costs compared to other components. The model utilizes historical data to calculate the wind farm CAPEX. However, the cost of wind energy may vary, as mentioned in Section 3.1.2. The outcomes of the sensitivity analysis on wind farm costs can be observed in Figure 4.6a and Figure 4.6b.

Regarding the EC ratio, there is no alteration in the system. In fact, both graphs exhibit similar behavior to each other and to the baseline case scenario. Since the other parameters remain unchanged, the optimal solution for maximizing yearly cash flows, and thus the optimal EC ratio, remains the same for both situations as in the baseline case.

However, the variation in the cost of wind energy significantly affects the NPV. A 15% deviation in the wind farm costs leads to a nearly 170% change in NPV. In the scenario where costs increase by 15%, the NPV drops considerably and becomes negative.

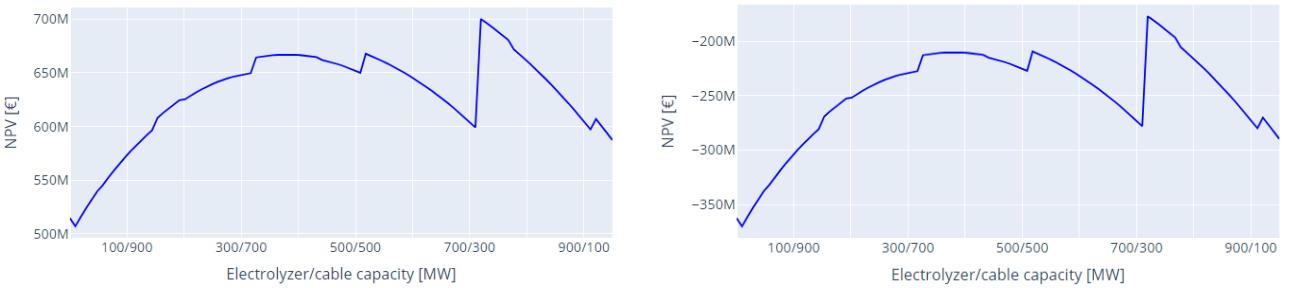

(a) (b)

Figure 4.6: Results of the sensitivity analysis on the wind farm costs. Figure (a) illustrates the NPV for a scenario with -15% cost of wind energy, and Figure (b) shows the NPV for a scenario with a wind farm that is 15% more expensive.

4.3.3 Electrolyzer costs

Electrolyzer technologies are currently undergoing active development, and various studies indicate a future decline in electrolyzer costs. The sensitivity analysis results concerning electrolyzer cost can be observed in Figure 4.7a and Figure 4.7b.

Intuitively, the NPV of a project changes when the electrolyzer costs are varied. On the leftmost sides of both graphs, where no electrolyzer capacity is included, the NPV remains unaffected, and both graphs exhibit the same starting point. However, when observing the optimum NPV

(a) (b)

Figure 4.7: Results of the sensitivity analysis on the electrolyzer cost. Figure (a) illustrates the NPV for a scenario with a 15% cost reduction, and Figure (b) shows the NPV for a scenario with a 15% cost increase.

for both scenarios, there is a significant difference. A lower electrolyzer cost leads to a higher NPV, while a higher electrolyzer cost corresponds to a lower NPV.

When the electrolyzer costs decrease by 15%, the system benefits from additional electrolyzer capacity. The slope progressively rises until reaching an EC ratio of 740/260. In comparison, for the baseline case scenario, this was up until an EC ratio of only 400/600. Conversely, when the price of the electrolyzer increases by 15%, the NPV experiences a decline upon adding more electrolyzer capacity more quickly. The tipping point for this scenario, where the slope of the curve starts to decrease, is already reached at an EC ratio of 170/830.

4.3.4 Electrolyzer stack lifetime

By altering the lifetime of the stack, its replacement schedule is affected, which is expected to influence the system according to Section 4.2.2. The results of the sensitivity analysis on the electrolyzer stack lifetime are depicted in Figures 4.8a and 4.8b.

When the stack lifespan is reduced by 15%, there is no longer any point on the graph where the stacks can only be replaced once. As a consequence, the significant increase in NPV that was observed in the baseline case scenario is no longer present. The absence of this jump eliminates the justification for choosing a larger electrolyzer size, resulting in a decrease in the optimal EC ratio. Additionally, the optimal NPV for this scenario declines as the model now needs to consider two stack replacements over the system's lifetime.

For a prolonged lifespan of the electrolyzer stack, the benefit of only one stack replacement occurs at a lower electrolyzer capacity relative to the baseline case. As a result, the jump in NPV is witnessed before the slope of the curve starts to decline. The optimal NPV is now found around the tipping point of the curve gradient rather than afterwards. Consequently, the optimal EC ratio drops relative to the baseline case, while the optimal NPV increases.

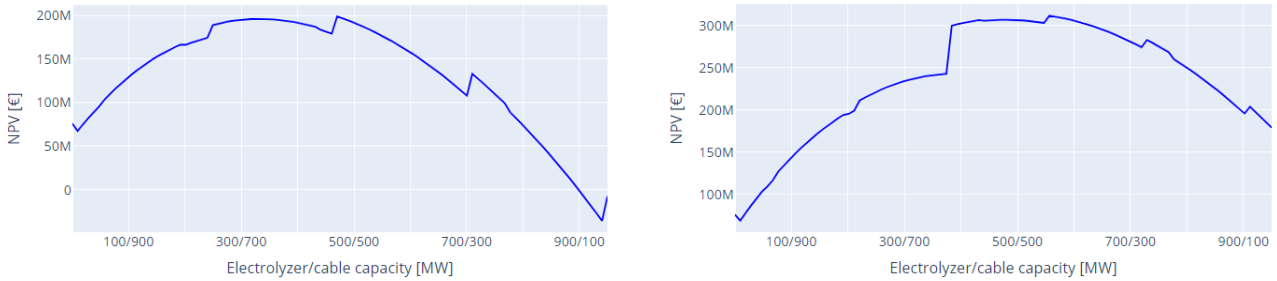

Figure 4.8: Results of the sensitivity analysis on the stack lifetime. Figure (a) illustrates the NPV for a scenario with a 15% lifetime reduction, and Figure (b) shows the NPV for a scenario with a 15% lifetime increase.

4.3.5 Electrolyzer efficiency

As outlined in Section 4.2.3, almost all of the required energy to produce hydrogen is accounted for by the electrolyzer. Therefore, a change in the operating efficiency of the electrolyzer is expected to affect the system. The results of the sensitivity analysis on the nominal efficiency of the electrolyzer are presented in Figure 4.9a and 4.9b. Note that a deviation of 15% is relative to the baseline case nominal efficiency of 64%. This means that the efficiency effectively changes with 9.6%.

Figure 4.9a depicts the relationship between NPV and connection configuration in a system where the electrolyzer efficiency is reduced. In this scenario, it is not beneficial to incorporate

any electrolyzer capacity into the system as the NPV continues to drop as more electrolyzer capacity is added. The optimal NPV is consequently achieved at an EC ratio of 0/1000.

Conversely, in a situation where the nominal efficiency of the electrolyzer is increased by 15% relative to the baseline case, the system experiences significant benefits from the addition of more electrolyzer capacity. Figure 4.9b clearly demonstrates this relationship. The maximum NPV is attained at an EC ratio of 920/80 and amounts to nearly one billion.

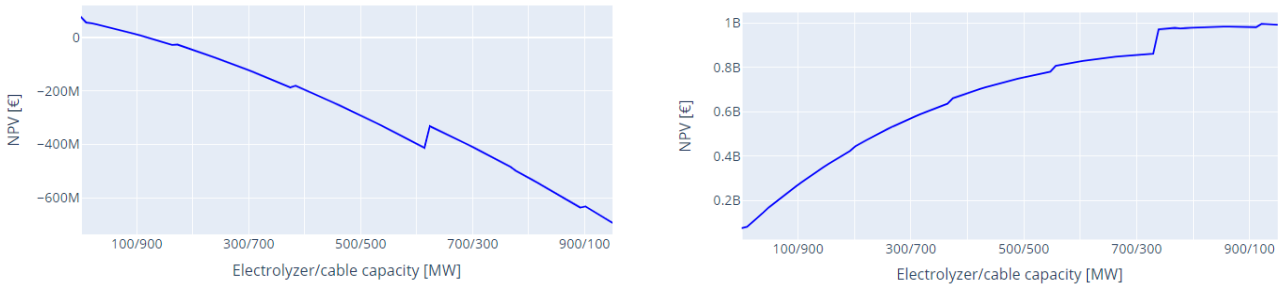

(a) (b)

Figure 4.9: Results of the sensitivity analysis on the electrolyzer efficiency. Figure (a) depicts the NPV for a scenario with a – 15% efficiency, and Figure (b) presents the NPV for a scenario with a + 15% efficiency.

4.3.6 Hydrogen price

The hydrogen price is one of the major assumptions in this study. Given the absence of a fully developed green hydrogen market, there remains uncertainty around the future cost of hydrogen. Figures 4.10a and 4.10b show the results of the sensitivity analysis on the hydrogen price.

Both graphs depicted in Figures 4.10a and 4.10b show similar behavior to those of the sensitivity analysis on the electrolyzer nominal efficiency. When the hydrogen price decreases by 15%, the addition of any electrolyzer capacity does not contribute to the NPV of the project.

However, when the hydrogen price is increased by 15%, it is beneficial to build a system with an almost fully electrolyzer-based connection. For this scenario, The optimum NPV is found at an EC ratio of 930/70 and surpasses one billion euros.

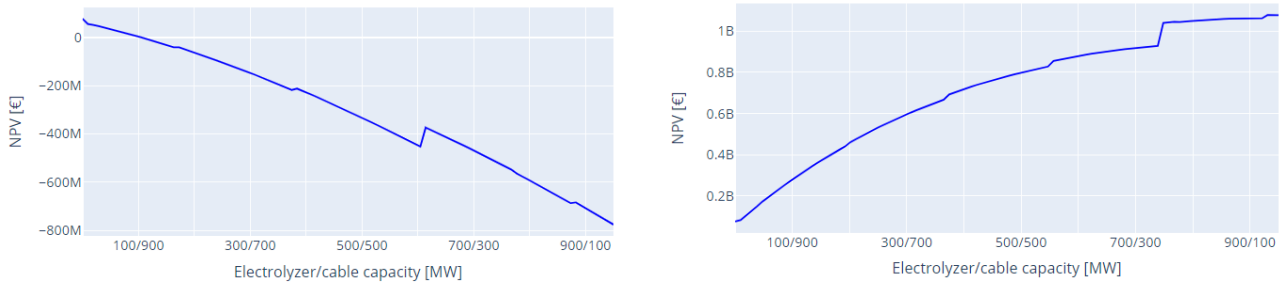

(a) (b)

Figure 4.10: Results of the sensitivity analysis on the hydrogen price. Figure (a) illustrates the NPV for a scenario where the hydrogen price is decreased by 15%, and figure (b) shows the NPV for a scenario with a cost of hydrogen that is 15% higher.

4.3.7 Electricity price

The electricity pricing in this study is based on historical data. For the baseline case, the mean electricity price was set to €75 per MWh. In the future, the electricity prices will deviate from the ones used in this research. The results of the sensitivity analysis on the electricity price are presented in Figure 4.11a and 4.11b.

The results demonstrate that electricity pricing has a significant impact on both the EC ratio and NPV. A 15% increase in the mean electricity price favors an all-electric wind farm without hydrogen production, whereas a reduction in electricity prices creates a favorable environment for integrating considerable electrolyzer capacity.

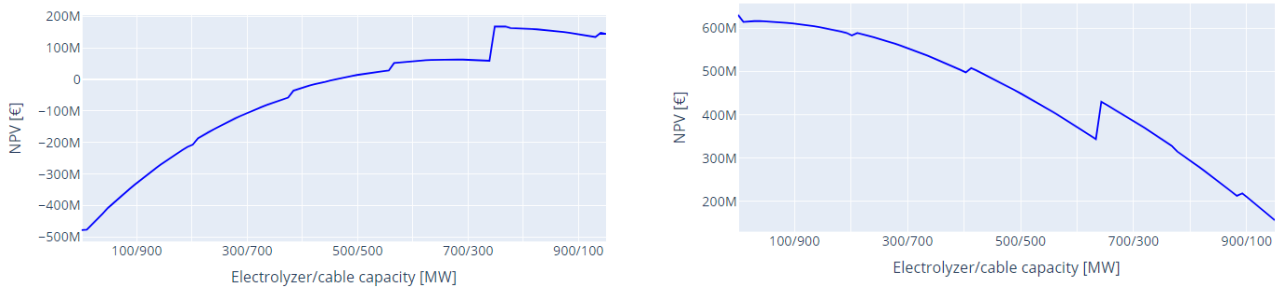

(a) (b)

Figure 4.11: Results of the sensitivity analysis on the mean electricity price. Figure (a) presents the NPV for a scenario with a 15% decline in electricity price, and figure (b) shows the NPV for a scenario with a cost of electricity that is 15% higher.

4.3.8 Summary of sensitivity analyses

The outcome of the sensitivity analyses is summarized in Table 4.4. The displayed changes in EC ratio and NPV are relative to the baseline case scenario. Key parameters that influence the EC ratio are the electrolyzer efficiency, the electricity price, and the hydrogen price.

Table 4.4: Summary of the sensitivity analyses.

Parameter	Offset	Optimal EC ratio	Change in EC ratio	Maximum NPV	Change in NPV
baseline case	± 0%	720/280	-	261M	-
Farm capacity	– 15%	610/240	± 0.0%	107M	– 59.0%
	+15%	830/320	± 0.0%	435M	+66.7%
Farm costs	– 15%	720/280	± 0.0%	700M	+168.2%
	+15%	720/280	± 0.0%	-178M	– 168.2%
Electrolyzer costs	– 15%	740/260	+10.6%	455M	+74.3%
	+15%	170/830	– 92.0%	104M	– 60.2%
Stack lifetime	– 15%	470/530	– 65.5%	199M	– 23.8%
	+15%	560/440	– 50.5%	311M	+19.2%
Electrolyzer efficiency	– 15%	0/1000	– 100.0%	76M	– 70.9%
	+15%	920/80	+347.2%	979M	+275.1%
Hydrogen price	– 15%	0/1000	– 100.0%	76M	– 70.9%
	+15%	930/70	+416.7%	1.08B	+313.8%
Electricity price	– 15%	750/250	+16.7%	168M	– 35.6%
	+15%	0/1000	– 100.0%	630M	+141.4%

4.4 Scenario analysis

In the previous section, sensitivity analyses were performed on several system parameters. As presented in Table 4.4, many of the parameters have a significant impact on both the optimal NPV and its corresponding EC ratio of the system. The parameters that were discussed for sensitivity will, in reality, deviate simultaneously rather than individually. In this section, the optimal NPV and its corresponding EC ratio are visualized as a function of the hydrogen price for different scenarios.

4.4.1 Scenario definitions

According to the sensitivity analysis, the optimal EC ratio was affected by the characteristics of the electrolyzer, the hydrogen price, and the electricity price. To reflect on simultaneous changes in these parameters, certain scenarios were defined.

For the purpose of this scenario analysis, three electrolyzer scenario's based on the potential future stage of development were considered. These scenarios are presented in Table 4.5. The case where the electrolyzer experiences low development reflects the scenario which was also used for the baseline case in Section 4.2. These costs and characteristics are based on vendor information and on the experience of Eneco and resemble the performance of an electrolyzer that is commercially available today. Scenarios 'Electrolyzer 2' and 'Electrolyzer 3' illustrate moderate and high development, respectively. In each subsequent development stage, the associated costs are slightly reduced while the stack lifetime and efficiency are increased.

Each electrolyzer scenario is evaluated for different prices of hydrogen and electricity. The following three mean electricity prices were considered:

1. €65 per MWh
2. €75 per MWh
3. €85 per MWh

The hydrogen price is arguably the most uncertain parameter in this research since a market for green hydrogen has not yet been established. The future pricing of hydrogen depends on the industry's willingness to pay and potential government subsidies that might be added to promote the development of green hydrogen facilities. Consequently, a wide range of hydrogen prices were considered. For the purpose of this scenario analysis, the hydrogen price is considered as a variable that ranges from €3/kg to €8/kg. This range of hydrogen pricing was set in consultation with Eneco.

The capacity of the wind farm and the associated costs were kept constant at the values used in the baseline case scenario. According to the sensitivity analysis, these parameters do not have an influence on the optimal EC ratio.

Table 4.5: Three different electrolyzer scenarios based on potential future development.

Scenario	**Development**	**Electrolyzer cost**	**BOS costs**	**Stack lifetime**	**Nominal efficiency**
Electrolyzer 1	Low	€1300/kW	€700/kW	70,000 hr	64%
Electrolyzer 2	Moderate	€1100/kW	€600/kW	80,000 hr	67%
Electrolyzer 3	High	€900/kW	€500/kW	90,000 hr	70%

4.4.2 Scenario results

In this section, the outcomes of the scenario analyses are presented. Each simulation maintains a total farm capacity of 1000 MW. Considering the minimal cable capacity constraint, which requires 5% of the total electrolyzer capacity, the maximum EC ratio was set at 950/50.

Figure 4.14 shows the results of the scenario for which the mean electricity price was set at €65 per MWh. The optimal EC ratio for the different electrolyzer scenarios as a function of the hydrogen price is depicted in Figure 4.14a. The graph clearly illustrates that whether it is beneficial to incorporate an electrolyzer into the design depends on the stage of development of the electrolyzer. If the technology experiences a high level of development in the coming years, incorporating an electrolyzer may be beneficial from a hydrogen price of €4 per kg. However, when no progress is being made, it would not make sense to incorporate any electrolyzer capacity for a hydrogen price lower than €5 per kg.

Figure 4.14b displays NPV corresponding to the optimal EC ratio for different scenarios. When considering an electricity price of €65 per MWh, theNPV for the all-electric case, with an EC ratio of 0/1000, is negative, indicating that the project is not economically viable from a developer's perspective. However, as the hydrogen price increases along the x-axis, the NPV of the project gradually improves and becomes positive. For the 'Electrolyzer 3' scenario, this shift to a positive NPV occurs at a hydrogen price of €4.70/kg, with an EC ratio of approximately 750/250. On the other hand, to achieve a positive NPV in the 'Electrolyzer 1' scenario, the hydrogen price must reach €5.80/kg.

Another noticeable aspect of this analysis is that for the highly developed electrolyzer, for which the lifespan was set at 90,000 full-load operating hours, the stacks only need one replacement regardless of the electrolyzer capacity. As a result, the curve of the 'Electrolyzer 3' scenario becomes more smooth.

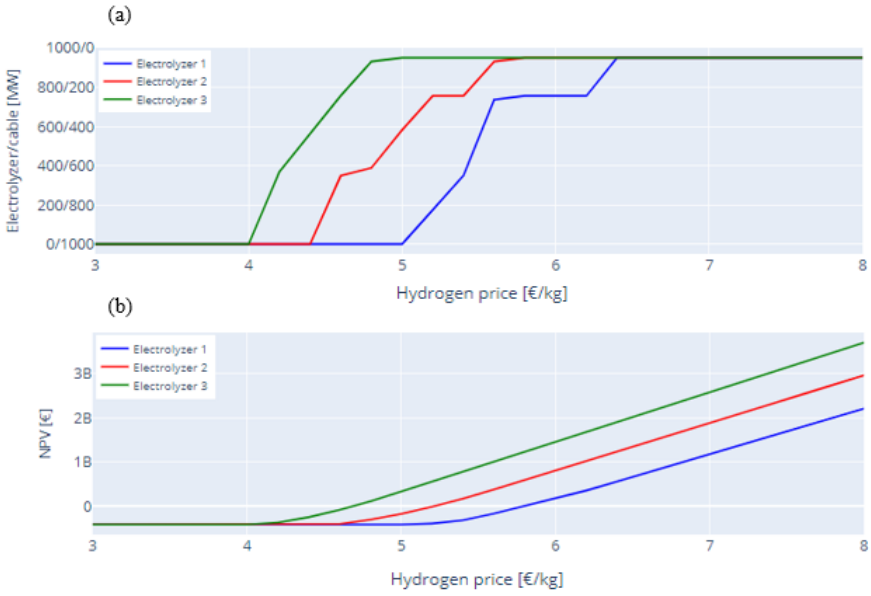

Figure 4.12: Results of the scenario analysis with a mean electricity price of €65 per MWh. In Figure (a), the optimal EC ratio as a function of the hydrogen price is presented. The corresponding NPV is found in Figure (b).

The results of the scenario analyses for an electricity price of €75 per MWh and €85 per MWh are presented in Figure 4.13 and Figure 4.14, respectively. Intuitively, when the mean electricity price is increased, it benefits the all-electric scenario. As a result, the incorporation

of an electrolyzer becomes favorable at higher hydrogen prices compared to the €65 per MWh scenario. The graphs show more or less similar behavior compared to Figure 4.14. However, the optimal EC ratio curves shift towards the right and the corresponding NPV's are all positive.

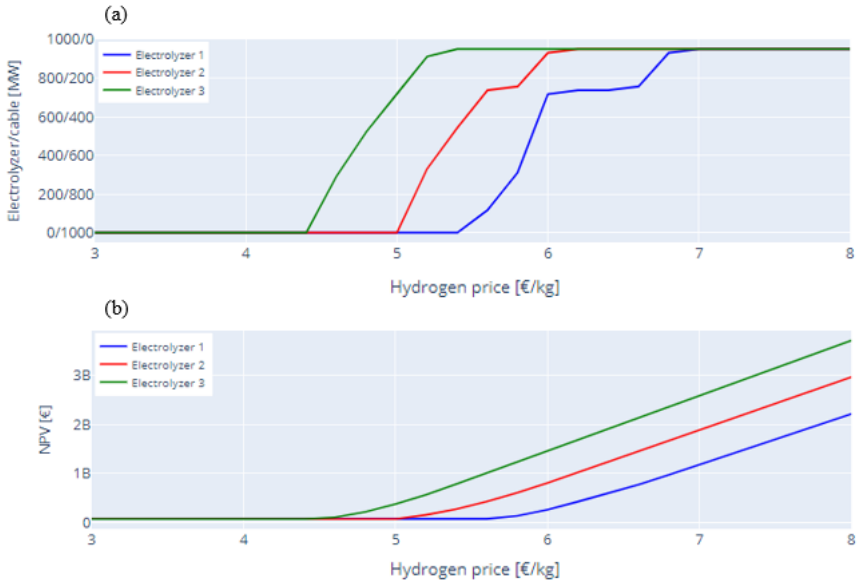

Figure 4.13: Results of the scenario analysis with a mean electricity price of €75 per MWh. In Figure (a), the optimal EC ratio as a function of the hydrogen price is presented. The corresponding NPV is found in Figure (b).

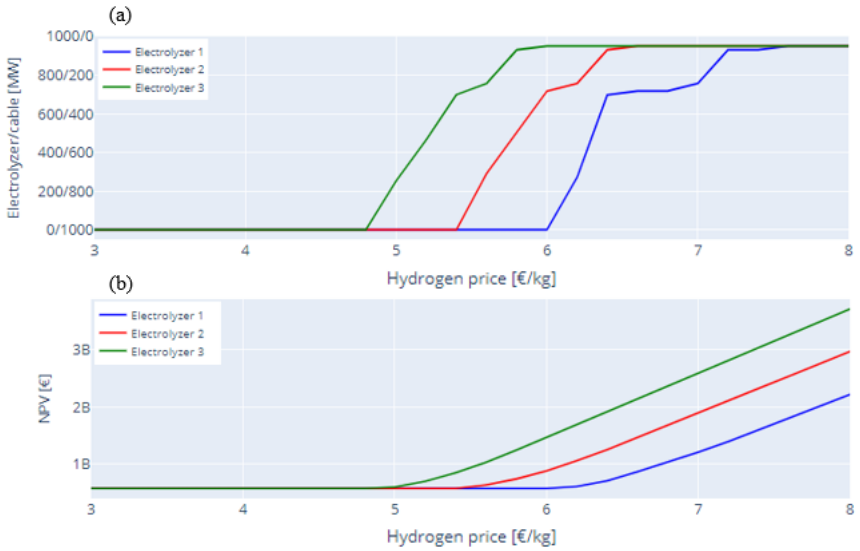

Figure 4.14: Results of the scenario analysis with a mean electricity price of €85 per MWh. In Figure (a), the optimal EC ratio as a function of the hydrogen price is presented. The corresponding NPV is found in Figure (b).

The figures presented in this section illustrate the significance of the electrolyzer's development stage when assessing the circumstances under which adding an electrolyzer becomes advantageous. Moreover, they reveal that the extent to which electrolyzer capacity should be integrated into the system is highly sensitive to the hydrogen price. The transition from an EC ratio of 0/1000 to 950/50 occurs within a relatively narrow hydrogen price range of approximately €1-€1.5 per kg for all electrolyzer scenarios.

Chapter 5

Conclusions

This master's thesis was concerned with the design and operation of a hybrid wind farm containing offshore electrolysis. In this chapter, the research is concluded and is structured as follows: In Section 5.1, the research is summarized, the research question of this study is answered and several conclusions are drawn from the findings. Some limitations of this research that the reader should be aware of are outlined in Section 5.2, and, finally, in Section 5.3, the research topic is discussed and recommendations for future research are made.

5.1 Summary

Due to its many applications, hydrogen is expected to play a vital role in a 100%-renewable future. Recognizing the importance of green hydrogen, the European Union has set goals to connect considerable renewable capacities to electrolysis. Given their strategic positioning to the North Sea, combining offshore wind energy with electrolysis is particularly of interest for North Western Europe. Therefore, in this research, an analysis was performed on a case study of a hybrid wind farm in the Dutch North Sea with the objective to answer the following research question:

"What is the optimal ratio between electricity and hydrogen connections to maximize the net present value of a wind farm with offshore electrolysis?"

The approach to answering this research question was made from a developer's perspective by assuming a perfect forecast and optimizing the sales of hydrogen and electricity per hour. A model was built in Python to execute the simulation for a certain set of input parameters. By incrementally altering the input parameters, the behavior of the system and the corresponding EC (Electrolyzer/Cable) ratio and NPV (Net Present Value) could be established.

The results show that the optimal EC ratio for maximizing the NPV is found at a linear relationship where the sum of the electrolyzer and electricity cable capacity equals the total capacity of the farm. Downsizing or oversizing the total connection capacity relative to the farm did not yield any benefits to the NPV, despite the electrolyzer's enhanced operation efficiency in the part-load regime. Where the actual optimum is found along this linear trend depends on a number of variables. To gain further insights, a sensitivity analysis was conducted to assess the impact of individual parameters. From this analysis, the following conclusions can be drawn:

1. The optimal EC ratio remained unaffected by both the farm capacity and the costs associated with the wind farm. Throughout the range of tested farm sizes, spanning from 850 MW to 1150 MW, the optimum connection sizes demonstrated a linear scaling,

resulting in the same EC ratio. While changes in the cost of wind energy do not alter the preferred EC ratio, they significantly impact the overall value of the NPV since the wind farm constitutes the largest expense within the system. Despite this, the EC ratio remains unchanged in optimizing the project's economic performance.

2. The characteristics of the electrolyzer, such as the stack lifetime, cost per kW, and efficiency, all affected both the NPV and the EC ratio. Among these characteristics, the nominal efficiency of the electrolyzer had the most significant impact on the system, followed by the costs and the stack lifetime, respectively. In the case of a hybrid wind farm with a projected lifetime of 25 years, particular attention should be given to the stack replacement. The study indicated that for stack lifetimes below 90,000 full-load operating hours, a second stack replacement can be avoided by appropriately sizing the electrolyzer capacity. When the electrolyzer lifetime surpasses 90,000 full-load operating hours, the stacks only require replacement once during the entire lifetime, regardless of the size of the electrolyzer.
3. Among the other parameters, the electricity and hydrogen pricing exerted the most influence on the system. Deviations in the mean electricity and hydrogen price can determine whether the system favors an all-eclectic system or a system where the full focus lies on producing hydrogen.

So, to concisely answer the research question on what the optimal configuration of electricity and hydrogen connection is to maximize the NPV:

While an optimum can be established, it depends on the circumstances that a developer is working with.

Deciding on an optimal EC ratio for a hybrid wind farm is particularly challenging due to the uncertainty of the parameters. The electrolyzer technology, especially in the context of large-scale systems, is still undergoing development and refinement. Additionally, the price of green hydrogen is influenced by factors such as industry willingness to pay and potential government subsidies. These uncertainties create a complex landscape for decision-making from a developer's perspective.

To address these uncertainties, several scenarios that could be representative of the near future were investigated. Each scenario considered a different developmental stage for the electrolyzer technology and a different mean electricity price. The system was then tested across various hydrogen prices, ranging from €3/kg to €8/kg. The results showed that, for none of the investigated scenarios, it was economically viable to incorporate an electrolyzer into the design when the hydrogen price was below €4/kg. On the other hand, as the hydrogen price exceeded €7.50/kg, the model favored a system where the total connection capacity was predominantly allocated to the electrolyzer. In between these hydrogen prices, hybrid solutions between electricity and hydrogen connection are found to maximize the NPV.

The results also revealed that, for each investigated scenario, the transition from an all-electric to a fully electrolyzer-employed system occurs within a hydrogen price range of approximately €1-€1.5. This suggests that there actually is a rather narrow hydrogen price range for which a hybrid system would make economic sense from a developer's perspective.

5.2 Limitations

Like any other techno-economic case study trying to forecast the profitability of a project containing an undeveloped technology, this research rests on many assumptions. Although the values used in this research were carefully considered by consulting multiple sources, deviation from reality is inevitable. It is obvious that the more research is performed on the cost estimations as offshore electrolysis develops over time, the more accurate a techno-economic study becomes. However, some limitations that are particularly relevant to this research are listed below:

1. A large underlying assumption in this thesis was that the developer possesses a perfect forecast of electricity and hydrogen prices. However, in practice, a developer relies on future projections rather than historical data to operate a hybrid wind farm. These future price projections are never a 100% accurate, leading to sub-optimal power allocation in reality. As a result, the system's electrolyzer full-operating hours and cash flows could be affected, potentially altering the final outcomes of the study.
2. The simulation relied solely on data from a single year for electricity pricing and wind power generation. The assumption was that this year's data is representative of the entire system's lifetime. Consequently, the model optimized the cash flow based on the data of this specific year and extrapolated the results. From an analytical point of view, using data from multiple years would provide a more accurate basis for estimating the NPV of a project. However, it is important to note that the electricity market is highly volatile and susceptible to unforeseen factors, as witnessed in recent years. This makes it challenging to create reliable forecasts, even with more data.
3. The optimal configuration of the electricity cable and electrolyzer connection was derived based on achieving the highest NPV. While NPV is a robust and reliable financial metric, it is advisable to evaluate the economic feasibility using multiple financial metrics. As mentioned in Section 1.3.1, one limitation of NPV is its inability to provide insights into the actual return on investment. Moreover, in this study, all configurations were assessed under the assumption of equal risk. However, it could be argued that the risk of a project rises with increasing electrolyzer capacity, given the current immaturity of the green hydrogen market. As a result, such projects would suffer from a higher discount rate, which would alter the results of this study.
4. Currently, there remains limited information about the impact of part-load operation on the lifetime of an electrolyzer. In this research, it was assumed that part-load operation does not lead to a reduction in the number of full-load operating hours. However, further investigations are needed to understand the effects of coupling intermittent sources to electrolyzers on their lifetimes. Since the stack replacement turned out to be a determining factor for where the optimal EC ratio was found, it is imperative to consider the lifetime more accurately in future research.

5.3 Recommendations

Coupling renewables to electrolysis in order to produce green hydrogen is a much-discussed topic in the literature. With the rising demand for green hydrogen, institutions and developers are investigating how to efficiently incorporate hydrogen production into their systems. This study adds knowledge to the design and operation of a wind farm containing offshore electrolysis from a developer's perspective. But how should these results be interpreted? And would this optimal solution for developers also be optimal for society?

In this study, the primary focus was on determining the optimal ratio between the electricity and hydrogen connection. As revealed by the sensitivity analysis described in Section 4.3, this optimum position is influenced by various system parameters, one of which is the cost of the electrolyzer. For this study, the total CAPEX of the electrolyzer was assumed at €2000/kW, a relatively high estimate compared to values reported in other literature. For instance, in the techno-economic studies conducted by Scolaro and Kittner [14] and Giampieri et al. [56], the electrolyzer CAPEX was considered as €700/kW and €1095/kW, respectively. It is evident that adopting either of these values for this study would have led to different conclusions, favoring the incorporation of an electrolyzer at lower hydrogen prices. Consequently, it is recommended to pursue ongoing and up-to-date techno-economic analyses. As the technology continues to mature, the estimation of prices and performances will improve.

Nonetheless, the estimated values in this research have been carefully considered by reviewing studies based on historical data, like the ones published by Kim et al. [34] and Viera et al. [61], vendor quotes, and the expertise of Eneco. So, assuming the values used in this study accurately describe reality, this study offers insights to developers on how to appropriately size the electricity and hydrogen connection for an offshore hybrid wind farm. Based on the scenario graphs in Section 4.4, a developer could learn how to size these connections under different circumstances of electricity pricing, hydrogen pricing, and electrolyzer development in order to maximize the profitability of the farm.

In practice, governments set out tenders for wind farm projects open to bids from developers. Recently, the Dutch government issued a tender for the construction of an offshore hybrid wind farm which is supposed to incorporate 500 MW of electrolysis. By using the findings presented in this study, developers can make estimations of the hydrogen price at which the project would achieve economic viability.

To compete with the current pricing of gray hydrogen, it is likely that the government will provide a subsidy on green hydrogen to make the projects financially feasible. Since it is plausible that society will partly cover the costs of green hydrogen, it brings us to the next question: Does the optimal solution perceived by developers, which is determined based on profitability and financial considerations, align with what is optimal for society as a whole? To answer this question, it is advised that a social-economic study regarding the implementation of wind-to-hydrogen systems is conducted.

The findings of this study suggest that whether a hybrid wind farm shifts from mainly electricity sales to primarily focusing on the sales of hydrogen occurs with small changes to the hydrogen and electricity price. The question is if society benefits from such an intermittent power allocation strategy. Although electrolyzers can help alleviate the electricity grid, they could also cause destabilization of the grid if all wind farm developers would operate their electrolyzers in times when producing hydrogen seems more profitable.

Whether the government should aim for hybrid farms or a combination of all-electric and all-hydrogen based systems is an interesting topic for further research. When addressing this question, a comparison should be made between hybrid systems and all-hydrogen ones. Systems

that are solely connected to an electrolyzer should have a battery bank incorporated into their designs to be able to sustain the minimal load of the electrolyzer but the costs associated with electricity transport are avoided.

Bibliography

[1] Lizer Ramirez, Daniel Fraile, and Guy Brindley. Offshore wind in europe: Key trends and statistics 2020. Technical report, Wind Europe, 2021.

[2] European Commission. A strategy to harness the potential of offshore renewable energy for a climate neutral future. Technical Report SWD(2020) 273, EU Commission, 2020.

[3] Hans Schermeyer, Michael Studer, Manuel Ruppert, and Wolf Fichtner. Understanding distribution grid congestion caused by electricity generation from renewables. In *Smart Energy Research. At the Crossroads of Engineering, Economics, and Computer Science: 3rd and 4th IFIP TC 12 International Conferences, SmartER Europe 2016 and 2017, Essen, Germany, February 16-18, 2016, and February 9, 2017, Revised Selected Papers 4*, pages 78–89. Springer, 2017.

[4] Iratxe Gonzalez-Aparicio, Anthony Vitulli, Siddharth Krishna-Swamy, Ricardo Hernandez-Serna, Niels Jansen, and Pieter Vertraten. Offshore wind business feasibility in a flexible and electrified dutch energy market by 2030. Technical report, TNO, 2022.

[5] Joakim Andersson and Stefan Grönkvist. Large-scale storage of hydrogen. *International journal of hydrogen energy*, 44(23):11901–11919, 2019.

[6] Jose Bellosta Von Colbe, Jose-Ramón Ares, Jussara Barale, Marcello Baricco, Craig Buckley, Giovanni Capurso, Noris Gallandat, David M Grant, Matylda N Guzik, Isaac Jacob, et al. Application of hydrides in hydrogen storage and compression: Achievements, outlook and perspectives. *international journal of hydrogen energy*, 44(15):7780–7808, 2019.

[7] Gonçalo Calado and Rui Castro. Hydrogen production from offshore wind parks: Current situation and future perspectives. *Applied Sciences*, 11(12):5561, 2021.

[8] Meiling Yue, Hugo Lambert, Elodie Pahon, Robin Roche, Samir Jemei, and Daniel Hissel. Hydrogen energy systems: A critical review of technologies, applications, trends and challenges. *Renewable and Sustainable Energy Reviews*, 146:111180, 2021.

[9] Christopher J Quarton and Sheila Samsatli. Power-to-gas for injection into the gas grid: What can we learn from real-life projects, economic assessments and systems modelling? *Renewable and sustainable energy reviews*, 98:302–316, 2018.

[10] Martin Thema, Franz Bauer, and Michael Sterner. Power-to-gas: Electrolysis and methanation status review. *Renewable and Sustainable Energy Reviews*, 112:775–787, 2019.

[11] IEA. Global hydrogen demand by sector in the Net Zero Scenario, 2019-2030. `https://www.iea.org/data-and-statistics/charts/global-hydrogen-demand-by-sector-in-the-net-zero-scenario-2019-2030`, 2021. Accessed: 2023-02-15.

[12] Nigel Rambhujun, Muhammad Saad Salman, Ting Wang, Chulaluck Pratthana, Prabal Sapkota, Mehdi Costalin, Qiwen Lai, and Kondo-Francois Aguey-Zinsou. Renewable hydrogen for the chemical industry. *MRS Energy & Sustainability*, 7:E33, 2020.

[13] Alexander Kättlitz, Guillermo Areosa Bäuml, Dante Powell, and Gideon Saunders. Tyndp 2022 scenario report. Technical report, ENTSOG & ENTSOE, 2022.

[14] Michele Scolaro and Noah Kittner. Optimizing hybrid offshore wind farms for cost-competitive hydrogen production in germany. *International Journal of Hydrogen Energy*, 47(10):6478–6493, 2022.

[15] Energinet, TenneT, and Gasunie. Grid-integrated offshore power-to-gas. Technical report, North Sea Wind Power Hub, 2022.

[16] Michael A Semeraro III. Renewable energy transport via hydrogen pipelines and hvdc transmission lines. *Energy Strategy Reviews*, 35:100658, 2021.

[17] A Taieb and M Shaaban. Cost analysis of electricity transmission from offshore wind farm by hvdc and hydrogen pipeline systems. In *2019 IEEE PES GTD Grand International Conference and Exposition Asia (GTD Asia)*, pages 632–636. IEEE, 2019.

[18] Bin Miao, Lorenzo Giordano, and Siew Hwa Chan. Long-distance renewable hydrogen transmission via cables and pipelines. *International journal of hydrogen energy*, 46(36):18699–18718, 2021.

[19] C Tsiklios, M Hermesmann, and TE Müller. Hydrogen transport in large-scale transmission pipeline networks: Thermodynamic and environmental assessment of repurposed and new pipeline configurations. *Applied Energy*, 327:120097, 2022.

[20] Deirdre Eradus. The techno-economic feasibility of green hydrogen storage in salt caverns in the dutch north sea. *TU Delft repository*, 2022.

[21] Armenio de Souza Rangel, Jose Carlos de Souza Santos, and Jose Robert F Savoia. Modified profitability index and internal rate of return. *Journal of International Business and Economics*, 4(2):13–18, 2016.

[22] Mikhail V Sokolov. NPV, IRR, PI, PP, and DPP: a unified view. *arXiv preprint arXiv:2302.02875*, 2023.

[23] Esra Bas. A robust approach to the decision rules of NPV and IRR for simple projects. *Applied Mathematics and Computation*, 219(11):5901–5908, 2013.

[24] Mihir Mehta, Michiel Zaaijer, and Dominic von Terzi. Optimum turbine design for hydrogen production from offshore wind. In *Journal of Physics: Conference Series*, volume 2265, page 042061. IOP Publishing, 2022.

[25] Alessandro Singlitico, Jacob Østergaard, and Spyros Chatzivasileiadis. Onshore, offshore or in-turbine electrolysis? techno-economic overview of alternative integration designs for green hydrogen production into offshore wind power hubs. *Renewable and Sustainable Energy Transition*, 1:100005, 2021.

[26] DNVGL. Power-to-hydrogen Ijmuiden ver. final report for TenneT and Gasunie. Technical report, DNVGL, 2018.

[27] Xiaojie Tian, Qingyang Wang, Guijie Liu, Yunxiang Liu, Yingchun Xie, and Wei Deng. Topology optimization design for offshore platform jacket structure. *Applied Ocean Research*, 84:38–50, 2019.

[28] Miralda Van Schot and Catrinus Jepma. A vision on hydrogen potential from the north sea. Technical report, North Sea Energy, 2020.

[29] Sepanta Dokhani, Mohsen Assadi, and Bruno G Pollet. Techno-economic assessment of hydrogen production from seawater. *International Journal of Hydrogen Energy*, 48(26):9592–9608, 2023.

[30] Saikat Bolar, Subhasis Shit, Naresh Chandra Murmu, and Tapas Kuila. Progress in theoretical and experimental investigation on seawater electrolysis: opportunities and challenges. *Sustainable Energy & Fuels*, 5(23):5915–5945, 2021.

[31] MA Khan, Tareq Al-Attas, Soumyabrata Roy, Muhammad M Rahman, Noreddine Ghaffour, Venkataraman Thangadurai, Stephen Larter, Jinguang Hu, Pulickel M Ajayan, and Md Golam Kibria. Seawater electrolysis for hydrogen production: a solution looking for a problem? *Energy & Environmental Science*, 14(9):4831–4839, 2021.

[32] Farah Ejaz Ahmed, Abdullah Khalil, and Nidal Hilal. Emerging desalination technologies: Current status, challenges and future trends. *Desalination*, 517:115183, 2021.

[33] Yu Jie Lim, Kunli Goh, Masaru Kurihara, and Rong Wang. Seawater desalination by reverse osmosis: Current development and future challenges in membrane fabrication–a review. *Journal of Membrane Science*, 629:119292, 2021.

[34] Jungbin Kim, Kiho Park, Dae Ryook Yang, and Seungkwan Hong. A comprehensive review of energy consumption of seawater reverse osmosis desalination plants. *Applied Energy*, 254:113652, 2019.

[35] Hyunkyung Lee, Yongxun Jin, and Seungkwan Hong. Recent transitions in ultrapure water (upw) technology: Rising role of reverse osmosis (ro). *Desalination*, 399:185–197, 2016.

[36] Lucía Alvarado and Aicheng Chen. Electrodeionization: principles, strategies and applications. *Electrochimica Acta*, 132:583–597, 2014.

[37] SA Grigoriev, VN Fateev, DG Bessarabov, and P Millet. Current status, research trends, and challenges in water electrolysis science and technology. *International Journal of Hydrogen Energy*, 45(49):26036–26058, 2020.

[38] Mohamed Nasser, Tamer F Megahed, Shinichi Ookawara, and Hamdy Hassan. A review of water electrolysis–based systems for hydrogen production using hybrid/solar/wind energy systems. *Environmental Science and Pollution Research*, pages 1–25, 2022.

[39] Christopher Varela, Mahmoud Mostafa, and Edwin Zondervan. Modeling alkaline water electrolysis for power-to-x applications: A scheduling approach. *International journal of hydrogen energy*, 46(14):9303–9313, 2021.

[40] S Shiva Kumar and V Himabindu. Hydrogen production by pem water electrolysis–a review. *Materials Science for Energy Technologies*, 2(3):442–454, 2019.

[41] Z Kexin, L Xiao, W Lina, S Ke, W Yuannan, X Zhoubing, W Qiannan, B Xinyu, H Mohamed, SC Hui, et al. Status and perspectives of key materials for pem electrolyzer. *Nano Res. Energy*, 2022.

[42] Kewei Hu, Jiakun Fang, Xiaomeng Ai, Danji Huang, Zhiyao Zhong, Xiaobo Yang, and Lei Wang. Comparative study of alkaline water electrolysis, proton exchange membrane water electrolysis and solid oxide electrolysis through multiphysics modeling. *Applied Energy*, 312:118788, 2022.

[43] Timur Gül and Dave Turk. The future of hydrogen. Technical report, IEA, 2019.

[44] Amin Mohammadi and Mehdi Mehrpooya. A comprehensive review on coupling different types of electrolyzer to renewable energy sources. *Energy*, 158:632–655, 2018.

[45] Meng Ni, Michael KH Leung, and Dennis YC Leung. Technological development of hydrogen production by solid oxide electrolyzer cell (soec). *International journal of hydrogen energy*, 33(9):2337–2354, 2008.

[46] Gyubin Min, Saeyoung Choi, and Jongsup Hong. A review of solid oxide steam-electrolysis cell systems: Thermodynamics and thermal integration. *Applied Energy*, 328:120145, 2022.

[47] Immanuel Vincent and Dmitri Bessarabov. Low cost hydrogen production by anion exchange membrane electrolysis: A review. *Renewable and Sustainable Energy Reviews*, 81:1690–1704, 2018.

[48] Hamish Andrew Miller, Karel Bouzek, Jaromir Hnat, Stefan Loos, Christian Immanuel Bernäcker, Thomas Weißgärber, Lars Röntzsch, and Jochen Meier-Haack. Green hydrogen from anion exchange membrane water electrolysis: a review of recent developments in critical materials and operating conditions. *Sustainable Energy & Fuels*, 4(5):2114–2133, 2020.

[49] Andrzej Witkowski, Andrzej Rusin, Mirosław Majkut, and Katarzyna Stolecka. Comprehensive analysis of hydrogen compression and pipeline transportation from thermodynamics and safety aspects. *Energy*, 141:2508–2518, 2017.

[50] IA Gondal. Hydrogen transportation by pipelines. In *Compendium of hydrogen energy*, pages 301–322. Elsevier, 2016.

[51] A european hydrogen infrastructure vision covering 28 countries, author=Van Rossum, Rik and Jens, Jaro and La Guardia, Gemma and Wang, Anthony and Kühnen, Luis and Overgaag, Martijn, year=2022, institution=EHB. Technical report.

[52] Syed Rahman, Irfan Khan, Hend I Alkhammash, and Muhammad Faisal Nadeem. A comparison review on transmission mode for onshore integration of offshore wind farms: Hvdc or hvac. *Electronics*, 10(12):1489, 2021.

[53] Kala Meah and Sadrul Ula. Comparative evaluation of hvdc and hvac transmission systems. In *2007 IEEE Power Engineering Society General Meeting*, pages 1–5. IEEE, 2007.

[54] Stephen Hardy, Kristof Van Brusselen, Stijn Hendrix, D Van Hertem, and H Ergun. Techno-economic analysis of hvac, hvdc and ofac offshore wind power connections. In *2019 IEEE Milan PowerTech*, pages 1–6. IEEE, 2019.

[55] Xin Xiang, Michael MC Merlin, and Tim C Green. Cost analysis and comparison of hvac, lfac and hvdc for offshore wind power connection. 2016.

[56] Alessandro Giampieri, Janie Ling-Chin, and Anthony Paul Roskilly. Techno-economic assessment of offshore wind-to-hydrogen scenarios: A uk case study. *International Journal of Hydrogen Energy*, 2023.

[57] Mohd Adnan Khan, Cameron Young, Catherine Mackinnon, and David B Layzell. The techno-economics of hydrogen compression. *Technical Briefs. Canada: Transition Accelerator*, 1(1):1e36, 2021.

[58] Giuseppe Sdanghi, Gaël Maranzana, Alain Celzard, and Vanessa Fierro. Review of the current technologies and performances of hydrogen compression for stationary and automotive applications. *Renewable and Sustainable Energy Reviews*, 102:150–170, 2019.

[59] Sebastian Schuster, Hans Josef Dohmen, and Dieter Brillert. Challenges of compressing hydrogen for pipeline transportation with centrifugal-compressors. *Proceedings of Global Power and Propulsion Society, GPPS Chania20, Sept*, pages 7–9, 2020.

[60] Evan Gaertner, Jennifer Rinker, Latha Sethuraman, Frederik Zahle, Benjamin Anderson, Garrett E Barter, Nikhar J Abbas, Fanzhong Meng, Pietro Bortolotti, Witold Skrzypinski, et al. Iea wind tcp task 37: definition of the iea 15-megawatt offshore reference wind turbine. Technical report, National Renewable Energy Lab.(NREL), Golden, CO (United States), 2020.

[61] M Vieira, Brian Snyder, Elsa Henriques, and Luis Reis. European offshore wind capital cost trends up to 2020. *Energy policy*, 129:1364–1371, 2019.

[62] Imran Hasan Tusar and Bhaba Ranjan Sarker. State-of-the-art operation and maintenance cost minimization strategies for offshore wind farms. In *IIE Annual Conference. Proceedings*, pages 1116–1121. Institute of Industrial and Systems Engineers (IISE), 2020.

[63] Rebecca Martin, Iraklis Lazakis, Sami Barbouchi, and Lars Johanning. Sensitivity analysis of offshore wind farm operation and maintenance cost and availability. *Renewable Energy*, 85:1226–1236, 2016.

[64] Anita Kusuma Wardani, Ahmad Nurul Hakim, and I Gede Wenten. Combined ultrafiltration-electrodeionization technique for production of high purity water. *Water Science and Technology*, 75(12):2891–2899, 2017.

[65] Daniel Janowitz, Sophie Groche, Süleyman Yüce, Thomas Melin, and Thomas Wintgens. Can large-scale offshore membrane desalination cost-effectively and ecologically address water scarcity in the middle east? *Membranes*, 12(3):323, 2022.

[66] Albashir KH Elfaqih and Said O Belhaj. Economic analysis of swro desalination plant design using three different power systems. In *2019 10th International Renewable Energy Congress (IREC)*, pages 1–6. IEEE, 2019.

[67] J Eichman, K Harrison, and Michael Peters. Novel electrolyzer applications: providing more than just hydrogen. Technical report, National Renewable Energy Lab.(NREL), Golden, CO (United States), 2014.

[68] Martin Kopp, David Coleman, Christoph Stiller, Klaus Scheffer, Jonas Aichinger, and Birgit Scheppat. Energiepark mainz: Technical and economic analysis of the worldwide largest power-to-gas plant with pem electrolysis. *International Journal of Hydrogen Energy*, 42(19):13311–13320, 2017.

[69] TenneT. 2gw program, more wind energy for europe. Technical report, TenneT, 2023.

[70] E Shashi Menon. *Pipeline planning and construction field manual*. Gulf Professional Publishing, 1978.

[71] Tomasz Włodek, Mariusz Łaciak, Katarzyna Kurowska, and Łukasz Wegrzyn. Thermodynamic analysis of hydrogen pipeline transportation–selected aspects. *AGH Drilling, Oil, Gas*, 33(2):379–396, 2016.

[72] Szymon Kuczyński, Mariusz Łaciak, Andrzej Olijnyk, Adam Szurlej, and Tomasz Włodek. Thermodynamic and technical issues of hydrogen and methane-hydrogen mixtures pipeline transmission. *Energies*, 12(3):569, 2019.

[73] Predrag Djapic and Goran Strbac. *Cost benefit methodology for optimal design of offshore transmission systems*. Department for Business, Enterprise & Regulatory Reform, 2008.

[74] Sofoklis Makridis. Hydrogen storage and compression. *arXiv preprint arXiv:1702.06015*, 2017.

[75] Catrinus J Jepma and M van Schot. On the economics of offshore energy conversion: smart combinations. *Converting Offshore Wind Energy into Green Hydrogen on Existing Oil and Gas Platforms in the North Sea. Energy Delta Institute (EDI)*, 3, 2017.

[76] Behrooz Ahmadzadeh. Efficiency in power transformers. 2016.

[77] IEA. Denmark, electricity generation by source, 2022.

[78] IEA. The netherlands, electricity generation by source, 2021.

Appendix A

Details on platform weight and cost

This appendix provides additional information concerning the weight and costs of the platform. The data presented here is sourced from a technical report commissioned by DNVGL for TenneT and Gasunie [26], the Dutch grid operators responsible for electricity and gas distribution. These estimates are based on the experience of TenneT and supplier information. A more comprehensive analysis of the weight and cost assessment is found in the report of DNVGL.

In the tables below, a cost and weight estimate has been given for 1000 MW platform, which contains 500 MW of electrolyzer equipment and 500 MW of electricity connection. Both the cost and weight scale linearly with the capacities as proposed by [26]. At the end of this Appendix, the derivation of the platform cost function is found. For the purpose of the simulation, the cost function has been written as a function of the capacity of the electrolyzer and cable capacity. A factor of 1.5 has been assumed to account for the installation costs of the platform.

Table A.1: Topside cost assumptions

Material	**Value**	**Unit**
Steel	3,500	€/tonne
Cladding	3,000	€/tonne
Grating	180	€/m^2
Coating	120	€/m^2

Table A.2: Support structure cost assumptions

Material	**Value**	**Unit**
Primary Steel	2,000	€/tonne
Secondary Steel	2,500	€/tonne
Anodes	6,500	€/m^2
Coating	120	€/m^2

500 MW electricity topside

Table A.3: Mass and volume assumptions

Material	**Value**	**Unit**
Volume	61,896	m^3
Steel structure	4,209	tonne
Equipment	1,816	tonne
Auxiliary equip.	2,228	tonne
Total mass	**8,253**	**tonne**

Table A.4: Cost assumption

Material	**Value**	**Unit**
Steelwork	4,209	tonne
Cladding	2,228	tonne
Gratings	6,809	m^2
Coating Area	82,011	m^2
Total cost	**32.485M**	**€**

500 MW electrolysis topside

Table A.5: Mass and volume assumptions

Material	Value	Unit
Volume	96,775	m^3
Steel structure	6,624	tonne
H_2 plant	6,400	tonne
Auxiliary equip.	3,302	tonne
Total mass	**16,326**	**tonne**

Table A.6: Cost assumption

Material	Value	Unit
Steelwork	6,624	tonne
Cladding	3,302	tonne
Gratings	10,645	m^2
Coating Area	126,448	m^2
Total cost	**50.180M €**	

Support structure

The mass and cost of the support structure are determined by both the water depth and the overall weight of the topside. DNVGL has taken a water depth of 30 meters into account, which represents the average depth of the Dutch North Sea, and is thus representative for this report.

Table A.7: Mass and volume assumptions

Material	Value	Unit
Topside mass	24,579	tonne
Jacket mass	12,964	tonne
Secondary steel	250	tonne
Anode	134	tonne
Coating area	14,513	m^2
Total mass	**13,348**	**tonne**
Total cost	**29.166M €**	

Derivation Cost function

It is assumed that the cost and weight of the topside scale linearly with cable and electrolyzer capacities. The following holds for the topside:

$$C_{tps}(S_{cab}, S_{elec}) = \frac{32.485 \times 10^6}{500} S_{cab} + \frac{50.180 \times 10^6}{500} S_{elec} \tag{A.1}$$

With S_{cab} the cable capacity [MW] and S_{elec} the electrolyzer capacity [MW]. For the support structure then follows:

$$C_{jck}(S_{cab}, S_{elec}) = \left(\frac{8253}{500} S_{cab} + \frac{16326}{500} S_{elec}\right) \frac{12964}{24579} \times \frac{29.166 \times 10^6}{12964} \tag{A.2}$$

By adding the Equations A.1 and A.2, the total CAPEX of the platform is derived:

$$C_{plat} = (C_{tps}(S_{cab}, S_{elec}) + C_{jck}(S_{cab}, S_{elec})) \times installationfactor \tag{A.3}$$

$$C_{plat} = (84.651 S_{cab} + 139.281 S_{elec}) \times 10^3 \times 1.5 \tag{A.4}$$

Appendix B

Map of the European hydrogen infrastructure

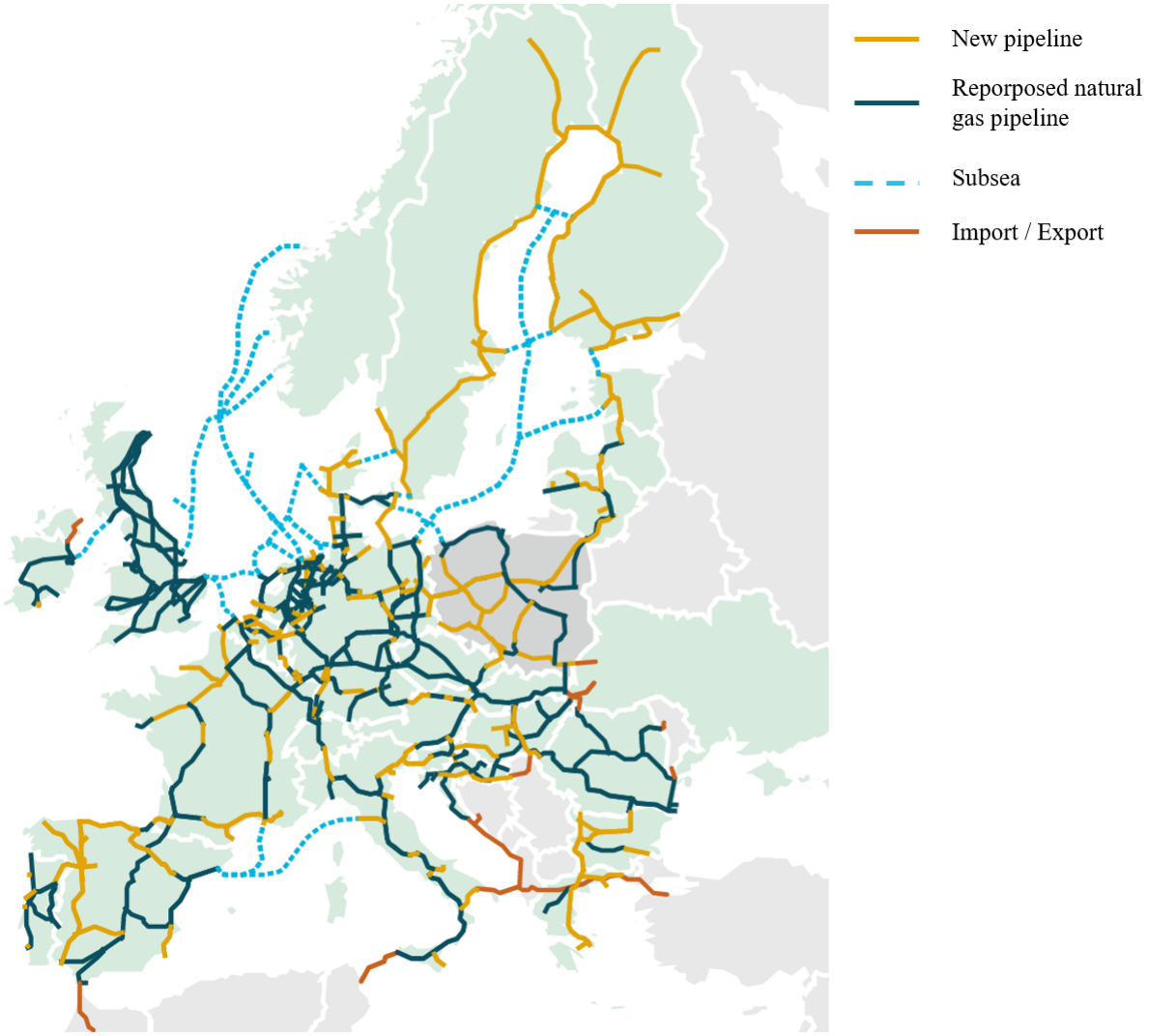

Figure B.1: Pan-European hydrogen infrastructure by 2040, envisioned by the EHB [51].

Appendix C

Location of the wind data

Figure C.1: Location of the wind data (55°N 7°E).

Appendix D

Input parameters of the simulations

Table D.1: Input parameters regarding the wind farm CAPEX

Parameter	**Symbol**	**Value**	**Unit**	**Reference**
Average water depth	D_{avg}	30	m	N/A
Turbine capacity	T_{cap}	15	MW	N/A
Function parameter	α_0	-776.2	-	[61]
Function parameter	α_1	115.1	-	[61]
Function parameter	α_2	-39.8	-	[61]
Function parameter	α_3	14.2	-	[61]
Function parameter	α_4	-153.5	-	[61]

Table D.2: Input parameters regarding the water treatment system.

Parameter	**Symbol**	**Value**	**Unit**	**Reference**
Gravimetric density seawater	ρ_{sw}	1025	kg/m^3	N/A
Gravitational constant	g	9.81	m/s^2	N/A
Feed pump efficiency	η_{fp}	70	%	N/A
Recovery RO	R_{RO}	45	%	[34]
Recovery EDI	R_{EDI}	90	%	[36]
Platform height	h	15	m	[28]

Appendix E

Offshore wind farm cost trends

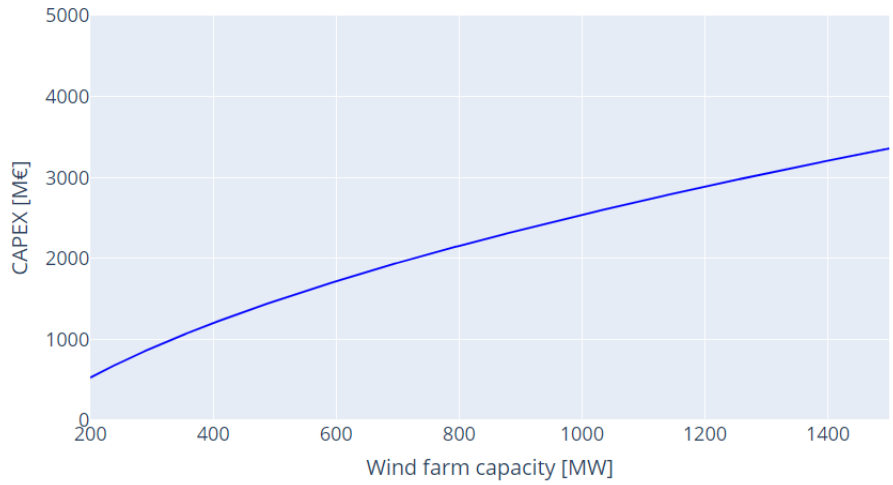

Figure E.1: Offshore wind farm CAPEX as a function of total farm capacity. This curve is based on historical data [61] and holds for a water depth of 30 meters and a turbine capacity of 15 MW

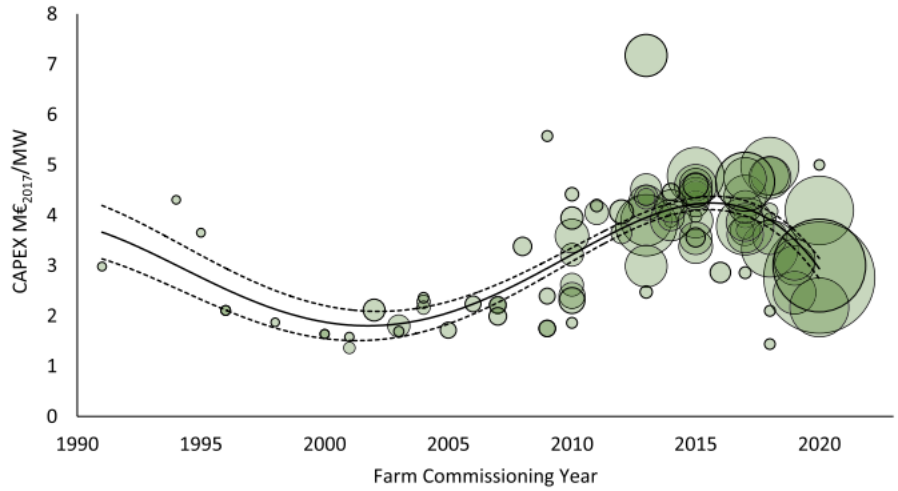

Figure E.2: Specific cost in M€/MW for offshore windfarms from 1991 to 2020. A 4th-order polynomial fit is included within the margins for its 95% confidence interval. The graph was taken from Viera et al. [61].

Derivation farm OPEX

Underneath, the derivation of the OPEX of the wind farm is presented. As explained in Section 3.1.2, the OPEX contributes to about 25% of the total costs over the lifetime of the wind farm.

$$\frac{O_{farm,tot}}{C_{farm} + O_{farm,tot}} = 0.25 \tag{E.1}$$

$$0.75O_{farm,tot} = 0.25C_{farm} \longrightarrow O_{farm,tot} = 0.33C_{farm} \tag{E.2}$$

Assuming the lifetime of the wind farm to be 25 years:

$$O_{farm,tot} = 25O_{farm,ann} = 0.33C_{farm} \tag{E.3}$$

$$O_{farm,ann} = 0.013C_{farm} \longrightarrow O_{farm,ann} = 1.3\% \times C_{farm} \tag{E.4}$$

Appendix F

Energy consumption and cost of seawater treatment

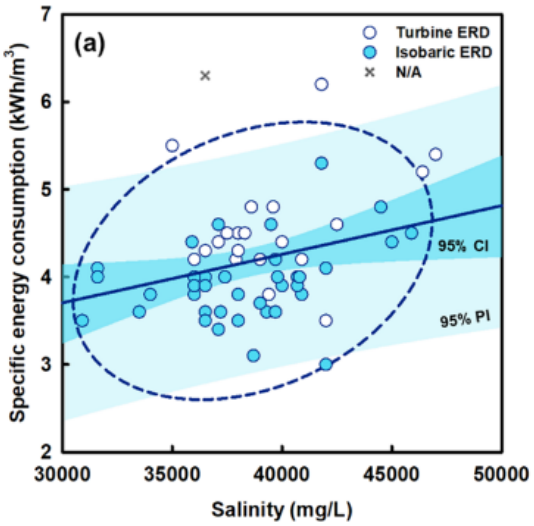

Figure F.1: Effects of feed salinity on the SEC of SWRO plants [34].

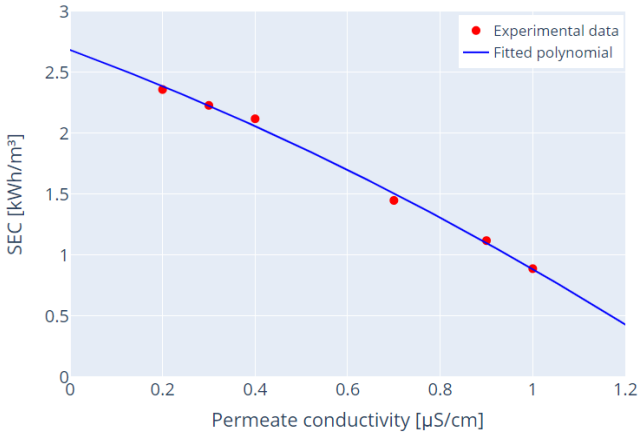

Figure F.2: SEC of deionizing tapwater (248 $\mu S/cm$) for various permeate conductivities. Experimental data were taken from Warandi et al. [64]. A 2nd-order polynomial was fitted through their data points: $y = -0.395x^2 - 1.404x + 2.684$

Derivation cost function

Depending on the size of the electrolyzer, a certain amount of hydrogen will be produced on a daily basis. In this example, it was assumed that the electrolyzer would be on full load for 90% of the time of the day:

$$X_{hy,dly} = S_{elec} \times \frac{\eta_{elec,nom}}{LHV_{hy}} \times 24 \times 0.90 \tag{F.1}$$

Where $X_{hy,dly}$ is the amount of produced hydrogen $[kg/day]$, S_{elec} the electrolyzer size $[MW]$, $\eta_{elec,nom}$ the nominal efficiency of the electrolyzer [%], and LHV_{hy} the lower heating value of hydrogen $[MWh]$. Calculating the above equation gives:

$$X_{hy,dly} = S_{elec} \times \frac{0.64}{33.3 * 10^{-3}} \times 24 \times 0.90 = 415 S_{elec} \tag{F.2}$$

The water intake of the electrolyzer can then be derived as follows:

$$Q_{elec,dly} = X_{hy,dly} \times \frac{Y_{elec}}{1000} \tag{F.3}$$

Where $Q_{elec,dly}$ is the demineralized water intake of the electrolyzer $[m^3/day]$, and Y_{elec} is the specific water intake of the electrolyzer $[L/kg]$. Calculating the above equation gives:

$$Q_{elec,dly} = 415 S_{elec} * \frac{10}{1000} = 4.15 S_{elec} \tag{F.4}$$

The CAPEX of the water treatment system can now be approximated as follows:

$$C_{wt} = 4.15 * S_{elec} * (c_{ro} + c_{edi}) = 20750 * S_{elec} \tag{F.5}$$

Where C_{wt} is the total capital cost of the water treatment system [€], and c_{ro} and c_{edi} are the specific capital costs of the RO and EDI unit, respectively $[€/m^3/day]$. Note that the specific capital costs of both the RO and EDI unit are assumed to be €2500 m^3/day as explained in Section 3.2.3.

It should be noted that, when assuming an electrolyzer operates at full capacity for 90% of the day, the desalination system will be oversized. To accurately determine the appropriate size for a desalination plant, it is necessary to incorporate a water storage tank and calculate the required daily UPW flow based on the projected annual hydrogen production. During periods of low production, the storage tank would gradually fill, and during high production periods, it would be drained. However, due to the relatively low financial impact together with a relatively low energy consumption, optimization was not pursued in this research.

Appendix G

Future layout of the Dutch North Sea

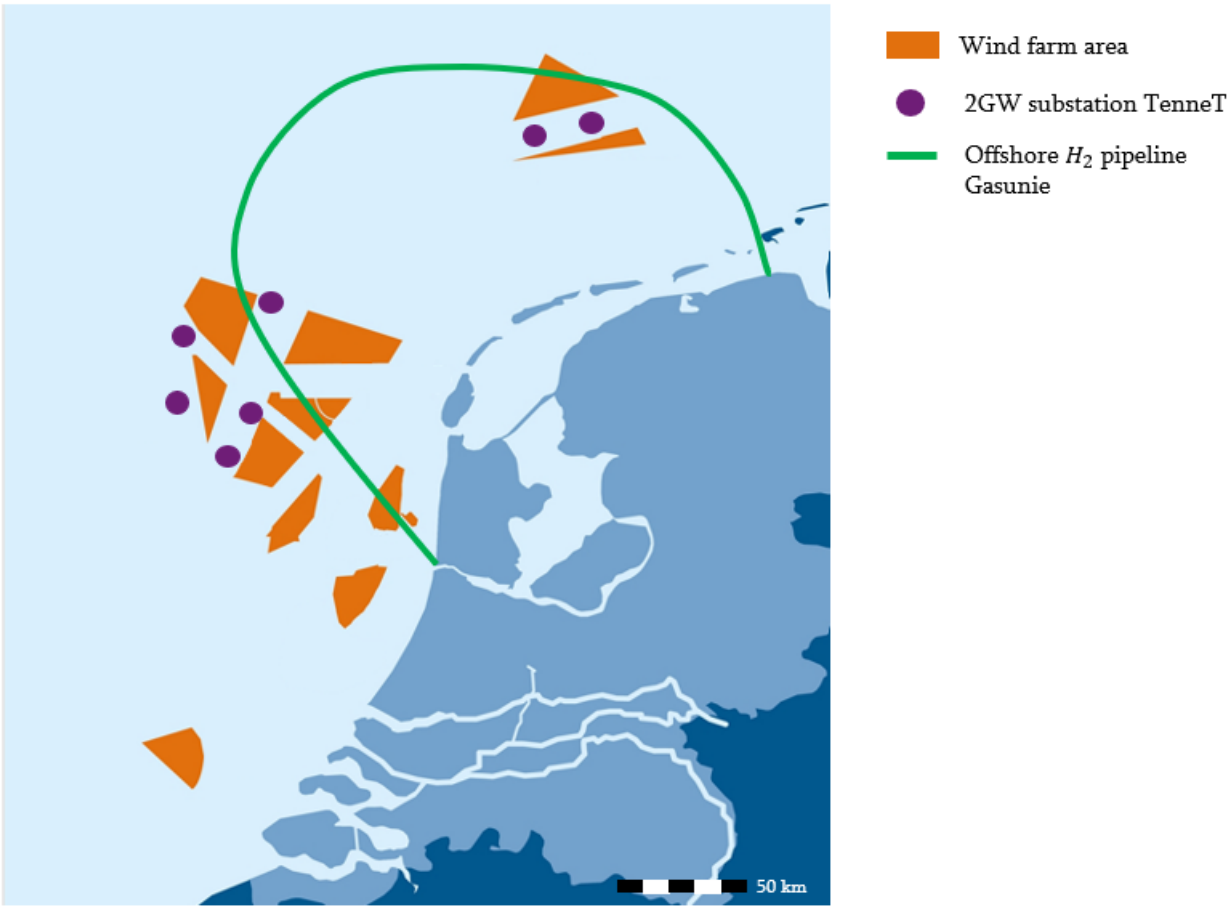

Figure G.1: Layout of the North Sea by 2030, envisioned by Tennet and Gasunie.

Appendix H

Pipeline sizing

This methodology for pipeline sizing was taken from [70]. As explained in Section 3.4.1, the model calculates the pressure drop for a certain hydrogen flow and pipe diameter.

Friction factor λ for turbulent gas flow through a pipe ($Re > 4000$), given by Colebrook-White equation:

$$\frac{1}{\sqrt{\lambda}} = -2\log_{10}\left(\frac{\epsilon}{3.7D} + \frac{2.51}{Re\sqrt{\lambda}}\right) \tag{H.1}$$

Where ϵ is the surface roughness of the pipe $[mm]$, and Re is the dimensionless Reynolds number given by:

$$Re = 0.5134\left(\frac{p_b}{T_b}\right)\left(\frac{G_{H_2}Q_{H_2}}{\mu_{hydr}D}\right) \tag{H.2}$$

Where μ_{hydr} is the dynamic viscosity of hydrogen gas, taken at STP [P].

The friction factor, λ, is solved iteratively with Equation H.1. In Table H.1, several input parameters used for the pipeline sizing are found.

Table H.1: Input parameters regarding HPL flow.

Parameter	**Symbol**	**Value**	**Unit**	**Reference**
Compressibility factor	Z	1.02	-	[71]
Pipe length	L	30.0	km	N/A
Average flow temperature	T_{avg}	288.15	K	N/A
Pipe surface roughness	ϵ	0.05	mm	[25]

Appendix I

Compressor details

In Figure I.1, a diagram for compressor technology selection based on volume flow and discharge pressure is presented. Based on the compression criteria in this research, a multi-stage reciprocating compressor system was proposed.

Some constants of hydrogen and other values regarding the calculation of the compression power are found in Table I.1.

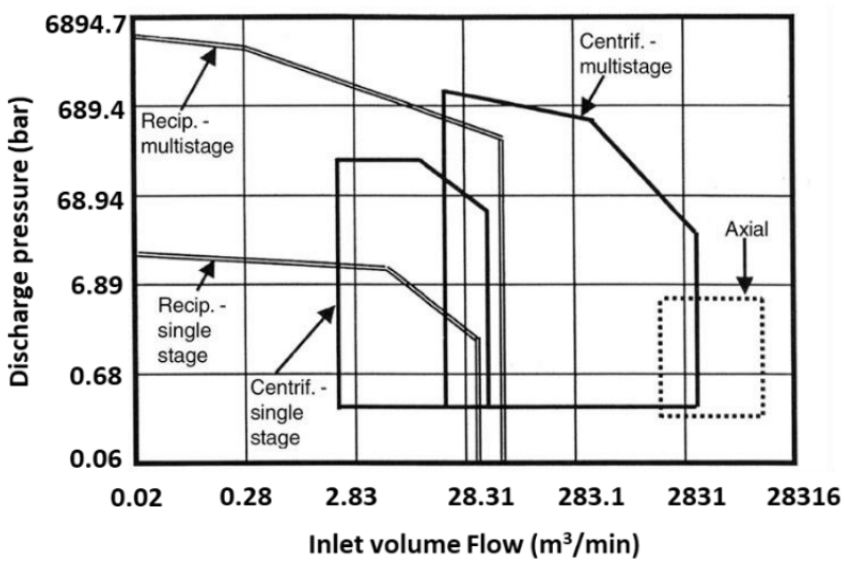

Figure I.1: Diagram for compressor selection. The diagram was adopted from [57].

Table I.1: Parameters regarding hydrogen compression.

Parameter	**Symbol**	**Value**	**Unit**
Specific heat at constant pressure	c_p	14.28	$kJkg^{-1}K^{-1}$
Specific heat at constant volume	c_v	10.11	$kJkg^{-1}K^{-1}$
Inlet temperature	T_{in}	298	K
Compression ratio	Π	1.58	-
Molar weight	M	1.00	g/mol

Compressor power

Knowing c_p and c_v of hydrogen, the gas isentropic coefficient can be calculated:

$$k = \frac{c_p}{c_v} = \frac{14.28}{10.11} = 1.41 \tag{I.1}$$

With the temperature of the gas at the inlet of the compressor and the compression ratio, an estimation of the temperature at the outlet can be derived:

$$\frac{T_{out}}{T_{in}} = \Pi^{(k-1)/k} = 1.58^{(1.41-1)/1.41} \rightarrow T_{out} = 340.4K \tag{I.2}$$

Assuming a 1 kg/s hydrogen flow, the isentropic compressor power can be calculated:

$$P_{comp,isen} = 2.31\frac{k}{k-1}\frac{T_{out} - T_{in}}{M}(Q_{comp} \times 10^{-3}) \tag{I.3}$$

$$P_{comp,isen} = 2.31\frac{1.41}{1.41-1}\frac{340.4 - 298}{1}(3600 \times 10^{-3}) = 1213kW \tag{I.4}$$

Using an assumed isentropic efficiency of 70% [57], the real compressor power is obtained:

$$P_{comp} = \frac{P_{comp,isen}}{\eta_{isen}} = \frac{1213}{0.70} = 1733kW \tag{I.5}$$

The calculated power above is for one compressor stage. As proposed by Section 3.5, the system will comprise two compressor stages with each a compression ratio of 1.58. The total compression power is therefore:

$$P_{comp,tot} = 2P_{comp} = 3466kW \tag{I.6}$$

With a flow rate of 1 kg/s, the amount of compression energy per kg can be calculated:

$$E_{comp} = \frac{3466}{3600} = 0.96kWh/kg \tag{I.7}$$

Cost function

The hydrogen flow can be related to the capacity of the electrolyzer by:

$$Q_{comp} = S_{elec}\frac{1000}{E_{elec}} \tag{I.8}$$

Where E_{elec} is the energy consumption of the electrolyzer (52 kWh/kg, Table 3.3) and Q_{comp} is the hydrogen flow to the compressor in kg/h.
For the example of 1 kg/s, the following is obtained:

$$S_{elec} = \frac{52 * 3600}{1000} = 187.2MW \tag{I.9}$$

Using the estimation of €2,800 per kW compressor power, the compressor cost as a function of electrolyzer capacity can be derived:

$$C_{comp} = \frac{2800 * 3466}{18.7}S_{elec} \tag{I.10}$$

$$C_{comp} \approx 52 \times 10^3 S_{elec} \tag{I.11}$$

Appendix J

Data sets for the simulations

As explained in Section 3.7.1, the Danish electricity market prices and wind data were used in this research. Figure J.1 shows the raw data set of the electricity market in Denmark in 2018 with an average price of €44.05 per MWh.

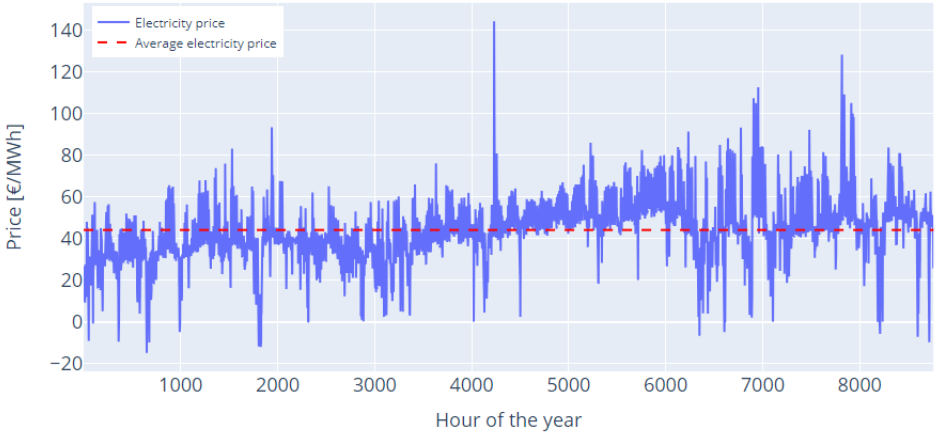

Figure J.1: Danish electricity prices in 2018 with an average electricity price of €44.05 per MWh.

Since this research considers a hybrid wind farm connected to the Dutch electricity grid, the data set has been indexed to mean price of €75 per MWh to represent the Dutch market more accurately. The result is presented in Figure J.2.

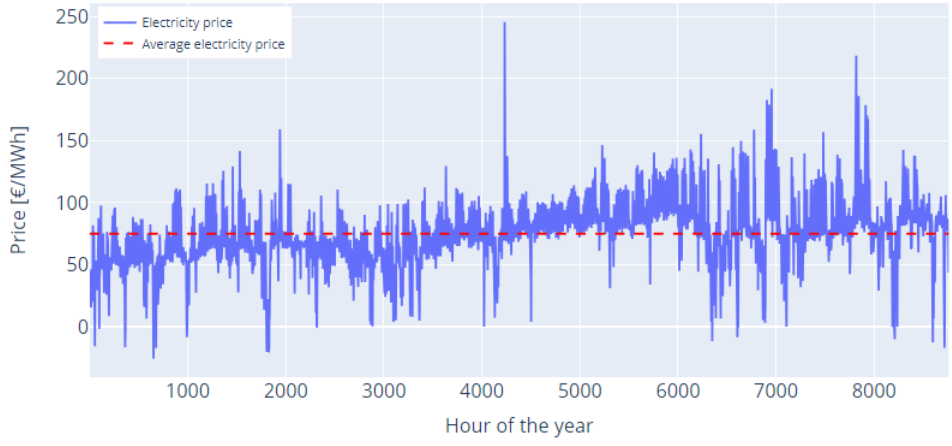

Figure J.2: Danish electricity prices indexed to a mean price of €75 per MWh.

As previously discussed in Section 3.7.1, the Danish electricity and wind data was adopted due to the large share of wind energy in Denmark. In Figure J.3, the relationship between the electricity price and the power output by the wind farm is depicted. Noticeable is that the majority of the negative price occurrences happen when the farm operates at maximum capacity.

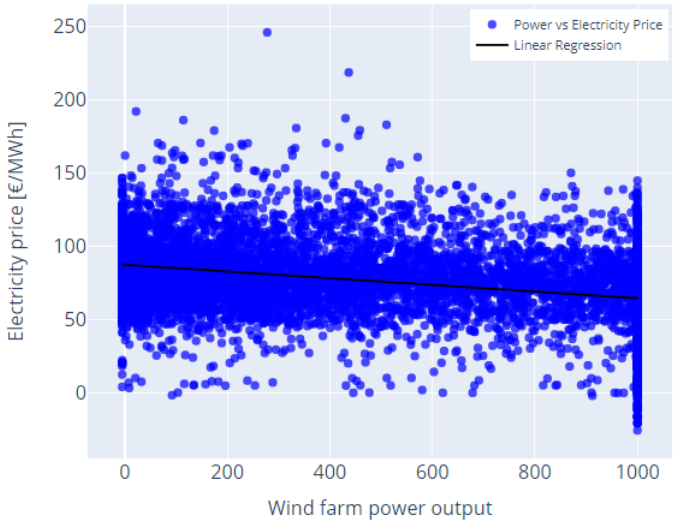

Figure J.3: Electricity price against wind farm power output. The black line indicates the correlation between the two.